Synthesis of Anisotropic Microparticles and Capsules *via* Droplet Microfluidics

By

Gabit E. Nurumbetov

A thesis submitted in fulfilment of the requirements for the degree of Doctor of Philosophy in Chemistry

University of Warwick, Department of Chemistry

February 2013

To Farida Dzhaparova, Assel Akhmetova and Emir Nurumbetov

Table of Contents

Figures

Tables

Acknowledgements

First of all, I would like to express my sincere gratitude to my supervisor Assoc. Prof. Stefan Bon for giving me an opportunity to be a member of his group, for constructive criticism, creative ideas, and many advices. Also, I would like to thank him for an opportunity to share the results of my work *via* top conferences and journals. It was a privilege for me to be a part of the BonLab.

I would like to thank my group mates for a good time spent. It would not be so exciting without our countless coffee breaks, group meetings and amazing off-lab times. Especially I would like to mention Andy, Nick, Roberto and Yunhua with whom I shared the office for three years, along with Tom and Adam for a successful collaboration. I would like to thank Holly, Attyah, Rong, Catheline, Nicole other researchers worked together with me. I would also like to thank Dr. Xiaolei Fan from Prof. Alexei Lapkin group for helping me with computational fluid dynamics simulations.

I would also like to mention the people who revealed me the fascination of the chemical science. First of all, my first teacher of chemistry, Tyo Eleonora Aleksandrovna, who managed to intrigue a troublesome teenager with symbols from the Periodic Table, which later had a huge impact on his life. Secondly, Prof. Enver R. Ishkenov, my mentor who significantly influenced the formation of my fundamental attitude to many aspects of the chemistry and life in general, whose merit in the existence of this thesis is difficult to overestimate.

Most importantly, I would like to thank members of my family, to whom this thesis is dedicated. Farida Dzhaparova, my grandmother who surrounded me with her boundless love and care for many years from the day of my birth. Emir Nurumbetov,

my father who is an example of the truly gentlemanly behaviour and wisdom for me. Assel Akhmetova, my mother to whom I owe absolutely everything in my life for her continuous titanic efforts to make it brighter. Every single letter, every single page in this thesis exists by virtue of these people to whom I am indebted.

Declaration

I hereby declare that this thesis consists of my own work, and that it has not previously been submitted for a degree at any other institution, except the following collaborations: (i) a nitrogen absorption experiment in Chapter IV was carried out by Adam Morgan; (ii) a confocal laser scanning image in Chapter IV was taken by Dr. Nicholas Ballard., (iii) a synthesis of block copolymer in Chapter VI was carried out by Rong Chen, (iv) experiments on interaction of polymersomes and hydrogen peroxide in Chapter VI were performed by Bruno Samorini, (v) Ansys CFD simulations were performed by Dr. Xiaolei Fan.

Signature: Date:

Abstract

We have developed simplified microfluidic droplet generators and employed them to fabricate anisotropic polymer particles and capsules in the size range of 100–500 μm. We used cheap and generally available materials and equipment to design and assemble microfluidic devices. All our devices were made of standard wall borosilicate capillaries (OD 1.0mm, ID 0.58mm), steel dispensing needles without bevel (30 G, 32 G), microscopy glass slides, fast-curing epoxy glue (Araldite-80805) and diamond scribe to process the glass. We designed four different geometries for each device, which can be separated for two groups: single and double droplet generators. The performance of the devices was validated using computational fluid dynamics and laboratory experiments.

First of all, we tried to fabricate intricate single emulsion droplets and then moved on to double emulsion droplets. The range of the fabricated particles and capsules includes anisotropically-shaped amphiphilic polymer "microbuckets", biphasic particles, capsules with various fillers and stimuli responsive polymer vesicles. To produce such objects we employed different functional monomers, for instance "clickable" glycidyl methacrylate or hydrophilic 2-hydroxyethyl methacrylate. We also utilized several chemical and physical phenomena such as internal phase separation, wettability or polymer chain cross-linking to tune the properties of the synthesized particles. We investigated properties of the above mentioned particles and capsules. For example, "microbuckets" which are hydrophilic at the exterior surface, but hydrophobic inside the cavity, were able to withdraw oil droplets from an aqueous phase and "arrest" them inside the cavity.

In short, a combination of easy-to-make microfluidic devices and traditional chemical methods greatly expanded synthetic routes towards particles and capsules fabrication.

Abbreviations

TEM	Transmission electron microscopy
SEM	Scanning electron microscopy
Cryo-SEM	Cryogenic scanning electron microscopy
GPC	Gel Permeation Chromatography
UV	Ultraviolet
Ca	Capillary number
We	Weber number
Re	Reynolds number
AMBN	2,2'-azobis(2-methylbutyronitrile)
DMPA	2,2-dimethoxy-2-phenylacetophenone
SSNa	Sodium 4-vinylbenzenesulfonate

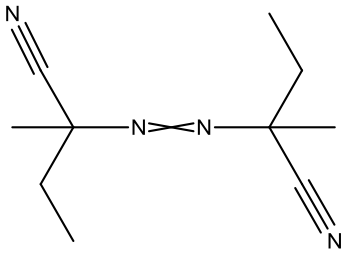

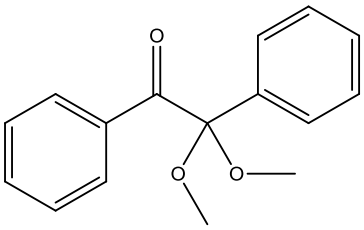

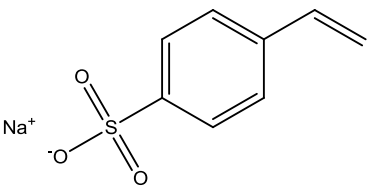

DBP	Dibutyl phthalate	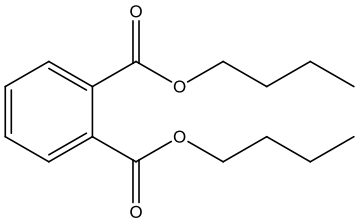
MMA	Methyl methacrylate	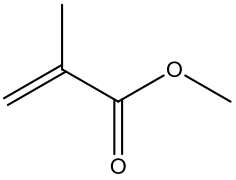
GMA	Glycidyl methacrylate	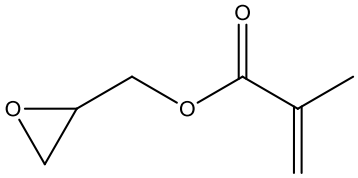
BMA	*n*-Butyl methacrylate	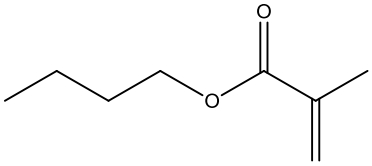
HEMA	2-hydroxyethyl methacrylate	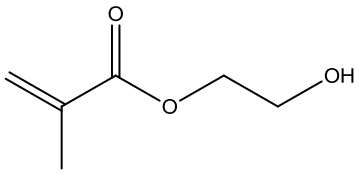
DMAEMA	2-(dimethylamino) ethyl methacrylate	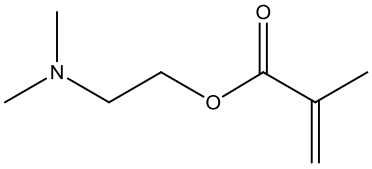
IBA	Isobornyl acrylate	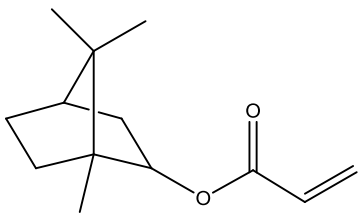
EGDMA	Ethylene glycol dimethacrylate	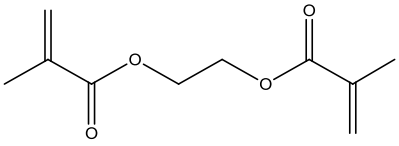

HDDA	1.6 Hexanediol diacrylate	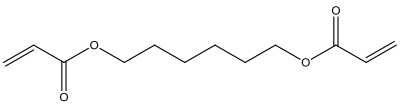
PVA	Poly(vinyl alcohol)	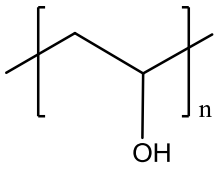
PVP	Poly(vinylpirrolidone)	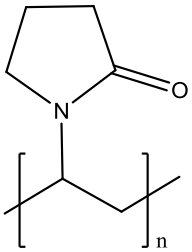
PMMA	Poly(methyl methacrylate)	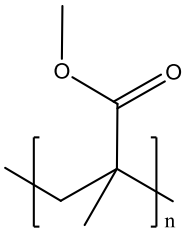
PBMA	Poly(butyl methacrylate)	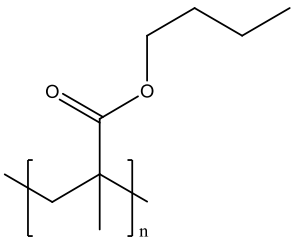
PIBA	Poly(isobornyl acrylate)	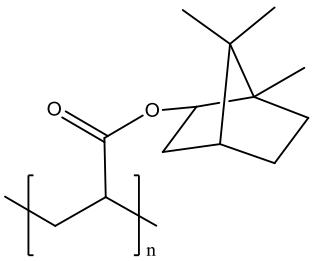

CHAPTER I

Introduction to the Basics and Applications of Droplet Microfluidics

In this chapter we discuss physical basics of droplet microfluidics, devices used to generate droplets, and their major applications. First of all, we introduce the types of frequently employed devices and methods to control parameters of droplet formation. We then turn to the synthetic possibilities provided by droplet microfluidics. We review bubbles-based materials, various types of particles and versatility of microfluidics as a route to encapsulate different matter. Finally, we conclude and give a brief description of the thesis.

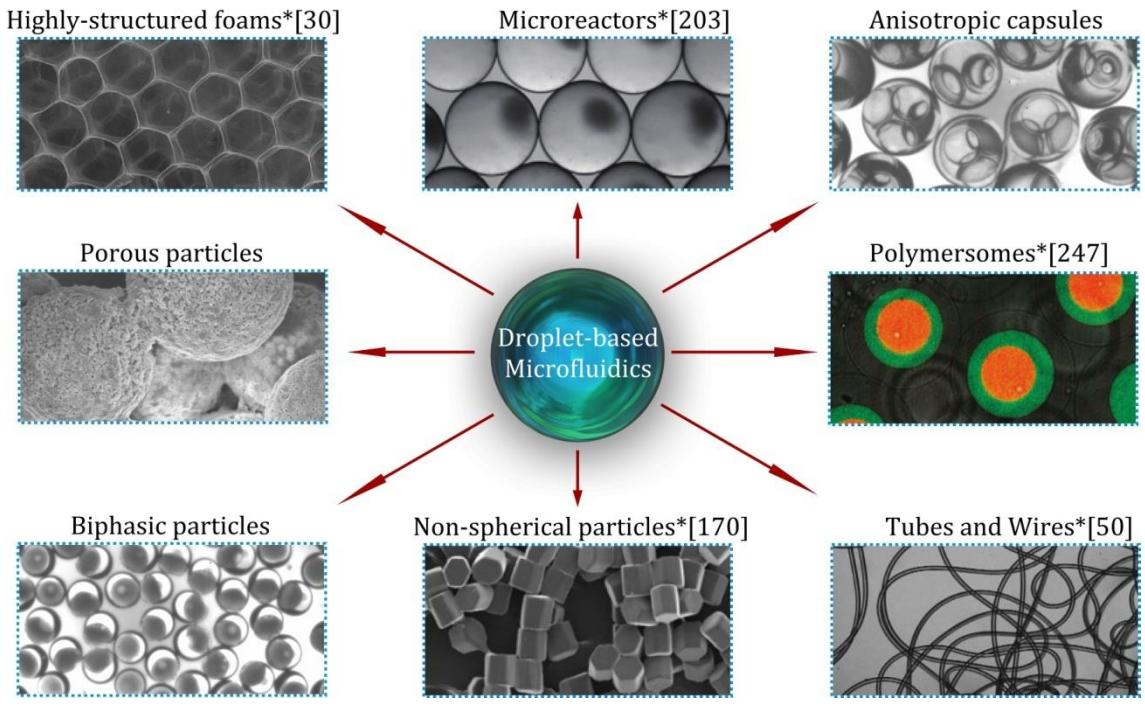

* These images were reproduced from following references [30], [50], [170], [203] and [247].

I.1 Introduction

Over the last two decades microfluidics, the discipline that deals with the control and manipulation of liquids on a miniaturized scale has developed itself as a generic platform contributing to the enhancement of science across a variety of fields. Its flexibility and relative simplicity led to integration of microfluidics in the fields of analytical chemistry, biology, engineering, soft matter physics and colloid science. As a result of hundreds of published papers related to the field of microfluidics is remarkable, as well as their interdisciplinary diversity. This chapter emphasizes droplet microfluidics and analyzes methods applicable to the field of colloidal materials; it focuses on the fundamental physics of droplet formation, types of microfluidic devices and the synthesis of various intricate particles and microcapsules.

The essential points of droplet-based microfluidics are the parameters and regimes of the droplet formation. A clear understanding of fluid dynamics and the droplet generation process enables precise control over the size, dispersity and anisotropy of the droplets and colloids synthesized thereof *via* microfluidics. A great variety of droplet-forming devices has been fabricated and studied. Researchers have clearly defined the principles of droplet formation in a microfluidics T-junction by comparing experimental data[1-12] with computational modelling simulations.[13-15] The control over the droplet formation in the co-flowing and, as a special case, flow-focusing microfluidics was also investigated in details,[16-21] allowing tuning of the frequency of the process and the dispersity of the droplets.[22-27]

There are other methods for droplet formation that differ from conventional liquid-liquid interactions. Pagonabarraga and co-workers[28] suggested an interesting technique for droplet formation by controlling the wetting properties in driven liquid

filaments. Cohen *et al.* reported a method based on a suction of the dispersed phase into a glass capillary filled with the continuous phase.[29] They created an oil/water interface and placed the capillary into the oil, so that the tip was close to the interface. Subsequent suction of the oil phase through the capillary dragged the aqueous phase into the capillary forming water-in-oil droplets. The types of the devices can be divided on the basis of the droplet generation principles and subdivided by the manufacturing materials.

Such extensive research in the field of droplet generation and device fabrication allowed the development of a plethora of methods and techniques for synthesising sophisticated colloidal materials. For instance, control over bubbles generation and manipulation using microfluidics resulted in the fabrication of highly-organized three dimensional scaffolds which have a great potential for tissue engineering.[30] Generated droplets were used as polymerization reactors,[31] to synthesize of porous structures,[32-34] inorganic particles,[35, 36] quantum dots[37, 38] and nanocrystals.[39-41] Furthermore, an employment of various droplet generation regimes, templated device surfaces and geometries led to the fabrication of non-spherical particles,[42-44] multiphase Janus particles[45-47] and polymer wires, fibres and tubes.[48-50] The generation of droplet-in-droplet, also known as double emulsion droplets, allowed controlled fabrication of capsules with tunable shell thickness and compositions,[51] droplets as magnetic transport systems[52, 53] and encapsulatable colour markers.[17] The precision of microfluidics raised encapsulation to a new level allowing encapsulation of cell cultures[54, 55] or even a single cell[56] generating great opportunities for biological studies.

In this chapter we review the current progress in the microfluidics field concerning synthesis of advanced colloidal materials. We provide a detailed description of the droplet generation processes and the devices that are usually employed in the

synthesis of diversity and intricate objects such as bubbles, particles and capsules of different varieties.

I.2 Types of microfluidic droplet generators

One of the fundamental parts of droplet-based microfluidics is the device used. Its significance is difficult to overemphasize, because of the direct influence on the shape, size, composition and functionality of any structure synthesized using droplet microfluidics. Despite the utilization of several types of devices such as Shirasu Porous Glass emulsifiers,[57, 58] straight-through devices,[59, 60] microvalve controlled,[61] and centrifugation driven capillary devices,[62] there are three major designs: T-junction, co-flow and counter-flow. We will discuss each of them in the following paragraphs focussing on the geometrical properties and ways of manufacturing.

Generally, T-junction geometries of microfluidic devices consist of two connected perpendicular channels, where the dispersed phase flows into the continuous phase at the right angle forming droplets in virtue of interactions between two phases (see Figure I-1A). This geometry can be a single-level, to generate single emulsion droplets, or hierarchical to fabricate double emulsion droplets (see Figure I-1B). An excellent illustration of the layouts was presented by Xu *et al.*,[8] Nisisako *et al.*[63] and Okushima *et al.*[64] Maintaining the basic principle, several variations of T-junction, also known as cross-flow layout were realised by researches. Luo and co-workers manufactured a micro-sieve device to increase the droplet generation frequency,[65] whereas a doubled T-junction droplet generator with subsequent coalescence induced a sol-gel reaction was reported by Seemann and co-workers[66] and Christopher *et al.*[67] Also, Yobas and colleagues presented a heat induced droplet generation using T-junctions,[68] while Weitz

and co-workers used air bubbles to trigger droplet formation by injecting the gas within the dispersed phase.[69] Another example is a device introduced by McQuade and co-workers,[20, 70] which is easy to manufacture and operate. In this device a plastic tube acts as the continuous phase channel while an orthogonally inserted needle delivering the dispersed phase into it. In addition to the droplet generation, orthogonally connected channels can be employed for droplet modification, for instance injection of another phase,[71] controlling the number of inner drops in double emulsions[72] or separation of the droplet contents.[73] An important point which is sometimes overlooked is that droplet generation is a complex phenomenon deserving independent scientific investigations. A reliable, reproducible and predictable droplet generation was achieved primarily due to these studies.[1-6, 9-15, 74-78] Nonetheless, we will not go into details, because they are mostly related more to the fluid dynamics and not to the chemical aspects.

However, in the majority of studies researchers prefer to employ the co-flow and counter-flow device layout, because they provide better control over the size, prevents channel wetting issues, and allows increased productivity. A classic illustration of the counter-flow layout often cited was introduced by Utada *et al.*[18] in 2005. The device consists of two capillaries with nozzles encased into a square glass tube, so that the capillaries were precisely aligned nozzle-to-nozzle. Moreover, each capillary had a separate injection channel as well as the inner space between the capillaries and the square tube. As a result, one of the capillaries was employed as the inner phase delivery channel. The middle phase was delivered through the space between the outer and inner tubes, flowing parallel to the inner phase. The continuous phase was also pumped into the inner space between the round and square capillaries, but oppositely to the middle phase forming the counter-flow. Remaining capillary was used as the collection tube for the droplets. In brief, the inner phase is dispersed in the parallel flowing middle phase,

while both phases subsequently redispersed in the counterly flowing outer (see Figure I-2A). This approach allows a precise control over the size and structure of the double emulsion droplets, but due to the simultaneous interactions of all three phases lacks reproducibility. Also, these types of devices are mostly used for double emulsion droplets fabrication, whilst single droplets easier to generate using conventional co-flow layout.

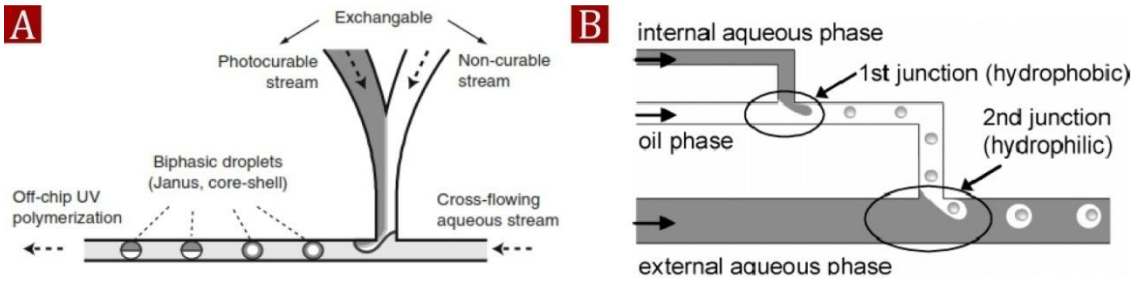

Figure I-1. T-junction layouts of microfluidic devices. (A) Combined dispersed phase delivery channel allowed fabrication of biphasic single emulsion droplets.[63] (B) An addition of another level of channels led to doubled emulsion droplets generation.[64]

In comparison to the T-junction layout, droplets are produced using the co-flow layout are the result of the parallel interaction between the dispersed and continuous phase. Of course, the geometry of the channels can be different forming variations of the co-flow layout, e.g. flow-focusing devices, but at the moment of droplet formation, both phases exist always in the same axis plane.

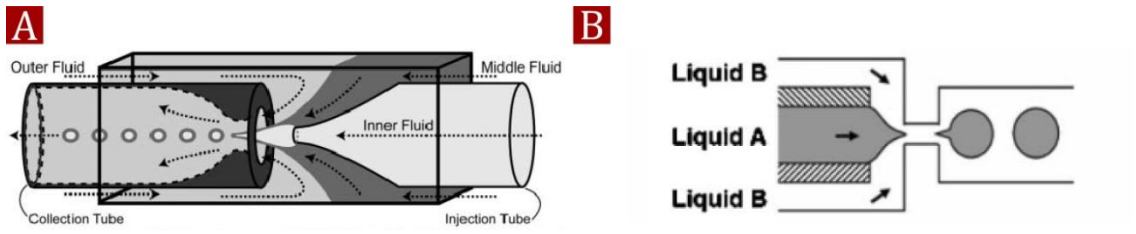

Figure I-2. Co-flow layouts of microfluidic devices. (A) Glass microcapillary device for fabrication monodisperse double emulsion droplets.[18] (B) A flow-focussing modification of co-flow systems allowing controlled dispersion of one phase in another.[82]

To take a good illustration we need to look at studies reported by Kumacheva and colleagues concerning consecutive flow-focussing droplet generators[79] (see Figure I-2B). The layout consisted of three channels which are focused onto the fourth. In such devices the dispersed phase remains in the central channel, while the continuous phase flows through the side, dragging all flows into the fourth channel and forcing the droplet formation. In turn, the collection channel can be the central part of the second level of the channels, again allowing double emulsion droplet generation.[80] Retaining the general principle many variations of such devices were developed, for instance modular microfluidic reactors,[81] parallel droplet generators,[82-84] multiple emulsion droplet devices[85] and simplified devices.[86] Furthermore, additional modification allowed the splitting of droplets after generation and thereby doubling the total amount,[87] separating droplets by size and functionality,[88, 89] controlling the droplet composition[90], and the monitoring of dispersity rate.[91] In addition, co-flow devices can be applied in conjunction with centrifugal force[92, 93] or electrospinning,[94, 95] increase the monodispersity and reduce the size respectively. As noted already, computational and experimental investigations are very important, and co-flow droplet generation using T-junctions were deeply studied.[16, 21, 96-103]

Despite the diversity of employed devices, materials for their production are limited. The primary material for both T-junction and co-flow devices is curable poly(dimethylsiloxane) compound, also known as Dow Corning Sylgard® 184 silicone elastomer. An opportunity to manufacture plain droplet generators[63] as well as complex microfluidic chips[81], along with a commercial availability, made it the number one choice for many researchers. The manufacturing of devices using poly(dimethylsiloxane) requires lithographical methods,[104, 105] or etching techniques.[106] The capillary based concepts[18] demand borosilicate glass capillaries, a special machine

to make nozzles (laser capillary puller) and epoxy glue to fix everything together. Simpler devices can be assembled without special equipment employing affordable materials, such as steel needles and plastic tubes.[20] To put it simply, the choice of devices appropriate for the variety of applications is great, but for the successful application it is essential to know how the droplet forms, which will be considered in the next section.

I.3 Physical basics of droplet generation

Droplet formation is a complex process, because of the simultaneous interplay of several physical phenomena. First of all, there is a hydrodynamic process for the interaction between two immiscible phases; therefore, such parameters like hydrodynamic radii of the main channel, fluid flow velocities, and potential flow turbulence are significant. An important point that sometimes is overlooked is that the actual local flow velocity directly depends on the hydrodynamic radius and differs from the prescribed overall value. Such a discrepancy can dramatically change the parameters for droplet formation, for instance, turning a theoretically monodisperse droplets generation into unstable polydisperse system. Furthermore, it affects structure of the flow by increasing the Reynolds number[107, 108] which can trigger a local flow disturbance, negatively influencing the overall process. Another parameter which should be considered is fluid viscosity, because it significantly affects the interaction of two liquids and Reynolds number, (Re):

$$Re = \frac{\rho V D}{\mu}$$ **Equation I-1**

where ρ represents fluid density, V – fluid velocity, D – hydrodynamic diameter of the channel, μ - fluid viscosity;

Secondly, droplet generation involves many aspects of surface and colloid science. The interaction of two immiscible phases presupposes the existence of a surface tension at the interface. An addition of molecular, or colloidal[109] surfactants allows for tuning interfacial tension, which has an influence on droplet size. Next to this, molecular and/or colloidal surfactants will provide colloidal stability to the droplets, which prevents them from coalescence.

The formation of droplets is a very complex phenomenon, and both physical and chemical components should be taken into account in order to make it coherent and comprehensive. We will describe the process focusing on the actions accomplished by the dispersed and continuous phases, and try to present a general explanation. Regardless of the type of the device, the dispersed phase is injected into the continuous phase under the action of pump pressure. Contact with the continuous phase induces shaping, namely conglobation of the dispersed phase, because of the tendency to minimize total surface area and energy of the system. At the same time the dispersed phase continues to flow in the channel which increasing the conglobating volume, until it detaches from the flow and forms a droplet. In essence, it is the action of surface tension versus fluid inertia[27] and is quantitatively determined by the dimensionless Weber number (We):

$$We = \frac{\rho V^2 D}{\sigma}$$ **Equation I-2**

where ρ represents fluid density, V – fluid velocity, D – hydrodynamic diameter of the dispersion channel, and σ – surface tension coefficient;

In parallel, the continuous phase having a considerably higher flow rate brings more pressure at the interface, accelerating the detachment of the conglobating volume of the dispersed phase. In effect, it is the action of surface tension versus dynamic viscous forces[19, 26] and is characterized by the dimensionless Capillary number (Ca):

$$Ca = \frac{\mu V}{\sigma}$$ **Equation I-3**

where μ - fluid dynamic viscosity, V – fluid velocity, and σ – surface tension;

In general, droplet formation is a result of the dynamic impact of the two immiscible phases on the interfacial interaction between these phases (see Figure I-3A).

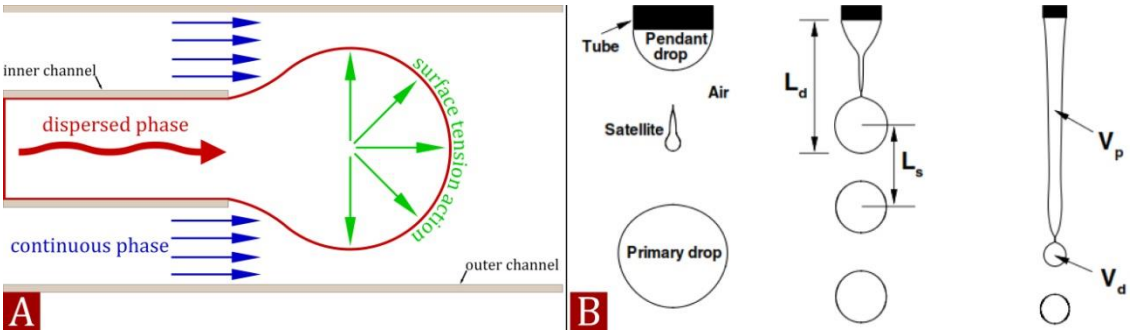

Figure I-3. The scheme and regimes of the droplet formation. (A) Cumulative impact of dynamic viscous forces of the continuous phase and fluid inertia of the dispersed phase on the surface tension action leading to the droplet formation. (B) From left to right dripping with satellite drop, dripping and jetting regimes of droplet formation.[23]

It is obvious that the above interactions can occur in various regimes depending on the values of flow velocities and surface tension coefficients. There are two main regimes for droplet formation: dripping and jetting (see Figure I-3B). Without going into technical details, the regime is considered as dripping if droplet forms immediately

after the contact between two phases, but jetting if the dispersed phase is dragged for an arbitrary distance into the continuous phase without droplet formation. These explanations show that a lower flow velocity is peculiar for the dripping regime, whereas higher velocity is indicative for jetting. A fundamental study concerning regimes of droplet formation, and the transitions between them, was presented by Lasheras and colleagues[22] in 1999 providing a comprehensive review of the problem. Thus, greater control over dispersity is more typical for the dripping regime, while the jetting regime allows reducing size of droplets, which in essence amounts to finding an appropriate ratio of the continuous/dispersed phases flow velocities. There are transitional regimes like dripping with satellite[23] or jetting with satellite[24] for the production of droplets and particles, but they are objectionable due to the uncontrolled formation of additional satellite droplets. To sum up, droplet generation is a complex process which can be controlled only by taking into consideration both physical and chemical components such as fluid dynamics and interfacial interaction between two phases.

I.4 Dispersion of gas and bubbles-based structures

Previous sections clearly described typical microfluidic devices and ways to control droplet generation. Using this knowledge we will further consider a variety of synthetic possibilities of microfluidics. First of all, we would like to introduce generation of monodisperse gas bubbles and materials obtainable through this method. Despite the apparent simplicity, this approach is a valid tool for the fabrication of several types of advanced materials.

The crucial question we need to answer is what differences are there between the droplet and bubble generation? Generally, both processes are identical from the point of device employment and physical principles, except the differences concerning gas-liquid interfacial interactions. Thus, Garstecki *et al.* introduced the formation of gas bubbles using microfluidic T-junction[7] and flow-focussing[110] device layouts, similar to the devices used for standard droplet generation. The successful adoption of the devices and perspectives of the method[7, 110] resulted in improved bubble generation and the development of potential applications. Thus, in attempts to diversify the process, researchers studied formation of bubbles in parallel and coupled flow-focussing geometries,[111] multisection junctions[112] and microbubble coalescence in microfluidic channels.[113] An interesting approach to control the size of the bubbles was reported by Kumacheva and co-workers[114] who suggested tuning of solubility of the dispersed CO_2 in the continuous phase by changing pH, thereby reducing the size of generated bubbles.

The practical aspects often cited are microfluidic bubble mixing,[115] and bubble motility logic,[116] which allow using bubbles to run chemical interactions at the micro scale in a controlled manner. Another excellent example of using bubbles was introduced by Matsuura and co-workers,[117] who showed a dispersion of vapour bubbles in the liquid continuous phase, which subsequently condensed, significantly reducing the size and transforming them into droplets.

More importantly, materials fabricated *via* microfluidic bubbles generation are very intricate. For example, Lin and co-workers presented fabrication of highly organized three-dimensional alginate scaffolds for cartilage tissue engineering[30] by generating N_2-in-alginate droplets and subsequent cross-linking of alginate using $CaCl_2$ (see Figure I-4C). The same approach was applied by Hutzler and co-workers for the synthesis of monodisperse liquid foams.[118] Another technique for fabrication of

structured foams was presented by Whitesides and co-workers (see Figure I-4B).[119] The method is based on simultaneous generations of bubbles of different sizes, thus allowing fine tuning of the size of the foam domains, producing more complex structures. Moreover, bubbles can be employed as ultrasound contrast agents. Wong and co-workers fabricated diacetylene polymerized shell microbubbles which showed stability against aggregation and gas dissolution,[120] by generating gas-in-liquid droplets, where a liquid was a photopolymerisable lipid/polymer rich phase, which led to the formation of the shell around the gas. Having high buoyancy in the liquid medium, the bubbles were stabilized in order to retain phase equilibrium and prevent aggregation. Nanoparticles can be employed as an alternative to molecular surfactants allowing stabilization and surface modification of the bubbles. For instance, pH driven stabilization of bubbles with surface active nanoparticles was demonstrated by Wiebke Drenckhan,[121] while Tumarkin *et al*. utilized temperature dependent dissolution of CO_2 leading to colloidal armour plating on the bubble surface.[122] The same strategy applied to fabricate gas-filled microparticles,[123] nanoparticle-shelled bubbles[124] and amphiphilic Janus bubbles.[125] Except for the above mentioned applications, production of microbubbles *via* microfluidics allows fabrication of porous structures (see Figure I-4A),[126, 127] or even fast gas-liquid interaction studies.[128] In short, controllable bubbles fabrication opens up a variety of synthetic possibilities interesting for both academic and industrial applications.

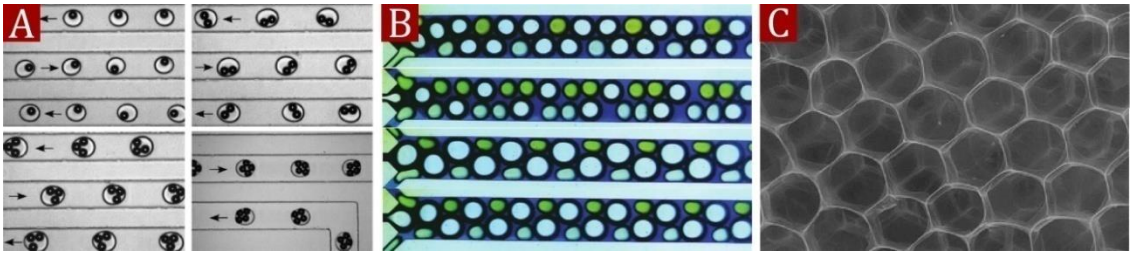

Figure I-4. Microbubbles-based structures fabricated *via* microfluidics. (A) Controlled encapsulation of bubbles into droplets.[126] (B) Production of multicomponent emulsions and foams by simultaneous dispersion of several phases.[119] (C)Highly organized alginate scaffold as the result of gas dispersion using microfluidic device.[30]

I.5. Particles synthesized *via* microfluidics

I.5.1 Porous materials

A shift of the dispersed phase to a liquid phase allows droplets generation which themselves can be intricate[129-131] or subsequently turned into particles with various properties.[31, 132-140] One such property is porosity. Porous materials are of interest as adsorbents, for controlled release of the encapsulated matter, drug delivery and microcontact printing. A basic route to introducing porosity to microfluidically synthesized particles is addition of a porogen. Kumacheva and co-workers[32] in 2008 presented a method based on copolymerization of ethylene glycol dimethacrylate (EGDMA) and glycidyl methacrylate (GMA) in the presence of esters of phthalic acid within a droplet producing macroporous particles (see Figure I-5A). This approach opened the way to production of Janus porous particles *via* microcontact printing by utilizing epoxy moieties[141] of poly(glycidyl methacrylate), introducing thiol-ene and thiol-yne chemistry in microfluidically produced porous beads[142] and hybrid gold coated porous materials.[33] Nonetheless, fabricated porous particles may have a “skin”, reducing adsorption, the formation of which was studied by Dubinsky *et al.*[34] In contrast to

induced phase separation occurring within the monomer/porogen droplets, application of high internal phase emulsions (HIPEs) for porous beads and rods fabrication was demonstrated by Gokmen and co-workers (see Figure I-5B).[143] This modification retained "clickability" of the porous structures and provided control over shape.

Another method is based on solvent evaporation/diffusion from the generated droplets consisting of stabilized particles or bubbles dispersed in a solvent. Thus, diffusive removal of solvent from generated droplets allowed production of monodisperse mesoporous silica particles[144] and nanopatterned porous microspheres (see Figure I-5C).[145] Evaporation of solvent also allowed formation of mesoporous silica structures,[146] latex-based supraparticles,[147] biodegradable porous microspheres[148] and porous polymeric microcapsules.[149]

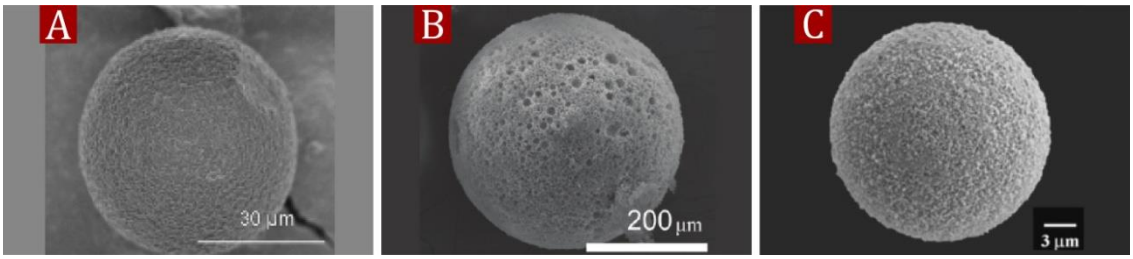

Figure I-5. Porous particles synthesized by employing droplet microfluidics. (A) The porosity achieved by virtue of porogen addition to the dispersed phase.[34] (B) The usage of HIPE as the dispersed phase also led to the fabrication of porous beads.[143] (C) Mesoporous silica microsphere.[144]

I.5.2 Multiphase anisotropic particles

Despite the fact that the single phase droplet generators can successfully be used for Janus particles fabrication[150-152] the level of intricacy of them is limited. A feature of microfluidic devices is the flexibility of the channel geometries allowing combining two or more phases producing multiphase Janus particles. In 2006 Nisisako and co-workers introduced a co-flow system to generate electrically anisotropic particles[47] which was

further employed for production of biphasic Janus droplets and shape-controlled particles (see Figure I-6A).[153] Applying the same principles of the droplet generation, fabrication of colour-filled hydrogel granules,[154] bi- and triphasic particles with a surface functionality,[155] electroresponsive photonic Janus balls (see Figure I-6B),[156] anisotropic microgels,[157] and drug nanocarriers[158] was introduced. A modification of the droplet generation process, specifically the implementation of electrospinning, allowed decreasing the size and fabricating Janus particles with nanoscale anisotropy[46] and multuphasic nanocolloids.[45, 159] Aside from combining the flows to generate Janus particles, double emulsion droplets can be employed as templates for amphiphilic particles fabrication.[160]

There are other methods which are not currently used for generation of droplets, but should be mentioned due to the outstanding synthetic opportunities. Hatton and co-workers presented fabrication of Janus magnetic microparticles with multiple functionalities, shapes and chemistries[161] by stopping the biphasic flow in the microfluidic channel and polymerizing a specific area at the two flow interfaces. A similar approach was used by Doyle and colleagues to fabricate amphiphilic polymer micrcoparticles.[162] Another beautiful method based on self-assembly of the prepolymer droplets leading to the production of complex multiphase structures was introduced by Grzybowsky and co-workers.[163] A phenomenon of dielectrophoresis applied in a microfluidic chip allowed to use droplets as reactors to synthesize anisotropic polymer particles in a controlled manner (see Figure I-6C).[164]

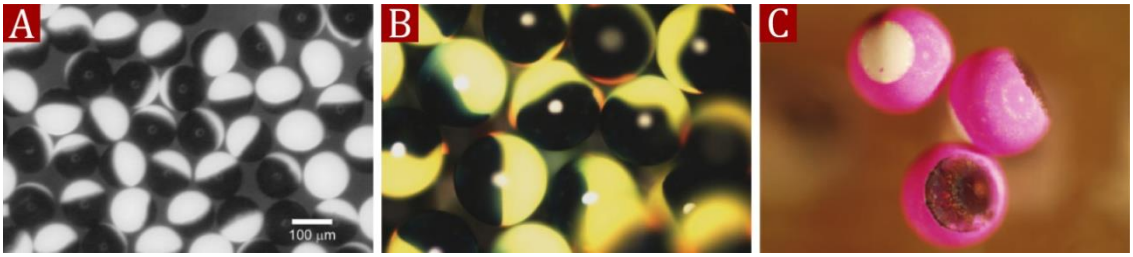

Figure I-6. A range of multiphase anisotropic particles. (A) Bicoloured electrically anisotropic Janus particles.[47] (B) Electroresponsive Janus photonic balls.[156] (C) Anisotropic particles produced by utilizing dielectrophoresis phenomenon.[164]

I.5.3 Non-spherical particles

Generally, the spherical shape of the droplets leads to the same shape of the synthesized particles. Nevertheless, droplet microfluidics allows fabrication of non-spherical particles employing geometrical flexibility of the devices, ancillary equipment and modifications. Thus, an alteration of the traditional circle cross-section of the microfluidic channel to the square allowed production of non-spherical particles by polymerizing non-spherical droplets (see Figure I-7A).[165-168] An integration of the stop flow lithography, electrospinning phenomena or utilization of surface modified channels resulted in production of multicompartmental microcylinders,[169] 3D designed microgels,[42] particles with various geometries[170] and toroidal-spiral particles (see Figure I-7B).[171] Along with these methods, traditional droplet generation allows fabrication of intricate non-spherical structures. For instance, Kumacheva and co-workers in 2005 introduced a microfluidic technique for producing particles with different shapes and morphologies.[172] Thereafter microfluidics successfully employed for fabrication of coalescence driven supracolloidal structures,[173] toroidal silica particles,[43] control texture and composition of polymer microparticles,[174] as well as liquid patterning as a strategy for control over the shape of the particles.[175]

As a special case of non-spherical structures, production of tubes, wires and fibres should be considered. The layout of the devices used for these applications are equal to the traditional, but instead of droplet generation they require elongation of the dispersed phase forming tube-like hollow structures. There are two main routes for production: the use of electrospinning phenomena and hydrodynamic approach which implies only usage of two flowing liquids. Both techniques allowed synthesis of nanofibres with various morphologies and compositions,[176-180] conductive nanowires,[49] and microtubes (see Figure I-7C).[48, 50, 181]

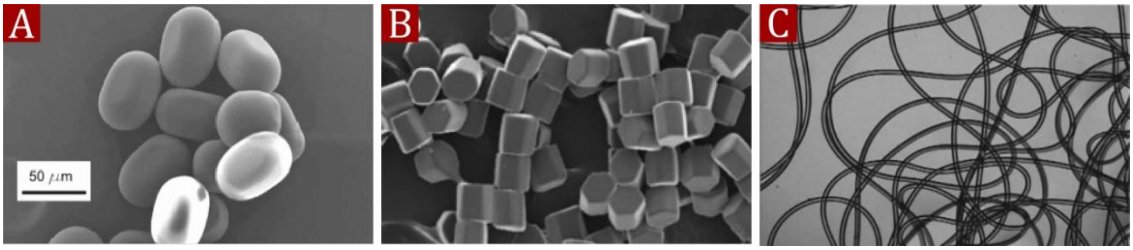

Figure I-7. A variety of non-spherical microfluidically synthesized structures. (A) Oval-shaped particles.[165] (B) Hexagonal microrods.[170] (C) Hydrodynamically fabricated microtube.[50]

I.5.4 Particles for biological applications

Microfluidics is an excellent tool for fabrication of particles for various biological applications such as drug delivery or cell encapsulation. Synthesis of such particles implies formation of microgels or particles made from biocompatible and biodegradable materials. The easiest way is the dispersion of aqueous solutions, for instance of alginate, gelatine or curable polymer, in the organic phase, forming a single emulsion droplet. Despite the simplicity, this method allowed to produce thermo-responsive microgels,[182] supramolecular hydrogel microspheres,[183, 184] biocatalyst immobilized particles[185] and encapsulate viruses into microgel particles.[186] Along with single emulsion devices, the double emulsion generators were successfully employed for

fabrication of "bucket-like" microgel particles (see Figure I-8C),[187] Janus microgel capsules[157] and highly monodisperse encapsulations.[188] Both approaches allow a general simplification of the process and retain the advantages of microfluidics.

Other methods suggest blending of two flows containing a cross-linker and gel-agent and dispersion in the continuous phase. Thus, Cooper-White and co-workers fabricated biopolymer particles by mixing $CaCl_2$ solution with alginate and subsequent dispersion in the organic solvent,[189] while Seiffert and co-workers introduced a radical-free synthesis of cell-laden microgels by dispersing premixed solutions of cells, polyethyleneglycol and hyperbranched polyglycerol in the oil.[190] Hoare and co-workers employed this strategy and pioneered covalently cross-linked degradable microgels by mixing premodified hydrazide-functionalized sodium carboxymethyl cellulose and aldehyde-functionalized dextran.[191] Also, various types of biodegradable polymer particles and microgels[192-194] were fabricated using different blending compounds (see Figure I-8A, B).

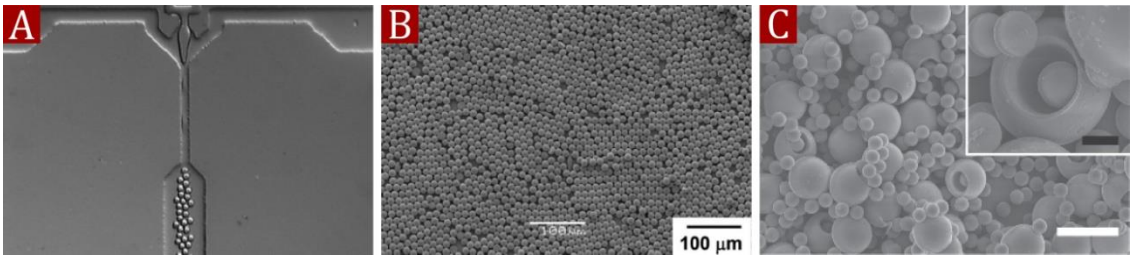

Figure I-8. Particles for biological applications. (A) Fabrication of biodegradable microgel particles using flow-focussing microfluidics device.[192] (B) Monodisperse polymer microparticles eligible for drug delivery.[193] (C) Microgel "buckets" filled with particles.[187]

I.5.5 Synthesis of inorganic particles

The vast majority of the microfluidically synthesized particles are organic structures.[195, 196] Nonetheless, various types of inorganic particles can also be produced.

For example, Martinez and co-workers reported fabrication of porous and non-porous ceramic particles and capsules (see Figure I-9A).[36] Gijs and co-workers presented synthesis of gold-titania hybrid particles by grafting gold nanoparticles on titanium dioxide within a droplet,[197] while fabrication of pure titanium dioxide particles was reported by Marlow and co-workers.[198] Research in this field introduced a method for the fabrication of spherical and non-spherical liquid metal droplets and microparticles.[199, 200]

So far we considered droplets as objects on which an action is performed in order to synthesize colloidal structures. However, microfluidically generated droplets can be used as auxiliary facilities, for instance as reactors providing a precise control over the amount and compositions of reacting compounds. Thus, synthesis of the magnetic iron oxide nanoparticles was presented by Baret and co-workers,[35] which in essence is monitored by the mixing of reagents in the microfluidic channel and subsequent dispersion of the mixture in the continuous phase. The droplets of the dispersed phase act as microreactors, within which a reaction occurs while they are moving in the microfluidic channel. A similar approach was employed for the production of nanocrystals,[39-41, 201, 202] quantum dots,[37, 38] biogenic paramagnetic nanoparticles[203] and copper nanofluids (see Figure I-9B, C).[204] Also, an interesting application of droplets is using magnetically driven transport to allow mixing and release of cargo in a controlled manner, introduced by Studart and co-workers.[52] In this method, instead of blending reagents within droplets, two droplet containing different reagents are magnetically "clinched" to squeeze them to initiate a reaction. After which the product of reaction can be released.

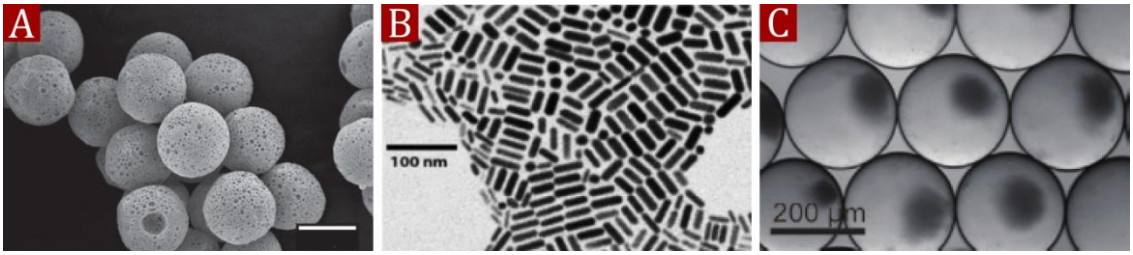

Figure I-9. Inorganic and composite particles produced using microfluidics. (A) Ceramic porous microparticles (scale bar = 100µm).[36] (B) Gold nanoparticles synthesized in droplet microreactors.[39] (C) Biogenic paramagnetic nanoparticles consisting of E.*coli* and iron oxide "arrested" in droplets.[203]

I.6 Encapsulation performance of microfluidics

I.6.1 Control over shell formation

Microfluidic droplet generators allow encapsulation of a variety of materials and fine tuning of many parameters such as shell composition and thickness, core diameter and contents. Control over shell formation can be subdivided in two categories: chemical, which employs single emulsion devices, and physical, which involves the use of double emulsion droplets generators.

A classic illustration of the single emulsion device application, often cited, was introduced by McQuade and co-workers.[20] The method employs an interfacial polymerization reaction at the dispersed/continuous phases interface which leads to the formation of the polyamide shell, thickness of which depends on the concentration of the reagents used. In spite of the straightforward capsule formation and use of affordable materials like PVC tubing and disposable needles, there are a number of difficulties with this method. Due to the immediate polycondensation reaction after phase contact the needle tip often becomes blocked. Moreover, the forming shell limits diffusion at the interface, thus slowing the shell growth. Nevertheless, the concept of

one-step shell formation was successfully used for the synthesis of core-shell organosilicon microcapsules (see Figure I-10C),[70] porous shell microcapsules,[205] block copolymer shells,[206] thermo-responsive[207] and polymer multilayered capusules.[208] Another example of the single emulsion droplets utilization was reported by Du Prez and co-workers.[209] The method is more complex due to the implementation of a template shell formation, despite the employment of a simple device. The first step is to obtain a dex-HEMA microgel template upon exposure of UV light to the generated droplets. This step is followed by deposition of negatively charged platinum nanoparticles and positively charged diazoresin[209] leading to the formation of a shell. Subsequent removal of the microgel core generated hollow capsules.

However, most methods allowing controlled shell formation employ double emulsion droplet generation. A general explanation is that the shell properties like thickness and composition are easier to adjust by tuning the flow rates rather than applying chemically driven processes.[210] Essentially, we need to look at the work introduced by Weitz and co-workers[18, 211] which describes the method of tuning the flow rates leading to formation of capsules with various thickness. Other methods apply different device layouts, but the principle remains the same. Thus, Tabeling and co-workers presented the fabrication of microcapsules with controlled geometrical and mechanical properties,[212] van Esch and co-workers[213] produced capsules which have aquatic cores and shells, while Studart and co-workers studied a correlation between theoretical and experimental shell thickness (see Figure I-10A).[51] More importantly, this approach allows tuning composition of the shell without requiring additional modifications. A simple substitution of the middle phase can lead to the fabrication of many intricate shell types. For example, fabrication of the shell made from colloidal crystals (see Figure I-10B),[214] as well as production of gel-based shells,[215]

biocompatible ethyl cellulose/alginate shells,[216, 217] nanoparticle armoured shells,[218] frozen shells for encapsulation and core release, near-infrared sensitive shells[219] and external stimuli responsive shells.[220]

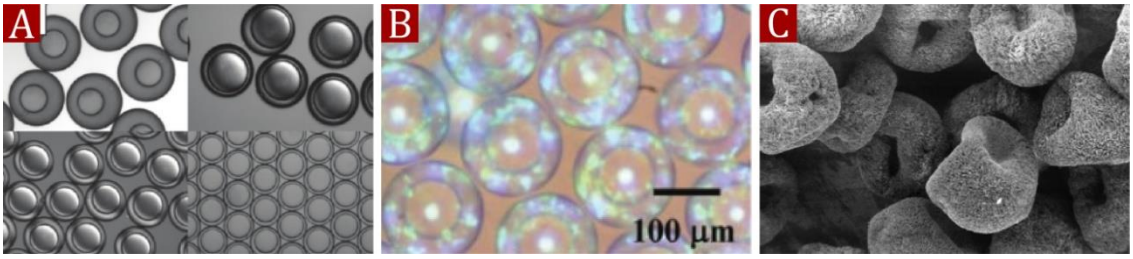

Figure I-10. Control over shell thickness and composition. (A) Polymer microcapsules with various shell thicknesses.[51] (B) Gel-immobilized colloidal crystal as the shell.[214] (C) Orgnosilane microcapsules obtained employing a simple microfluidic device.[70]

I.6.2 Variety of encapsulated materials

The previous paragraphs considered only the shell formation options. Now we are looking at the materials which can be successfully encapsulated *via* microfluidics. We separated all methods in the previous section with respect to the types of droplet generators, but the following section will only emphasize the materials.

Thus, encapsulation of multiple cores within a single shell led to production of many intricate structures. A beautiful approach was presented by Weitz and co-workers in 2007 which allowed generation of droplets-in-droplets[221] and further developed by Chu and co-workers for controllable multicomponent emulsion fabrication,[222] which in essence is the sequential dispersion of multiple phases (see Figure I-11A). Another technique was realised by Yang and co-workers which is based on tuning of the inner/middles phase volumetric flow rate ratio, leading to the fabrication of multi-cored microcapsules.[223] Moreover, multiple encapsulations allows incorporation of two types of materials, for instance oil droplets and microgel particles.[224] Also, a variety of inorganic materials can be encapsulated, for example magnetic hydrogels (see Figure I-

11C),[53] gold nanoparticles,[225] or filled with silver ions for producing nanocomposite beads upon reduction.[226] Another interesting material to encapsulate is cells and viruses as a tool for biological studies. For example, Viovy and co-workers demonstrated a strategy for the cell encapsulation and hydrodynamic sorting[227] using microfluidics; Kumacheva and co-workers presented fabrication of agarose-based 3D environments for cells[228] and encapsulation of cell co-cultures to study their interaction.[54] We saw in the above descriptions that cell cultures can be easily encapsulated *via* microfluidics, but it gives an opportunity to "arrest" even a single cell. For instance, Toner and co-workers introduced controlled encapsulation of a single cell into picolitre droplets (see Figure I-11B).[56] Another example of this technique was introduced by Weitz and co-workers[229] where they analysed the life cycle of a single cell and also looked at scalability of the whole process. In comparison to dispersive encapsulation methods, Zhao and co-workers introduced a droplet merging method which uses droplets of different composition followed by subsequent merging which results in the encapsulation of the cells.[230] Control over the number of encapsulated cells can also be performed by applying the above mentioned electrospinning phenomena.[231] As we noted already, in addition to cells, encapsulants can contain a virus,[186] thus extending capabilities of microfluidics. In short, microfluidics is a versatile tool for the encapsulation of various types of materials for many purposes (see Figure I-11).

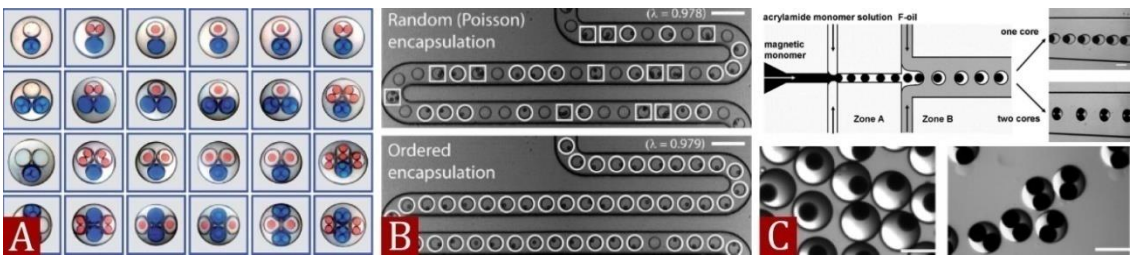

Figure I-11. Encapsulation performance of droplet microfluidics. (A) Controlled synthesis of the multiple-cored droplets-in-droplets.[17] (B) A single cell encapsulation into picolitre droplet.[56] (C) Production of magnetic single or double-cored hydrogel particles (scale bars = 100μm).[53]

I.6.3 Fabrication of vesicles and polymersomes

Another variation of the capsules produced *via* microfluidics is vesicles and polymersomes. One of the differences between capsules and vesicles is the thickness of the shell which is noticeably thinner than in the case of vesicles. But the most important distinction is the structure of the shell, which should be a bilayer, mimicking natural vesicles like a liposome. There are several techniques which are used to fabricate vesicles such as conventional single or double emulsion droplet generation and processing, and an alternative known as microfluidic jetting.[232, 233] We will discuss them in the following paragraphs.

The formation of the bilayer using the microfluidic jetting technique[232, 233] requires additional preparation and proceeds in two stages. The initial step is the production of a bilayer at the interface between the two phases. Fletcher and co-workers suggested the following procedure. [232, 233] An acrylic chamber was divided by a thin shield forming two compartments, this was filled with oil as the medium and water droplet containing oil-insoluble lipids as the dispersed phase. Thereby, each compartment had the oil-water interface on which a lipid monolayer formed. Shield removal induced a contact between the two monolayers and formed a layer in each compartment leading to a bilayer. Thereafter a water jet was focussed on it using a microfluidic device causing formation of vesicles around the vortex. Nevertheless, being an appropriate method for the vesicle synthesis, it has disadvantages such as the multi-step procedure and low productivity (see Figure I-13C).

Employment of single and double emulsion droplet generators allows for straightforward fabrication of polymer vesicles[234] at high production rates. Figure I-12 shows a general principle of polymer vesicle formation.

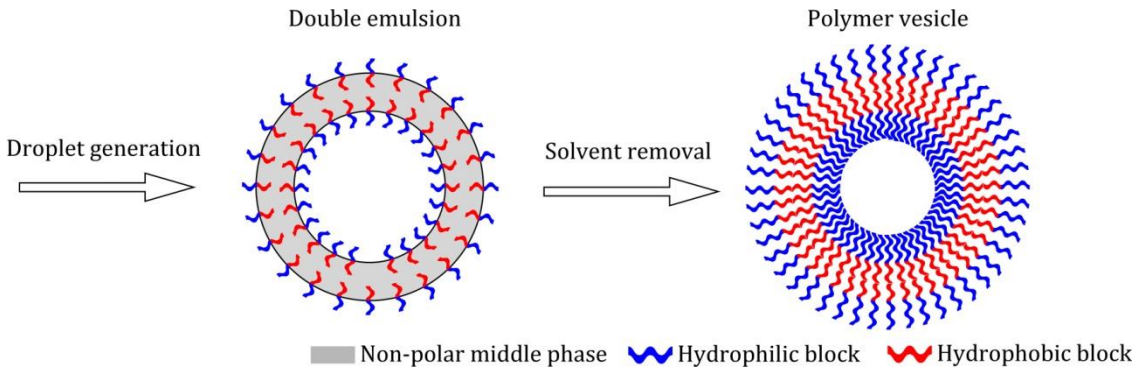

Figure I-12. Schematic representation of the polymer vesicle formation from the double emulsion droplets.[235]

For instance, Yomo and co-workers fabricated unilamellar layer vesicles by stabilizing microfluidically generated water droplets with phospholipids which were in the continuous phase,[236] while Battaglia and co-workers introduced synthesis of pH-sensitive block-copolymer vesicles using a flow-focussing microfluidic platform.[237] Another method based on molecular surfactant replacement with lipids on the surface of monodisperse droplets leading to formation of vesicles was reported by Ichikawa and co-workers[238, 239] and various others.[240] An interesting technique of bilayer "printing" using a microfluidic device was presented by Takeuchi and co-workers,[241] which involves squeezing a lipid containing oil droplet between two aqueous layers leading to the formation of a lipid-bilayer oil phase, which subsequently was pushed into the aqueous medium. Upon pushing out the aqueous medium the oil lipid-rich phase conglobated forming the vesicle.

While single emulsion droplets require additional processing to form a bilayer at their surface, double emulsion droplets allow deposition of a bilayer forming material in the middle phase directly. Thus, Weitz and co-workers in 2005 reported fabrication of polymersomes by generating water-in-oil-in-water droplets, where the oil phase contained a dissolved diblock copolymer which formed a bilayer after solvent evaporation.[242] The same approach was employed for the fabrication of biodegradable

and biocompatible polymersomes,[235, 243] process scalability studies,[244] polymer-lipid microbubbles,[245] and monodisperse phospholipid vesicles.[246] Moreover, it allowed fabrication of polymersomes with intricate morphologies such as multiple polymersomes with several levels of bilayers[247, 248] and multicompartmental polymersomes (see Figure I-13A, B).[249, 250] However, double emulsion methods have some difficulties such as selection of appropriate solvents for diblock copolymers or dewetting instabilities[251, 252] which prevent the formation of the bilayer. It seems clear that microfluidics gives a great opportunity to fabricate and study bio-inspired materials for future applications (see Figure I-12).

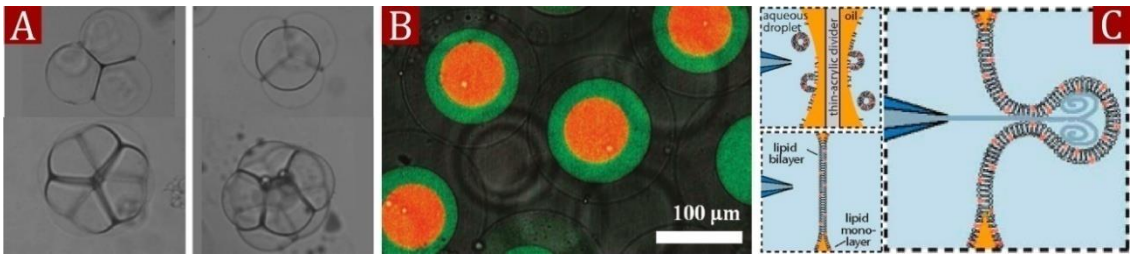

Figure I-13. Types of microfluidically obtained polymersomes and vesicles. (A) Complex polymersomes fabricated using a simple co-flow device.[250] (B) Confocal microscope image of multi-layered polymersomes.[247] (C) The microfluidic jetting technique for the fabrication of giant vesicles.[233]

I.7 Conclusions and scope of the thesis

It is difficult to escape the conclusion that droplet microfluidics is a great tool for the synthesis of a variety of micro structures by virtue of the versatility and relative simplicity. In comparison to conventional methods, such as emulsion or dispersion polymerization, droplet microfluidics provides a custom synthesis of each particle or capsule boosting their performance. Furthermore, it has a great potential as an industrial method, because particular types of devices can be manufactured en masse. Nevertheless, despite the numerous studies, reflected in the amount of related

publications, there are areas that are still of interest for further studies. These include the design and manufacture of simplified microfluidic devices, fabrication of advanced colloidal structures with tuneable functionalities, along with investigations concerning their behaviour.

In this thesis we explore fabrication of polymer microparticles and capsules by employing droplet microfluidics as a strategy to produce intricate structures in a controlled manner. We use simplified devices assembled using affordable materials and equipment as a fabrication tool. We employ combinations of monomers and polymer colloids to advance the fabricated particles and capsules, and also study consequences of these modifications and how they affect the chemical and physical characteristics of the product.

Chapter II contains experimental methods and materials used across the thesis.

Chapter III focuses on the fabrication of amphiphilic polymer "microbuckets" which have hydrophilic and hydrophobic surface areas allowing selective filling of the cavities, or "microbuckets". A simplified droplet generator was employed to control the size and dispersity. A mixture of monomers and non-polymerisable oil was used to achieve desired morphologies and surface characteristics.

Chapter IV is dedicated to the synthesis of Janus particles using a simple microfluidic device, mainly emphasizing the production of porous, magnetic and chameleonic (or photonic) structures. A scheme of the device assembly and methods of operation are presented in detail. Preparation methods of functional monomers applicable for the generation of Janus droplets and subsequent transformation into particles are explained.

Chapter V describes the manufacturing procedure for the microfluidic device, which implements combined T-junction/co-flow layouts. Fluid flow simulations using CAD software were used to achieve an optimal device design for generating single and double emulsion droplets. The device performance was tested by fabricating a variety of microcapsules.

Chapter VI outlines a microfluidic approach for the production of polymersomes along with their armouring with polymer colloids. The synthesis of amphiphilic diblock copolymers forming the bilayer, and using particles to act as colloidal "armour" is considered separately. Manufacturing procedures of employed microfluidic device are illustrated in photographs showing the step by step process.

Chapter VII highlights main conclusions and suggests directions for future investigations.

I.8 References

[1] Nisisako, T.; Torii, T.; Higuchi, T., Droplet formation in a microchannel network. *Lab Chip* **2002**, 2, 24-26.

[2] Ménétrier-Deremble, L.; Tabeling, P., Droplet breakup in microfluidic junctions of arbitrary angles. *Phys. Rev. E* **2006**, 74, 035303-035307.

[3] Jullien, M. C.; Ching, M. J. T. M.; Cohen, C.; Menetrier, L.; Tabeling, P., Droplet breakup in microfluidic T-junctions at small capillary numbers. *Phys. Fluids* **2009**, 21, 072001-6.

[4] Gupta, A.; Murshed, S.; Kumar, R., Droplet formation and stability of flows in a microfluidic T-junction. *Appl. Phys. Lett.* **2009**, 94-97.

[5] Bedram, A.; Moosavi, A., Droplet breakup in an asymmetric microfluidic T junction. *Eur. Phys. J. E: Soft Matter Biol. Phys.* **2011**, 34, 1-8.

[6] Glawdel, T.; Elbuken, C.; Ren, C. L., Droplet formation in microfluidic T-junction generators operating in the transitional regime. I. Experimental observations. *Phys. Rev. E* **2012**, 85, 016322-016334.

[7] Garstecki, P.; Fuerstman, M. J.; Stone, H. A.; Whitesides, G. M., Formation of droplets and bubbles in a microfluidic T-junction-scaling and mechanism of break-up. *Lab Chip* **2006**, 6, 437-446.

[8] Xu, J. H.; Li, S. W.; Tan, J.; Wang, Y. J.; Luo, G. S., Controllable Preparation of Monodisperse O/W and W/O Emulsions in the Same Microfluidic Device. *Langmuir* **2006**, 22, 7943-7946.

[9] Xu, J. H.; Li, S. W.; Tan, J.; Wang, Y. J.; Luo, G. S., Preparation of highly monodisperse droplet in a T-junction microfluidic device. *AIChE Journal* **2006**, 52, 3005-3010.

[10] Xu, J. H.; Luo, G. S.; Li, S. W.; Chen, G. G., Shear force induced monodisperse droplet formation in a microfluidic device by controlling wetting properties. *Lab Chip* **2006**, 6, 131-136.

[11] Xu, J.; Li, S.; Tan, J.; Luo, G., Correlations of droplet formation in T-junction microfluidic devices: from squeezing to dripping. *Microfluid. Nanofluid.* **2008**, 5, 711-717.

[12] Xu, J.; Li, S.; Tostado, C.; Lan, W.; Luo, G., Preparation of monodispersed chitosan microspheres and in situ encapsulation of BSA in a co-axial microfluidic device. *Biomed.l Microdevices* **2009**, 11, 243-249.

[13] van der Graaf, S.; Nisisako, T.; Schroën, C. G. P. H.; van der Sman, R. G. M.; Boom, R. M., Lattice Boltzmann Simulations of Droplet Formation in a T-Shaped Microchannel. *Langmuir* **2006**, 22, 4144-4152.

[14] Gupta, A.; Kumar, R., Effect of geometry on droplet formation in the squeezing regime in a microfluidic T-junction. *Microfluid. Nanofluid.* **2010**, 8, 799-812.

[15] De Menech, M., Modeling of droplet breakup in a microfluidic T-shaped junction with a phase-field model. *Phys. Rev. E* **2006**, 73, 031505-031514.

[16] Joanicot, M.; Ajdari, A., Droplet Control for Microfluidics. *Science* **2005**, 309, 887-888.

[17] Wang, W.; Xie, R.; Ju, X.-J.; Luo, T.; Liu, L.; Weitz, D. A.; Chu, L.-Y., Controllable microfluidic production of multicomponent multiple emulsions. *Lab Chip* **2011**, 11, 1587-1592.

[18] Utada, A. S.; Lorenceau, E.; Link, D. R.; Kaplan, P. D.; Stone, H. A.; Weitz, D. A., Monodisperse Double Emulsions Generated from a Microcapillary Device. *Science* **2005**, 308, 537-541.

[19] Umbanhowar, P. B.; Prasad, V.; Weitz, D. A., Monodisperse Emulsion Generation via Drop Break Off in a Coflowing Stream. *Langmuir* **1999**, 16, 347-351.

[20] Quevedo, E.; Steinbacher, J.; McQuade, D. T., Interfacial Polymerization within a Simplified Microfluidic Device: Capturing Capsules. *J. Am. Chem. Soc.* **2005**, 127, 10498-10499.

[21] Sullivan, M. T.; Stone, H. A., The role of feedback in microfluidic flow-focusing devices. *Philos. Trans. R. Soc., A* **2008**, 366, 2131-2143.

[22] Clanet, C.; Lasheras, J. C., Transition from dripping to jetting. *J. Fluid Mech.* **1999**, 383, 307-326.

[23] Ambravaneswaran, B.; Subramani, H. J.; Phillips, S. D.; Basaran, O. A., Dripping-Jetting Transitions in a Dripping Faucet. *Phys. Rev. Lett.* **2004**, 93, 034501-034505 .

[24] Utada, A. S.; Fernandez-Nieves, A.; Stone, H. A.; Weitz, D. A., Dripping to Jetting Transitions in Coflowing Liquid Streams. *Phys. Rev. Lett.* **2007**, 99, 094502-094506.

[25] Marre, S.; Aymonier, C.; Subra, P.; Mignard, E., Dripping to jetting transitions observed from supercritical fluid in liquid microcoflows. *Appl. Phys. Lett.* **2009**, 95, 134105-134108.

[26] Cohen, I.; Brenner, M. P.; Eggers, J.; Nagel, S. R., Two Fluid Drop Snap-Off Problem: Experiments and Theory. *Phys. Rev. Lett.* **1999**, 83, 1147-1150.

[27] Meyer, R. F.; Crocker, J. C., Universal Dripping and Jetting in a Transverse Shear Flow. *Phys. Rev. Lett.* **2009**, 102, 194501-194505.

[28] Ledesma-Aguilar, R.; Nistal, R.; Hernández-Machado, A.; Pagonabarraga, I., Controlled drop emission by wetting properties in driven liquid filaments. *Nat. Mater.* **2011**, 10, 367-371.

[29] Cohen, I.; Li, H.; Hougland, J. L.; Mrksich, M.; Nagel, S. R., Using Selective Withdrawal to Coat Microparticles. *Science* **2001**, 292, 265-267.

[30] Wang, C.-C.; Yang, K.-C.; Lin, K.-H.; Liu, H.-C.; Lin, F.-H., A highly organized three-dimensional alginate scaffold for cartilage tissue engineering prepared by microfluidic technology. *Biomaterials* **2011**, 32, 7118-7126.

[31] Lewis, P. C.; Graham, R. R.; Nie, Z.; Xu, S.; Seo, M.; Kumacheva, E., Continuous Synthesis of Copolymer Particles in Microfluidic Reactors. *Macromolecules* **2005**, 38, 4536-4538.

[32] Dubinsky, S.; Zhang, H.; Nie, Z.; Gourevich, I.; Voicu, D.; Deetz, M.; Kumacheva, E., Microfluidic Synthesis of Macroporous Copolymer Particles. *Macromolecules* **2008**, 41, 3555-3561.

[33] Dubinsky, S.; Petukhova, A.; Gourevich, I.; Kumacheva, E., Hybrid porous material produced by polymerization-induced phase separation. *Chem. Commun.* **2010**, 46, 2578-2580.

[34] Dubinsky, S.; Park, J. I.; Gourevich, I.; Chan, C.; Deetz, M.; Kumacheva, E., Toward Controlling the Surface Morphology of Macroporous Copolymer Particles. *Macromolecules* **2009**, 42, 1990-1994.

[35] Frenz, L.; El Harrak, A.; Pauly, M.; Bégin-Colin, S.; Griffiths, A. D.; Baret, J.-C., Droplet-Based Microreactors for the Synthesis of Magnetic Iron Oxide Nanoparticles. *Angew. Chem. Int. Ed.* **2008**, 47, 6817-6820.

[36] Ye, C.; Chen, A.; Colombo, P.; Martinez, C., Ceramic microparticles and capsules via microfluidic processing of a preceramic polymer. *J. R. Soc., Interface* **2010**, 7, S461-S473.

[37] Ji, X.-H.; Cheng, W.; Guo, F.; Liu, W.; Guo, S.-S.; He, Z.-K.; Zhao, X.-Z., On-demand preparation of quantum dot-encoded microparticles using a droplet microfluidic system. *Lab Chip* **2011**, 11, 2561-2568.

[38] Schabas, G.; Wang, C.-W.; Oskooei, A.; Yusuf, H.; Moffitt, M. G.; Sinton, D., Formation and Shear-Induced Processing of Quantum Dot Colloidal Assemblies in a Multiphase Microfluidic Chip. *Langmuir* **2008**, 24, 10596-10603.

[39] Duraiswamy, S.; Khan, S. A., Droplet-Based Microfluidic Synthesis of Anisotropic Metal Nanocrystals. *Small* **2009**, 5, 2828-2834.

[40] Gendrineau, T.; Marre, S.; Vaultier, M.; Pucheault, M.; Aymonier, C., Microfluidic Synthesis of Palladium Nanocrystals Assisted by Supercritical CO2: Tailored Surface Properties for Applications in Boron Chemistry. *Angew. Chem. Int. Ed.* **2012**, 124, 8653-8656.

[41] Chan, E. M.; Alivisatos, A. P.; Mathies, R. A., High-Temperature Microfluidic Synthesis of CdSe Nanocrystals in Nanoliter Droplets. *J. Am. Chem. Soc.* **2005**, 127, 13854-13861.

[42] Hancock, M. J.; Yanagawa, F.; Jang, Y.-H.; He, J.; Kachouie, N. N.; Kaji, H.; Khademhosseini, A., Designer Hydrophilic Regions Regulate Droplet Shape for Controlled Surface Patterning and 3D Microgel Synthesis. *Small* **2012**, 8, 393-403.

[43] Fang, A.; Gaillard, C.; Douliez, J.-P., Template-Free Formation of Monodisperse Doughnut-Shaped Silica Microparticles by Droplet-Based Microfluidics. *Chem. Mater.***2011**, 23, 4660-4662.

[44] Bon, S. A. F.; Mookhoek, S. D.; Colver, P. J.; Fischer, H. R.; van der Zwaag, S., Route to stable non-spherical emulsion droplets. *Eur. Polym. J.* **2007**, 43, 4839-4842.

[45] Roh, K.-H.; Martin, D. C.; Lahann, J., Triphasic Nanocolloids. *J. Am. Chem. Soc.* **2006**, 128, 6796-6797.

[46] Roh, K.-H.; Martin, D. C.; Lahann, J., Biphasic Janus particles with nanoscale anisotropy. *Nat. Mater.* **2005**, 4, 759-763.

[47] Nisisako, T.; Torii, T.; Takahashi, T.; Takizawa, Y., Synthesis of Monodisperse Bicolored Janus Particles with Electrical Anisotropy Using a Microfluidic Co-Flow System. *Adv. Mater.* **2006**, 18, 1152-1156.

[48] Dror, Y.; Salalha, W.; Avrahami, R.; Zussman, E.; Yarin, A. L.; Dersch, R.; Greiner, A.; Wendorff, J. H., One-Step Production of Polymeric Microtubes by Co-electrospinning. *Small* **2007**, 3, 1064-1073.

[49] Puigmartí-Luis, J.; Schaffhauser, D.; Burg, B. R.; Dittrich, P. S., A Microfluidic Approach for the Formation of Conductive Nanowires and Hollow Hybrid Structures. *Adv. Mater.* **2010**, 22, 2255-2259.

[50] Jeong, W.; Kim, J.; Kim, S.; Lee, S.; Mensing, G.; Beebe, D. J., Hydrodynamic microfabrication via "on the fly" photopolymerization of microscale fibers and tubes. *Lab Chip* **2004**, 4, 576-580.

[51] Chen, P. W.; Erb, R. M.; Studart, A. R., Designer Polymer-Based Microcapsules Made Using Microfluidics. *Langmuir* **2011**, 28, 144-152.

[52] Sander, J. S.; Erb, R. M.; Denier, C.; Studart, A. R., Magnetic Transport, Mixing and Release of Cargo with Tailored Nanoliter Droplets. *Adv. Mater.* **2012**, 24, 2582-2587.

[53] Chen, C.-H.; Abate, A. R.; Lee, D.; Terentjev, E. M.; Weitz, D. A., Microfluidic Assembly of Magnetic Hydrogel Particles with Uniformly Anisotropic Structure. *Adv. Mater.* **2009**, 21, 3201-3204.

[54] Tumarkin, E.; Tzadu, L.; Csaszar, E.; Seo, M.; Zhang, H.; Lee, A.; Peerani, R.; Purpura, K.; Zandstra, P. W.; Kumacheva, E., High-throughput combinatorial cell co-culture using microfluidics. *Integr. Biol.* **2011**, 3, 653-662.

[55] Velasco, D.; Tumarkin, E.; Kumacheva, E., Microfluidic Encapsulation of Cells in Polymer Microgels. *Small* **2012**, 8, 1633-1642.

[56] Edd, J. F.; Di Carlo, D.; Humphry, K. J.; Koster, S.; Irimia, D.; Weitz, D. A.; Toner, M., Controlled encapsulation of single-cells into monodisperse picolitre drops. *Lab Chip* **2008**, 8, 1262-1264.

[57] Ma, G.-H.; Nagai, M.; Omi, S., Study on preparation of monodispersed poly(styrene-co-N-dimethylaminoethyl methacrylate) composite microspheres by SPG (Shirasu Porous Glass) emulsification technique. *J. Appl. Polym. Sci.* **2001**, 79, 2408-2424.

[58] Ma, G. H.; Su, Z. G.; Omi, S.; Sundberg, D.; Stubbs, J., Microencapsulation of oil with poly(styrene-N,N-dimethylaminoethyl methacrylate) by SPG emulsification technique: Effects of conversion and composition of oil phase. *J. Colloid Interface Sci.* **2003**, 266, 282-294.

[59] Kobayashi, I.; Takano, T.; Maeda, R.; Wada, Y.; Uemura, K.; Nakajima, M., Straight-through microchannel devices for generating monodisperse emulsion droplets several microns in size. *Microfluid. Nanofluid.* **2008**, 4, 167-177.

[60] Kobayashi, I.; Murayama, Y.; Kuroiwa, T.; Uemura, K.; Nakajima, M., Production of monodisperse water-in-oil emulsions consisting of highly uniform droplets using asymmetric straight-through microchannel arrays. *Microfluid. Nanofluid.* **2009**, 7, 107-119.

[61] Churski, K.; Michalski, J.; Garstecki, P., Droplet on demand system utilizing a computer controlled microvalve integrated into a stiff polymeric microfluidic device. *Lab Chip* **2010**, 10, 512-518.

[62] Maeda, K.; Onoe, H.; Takinoue, M.; Takeuchi, S., Controlled Synthesis of 3D Multi-Compartmental Particles with Centrifuge-Based Microdroplet Formation from a Multi-Barrelled Capillary. *Adv. Mater.* **2012**, 24, 1340-1346.

[63] Nisisako, T.; Hatsuzawa, T., A microfluidic cross-flowing emulsion generator for producing biphasic droplets and anisotropically shaped polymer particles. *Microfluid. Nanofluid.* **2010**, 9, 427-437.

[64] Okushima, S.; Nisisako, T.; Torii, T.; Higuchi, T., Controlled Production of Monodisperse Double Emulsions by Two-Step Droplet Breakup in Microfluidic Devices. *Langmuir* **2004**, 20, 9905-9908.

[65] Wang, K.; Lu, Y.; Xu, J.; Luo, G., Droplet generation in micro-sieve dispersion device. *Microfluid. Nanofluid.* **2011**, 10, 1087-1095.

[66] Chokkalingam, V.; Weidenhof, B.; Kramer, M.; Maier, W. F.; Herminghaus, S.; Seemann, R., Optimized droplet-based microfluidics scheme for sol-gel reactions. *Lab Chip* **2010**, 10, 1700-1705.

[67] Christopher, G. F.; Bergstein, J.; End, N. B.; Poon, M.; Nguyen, C.; Anna, S. L., Coalescence and splitting of confined droplets at microfluidic junctions. *Lab Chip* **2009**, 9, 1102-1109.

[68] Murshed, S.; Tan, S.; Nguyen, N.; Wong, T.; Yobas, L., Microdroplet formation of water and nanofluids in heat-induced microfluidic T-junction. *Microfluid. Nanofluid.* **2009**, 6, 253-259.

[69] Abate, A. R.; Weitz, D. A., Air-bubble-triggered drop formation in microfluidics. *Lab Chip* **2011**, 11, 253-259.

[70] Steinbacher, J. L.; Moy, R. W. Y.; Price, K. E.; Cummings, M. A.; Roychowdhury, C.; Buffy, J. J.; Olbricht, W. L.; Haaf, M.; McQuade, D. T., Rapid Self-Assembly of Core−Shell Organosilicon Microcapsules within a Microfluidic Device. *J. Am. Chem. Soc.* **2006**, 128, 9442-9447.

[71] Abate, A. R.; Hung, T.; Mary, P.; Agresti, J. J.; Weitz, D. A., High-throughput injection with microfluidics using picoinjectors. *Proc. Natl. Acad.* **2010**, 107, 19163-19166.

[72] Lao, K.-L.; Wang, J.-H.; Lee, G.-B., A microfluidic platform for formation of double-emulsion droplets. *Microfluid. Nanofluid.* **2009**, 7, 709-719.

[73] Lee, H.; Xu, L.; Ahn, B.; Lee, K.; Oh, K., Continuous-flow in-droplet magnetic particle separation in a droplet-based microfluidic platform. *Microfluid. Nanofluid.* **2012**, online first.

[74] van der Graaf, S.; Steegmans, M. L. J.; van der Sman, R. G. M.; Schroën, C. G. P. H.; Boom, R. M., Droplet formation in a T-shaped microchannel junction: A model system for membrane emulsification. *Colloids Surf.* **2005**, 266, 106-116.

[75] Abate, A. R.; Mary, P.; van Steijn, V.; Weitz, D. A., Experimental validation of plugging during drop formation in a T-junction. *Lab Chip* **2012**, 12, 1516-1521.

[76] Lee, W.; Jambovane, S.; Kim, D.; Hong, J., Predictive model on micro droplet generation through mechanical cutting. *Microfluid. Nanofluid.* **2009**, 7, 431-438.

[77] van Steijn, V.; Kleijn, C. R.; Kreutzer, M. T., Predictive model for the size of bubbles and droplets created in microfluidic T-junctions. *Lab Chip* **2010**, 10, 2513-2518.

[78] van der Zwan, E.; van der Sman, R.; Schroën, K.; Boom, R., Lattice Boltzmann simulations of droplet formation during microchannel emulsification. *J. Colloid Interface Sci.* **2009**, 335, 112-122.

[79] Seo, M.; Paquet, C.; Nie, Z.; Xu, S.; Kumacheva, E., Microfluidic consecutive flow-focusing droplet generators. *Soft Matter* **2007**, 3, 986-992.

[80] Berkland, C.; Pollauf, E.; Varde, N.; Pack, D.; Kim, K., Monodisperse Liquid-filled Biodegradable Microcapsules. *Pharm. Res.* **2007**, 24, 1007-1013.

[81] Li, W.; Greener, J.; Voicu, D.; Kumacheva, E., Multiple modular microfluidic (M3) reactors for the synthesis of polymer particles. *Lab Chip* **2009**, 9, 2715-2721.

[82] Li, W.; Young, E. W. K.; Seo, M.; Nie, Z.; Garstecki, P.; Simmons, C. A.; Kumacheva, E., Simultaneous generation of droplets with different dimensions in parallel integrated microfluidic droplet generators. *Soft Matter* **2008**, 4, 258-262.

[83] Mulligan, M.; Rothstein, J., Scale-up and control of droplet production in coupled microfluidic flow-focusing geometries. *Microfluid. Nanofluid.*, **2012**, 13 65-73.

[84] Gupta, R.; Baldock, S. J.; Carreras, P.; Fielden, P. R.; Goddard, N. J.; Mohr, S.; Razavi, B. S.; Treves Brown, B. J., A microfluidic device for self-synchronised production of droplets. *Lab Chip* **2011**, 11, 4052-4056.

[85] Abate, A. R.; Weitz, D. A., High-Order Multiple Emulsions Formed in Poly(dimethylsiloxane) Microfluidics. *Small* **2009**, 5, 2030-2032.

[86] Deng, N.-N.; Meng, Z.-J.; Xie, R.; Ju, X.-J.; Mou, C.-L.; Wang, W.; Chu, L.-Y., Simple and cheap microfluidic devices for the preparation of monodisperse emulsions. *Lab Chip* **2011**, 11, 3963-3969.

[87] Abate, A. R.; Weitz, D. A., Faster multiple emulsification with drop splitting. *Lab Chip* **2011**, 11, 1911-1915.

[88] Tan, Y.-C.; Lee, A. P., Microfluidic separation of satellite droplets as the basis of a monodispersed micron and submicron emulsification system. *Lab Chip* **2005**, 5, 1178-1183.

[89] Link, D. R.; Grasland-Mongrain, E.; Duri, A.; Sarrazin, F.; Cheng, Z.; Cristobal, G.; Marquez, M.; Weitz, D. A., Electric Control of Droplets in Microfluidic Devices. *Angew. Chem. Int. Ed.* **2006**, 45, 2556-2560.

[90] Yeh, C.-H.; Chen, Y.-C.; Lin, Y.-C., Generation of droplets with different concentrations using gradient-microfluidic droplet generator. *Microfluid. Nanofluid.* **2011**, 11, 245-253.

[91] Woodward, A.; Cosgrove, T.; Espidel, J.; Jenkins, P.; Shaw, N., Monodisperse emulsions from a microfluidic device, characterised by diffusion NMR. *Soft Matter* **2007**, 3, 627-633.

[92] Haeberle, S.; Zengerle, R.; Ducrée, J., Centrifugal generation and manipulation of droplet emulsions. *Microfluid. Nanofluid.* **2007**, 3, 65-75.

[93] Mark, D.; Haeberle, S.; Zengerle, R.; Ducree, J.; Vladisavljević, G. T., Manufacture of chitosan microbeads using centrifugally driven flow of gel-forming solutions through a polymeric micronozzle. *J. Colloid Interface Sci.* **2009**, 336, 634-641.

[94] Loscertales, I. G.; Barrero, A.; Guerrero, I.; Cortijo, R.; Marquez, M.; Gañán-Calvo, A. M., Micro/Nano Encapsulation via Electrified Coaxial Liquid Jets. *Science* **2002**, 295, 1695-1698.

[95] Chang, M.-W.; Stride, E.; Edirisinghe, M., Controlling the thickness of hollow polymeric microspheres prepared by electrohydrodynamic atomization. *J. R. Soc., Interface* **2010**, 7, S451-S460.

[96] Xu, Q.; Nakajima, M., The generation of highly monodisperse droplets through the breakup of hydrodynamically focused microthread in a microfluidic device. *Appl. Phys. Lett.* **2004**, 85, 3726-3728.

[97] Xing, X. Q.; Butler, D. L.; Ng, S. H.; Wang, Z.; Danyluk, S.; Yang, C., Simulation of droplet formation and coalescence using lattice Boltzmann-based single-phase model. *J. Colloid Interface Sci.* **2007**, 311, 609-618.

[98] Ward, T.; Faivre, M.; Abkarian, M.; Stone, H. A., Microfluidic flow focusing: Drop size and scaling in pressure versus flow-rate-driven pumping. *Electrophoresis* **2005**, 26, 3716-3724.

[99] Anna, S. L.; Bontoux, N.; Stone, H. A., Formation of dispersions using ``flow focusing'' in microchannels. *Appl. Phys. Lett.* **2003**, 82, 364-366.

[100] Nie, Z.; Seo, M.; Xu, S.; Lewis, P.; Mok, M.; Kumacheva, E.; Whitesides, G.; Garstecki, P.; Stone, H., Emulsification in a microfluidic flow-focusing device: effect of the viscosities of the liquids. *Microfluid. Nanofluid.* **2008**, 5, 585-594.

[101] Park, J. M.; Anderson, P. D., A ternary model for double-emulsion formation in a capillary microfluidic device. *Lab Chip* **2012**, 12, 2672-2677.

[102] Priest, C.; Reid, M. D.; Whitby, C. P., Formation and stability of nanoparticle-stabilised oil-in-water emulsions in a microfluidic chip. *J. Colloid Interface Sci.* **2011**, 363, 301-306.

[103] Serra, C.; Berton, N.; Bouquey, M.; Prat, L.; Hadziioannou, G., A Predictive Approach of the Influence of the Operating Parameters on the Size of Polymer Particles Synthesized in a Simplified Microfluidic System. *Langmuir* **2007**, 23, 7745-7750.

[104] Duffy, D. C.; McDonald, J. C.; Schueller, O. J. A.; Whitesides, G. M., Rapid Prototyping of Microfluidic Systems in Poly(dimethylsiloxane). *Anal. Chem.* **1998**, 70, 4974-4984.

[105] McDonald, J. C.; Whitesides, G. M., Poly(dimethylsiloxane) as a Material for Fabricating Microfluidic Devices. *Accounts of Chemical Research* **2002**, 35, 491-499.

[106] Perry, J. M.; Harms, Z. D.; Jacobson, S. C., 3D Nanofluidic Channels Shaped by Electron-Beam-Induced Etching. *Small* **2012**, 8, 1521-1526.

[107] Stokes, G. G., On the Effect of the Internal Friction of Fluids on the Motion of Pendulums. *Trans. Cambridge Philos. Soc.* **1850**, 9, 8-18.

[108] Reynolds, O., An Experimental Investigation of the Circumstances Which Determine Whether the Motion of Water Shall Be Direct or Sinuous, and of the

Law of Resistance in Parallel Channels. *Philos. Trans. R. Soc. London* **1883**, 174, 935-982.

[109] Nie, Z.; Park, J. I.; Li, W.; Bon, S. A. F.; Kumacheva, E., An "Inside-Out" Microfluidic Approach to Monodisperse Emulsions Stabilized by Solid Particles. *J. Am. Chem. Soc.* **2008**, 130, 16508-16509.

[110] Garstecki, P.; Gitlin, I.; DiLuzio, W.; Whitesides, G. M.; Kumacheva, E.; Stone, H. A., Formation of monodisperse bubbles in a microfluidic flow-focusing device. *Appl. Phys. Lett.* **2004**, 85, 2649-2651.

[111] Hashimoto, M.; Shevkoplyas, S. S.; Zasońska, B.; Szymborski, T.; Garstecki, P.; Whitesides, G. M., Formation of Bubbles and Droplets in Parallel, Coupled Flow-Focusing Geometries. *Small* **2008**, 4, 1795-1805.

[112] Hashimoto, M.; Whitesides, G. M., Formation of Bubbles in a Multisection Flow-Focusing Junction. *Small* **2010**, 6, 1051-1059.

[113] Yang, L.; Wang, K.; Tan, J.; Lu, Y.; Luo, G., Experimental study of microbubble coalescence in a T-junction microfluidic device. *Microfluid. Nanofluid.* **2012**, 12, 715-722.

[114] Park, J. I.; Nie, Z.; Kumachev, A.; Kumacheva, E., A microfluidic route to small CO2 microbubbles with narrow size distribution. *Soft Matter* **2010**, 6, 630-634.

[115] Garstecki, P.; J. Fuerstman, M.; Fischbach, M. A.; Sia, S. K.; Whitesides, G. M., Mixing with bubbles: a practical technology for use with portable microfluidic devices. *Lab Chip* **2006**, 6, 207-212.

[116] Prakash, M.; Gershenfeld, N., Microfluidic Bubble Logic. *Science* **2007**, 315, 832-835.

[117] Seo, M.; Matsuura, N., Monodisperse, Submicrometer Droplets via Condensation of Microfluidic-Generated Gas Bubbles. *Small* **2012**, 8, 2704-2714.

[118] van der Net, A.; Delaney, G. W.; Drenckhan, W.; Weaire, D.; Hutzler, S., Crystalline arrangements of microbubbles in monodisperse foams. *Colloids Surf.* **2007**, 309, 117-124.

[119] Hashimoto, M.; Garstecki, P.; Whitesides, G. M., Synthesis of Composite Emulsions and Complex Foams with the use of Microfluidic Flow-Focusing Devices. *Small* **2007**, 3, 1792-1802.

[120] Park, Y.; Luce, A. C.; Whitaker, R. D.; Amin, B.; Cabodi, M.; Nap, R. J.; Szleifer, I.; Cleveland, R. O.; Nagy, J. O.; Wong, J. Y., Tunable Diacetylene Polymerized Shell Microbubbles as Ultrasound Contrast Agents. *Langmuir* **2012**, 28, 3766-3772.

[121] Drenckhan, W., Generation of Superstable, Monodisperse Microbubbles Using a pH-Driven Assembly of Surface-Active Particles. *Angew. Chem. Int. Ed.* **2009**, 48, 5245-5247.

[122] Tumarkin, E.; Park, J. I.; Nie, Z.; Kumacheva, E., Temperature mediated generation of armoured bubbles. *Chem. Commun.* **2011**, 47, 12712-12714.

[123] Duncanson, W. J.; Abbaspourrad, A.; Shum, H. C.; Kim, S.-H.; Adams, L. L. A.; Weitz, D. A., Monodisperse Gas-Filled Microparticles from Reactions in Double Emulsions. *Langmuir* **2012**, 28, 6742-6745.

[124] Lee, M. H.; Prasad, V.; Lee, D., Microfluidic Fabrication of Stable Nanoparticle-Shelled Bubbles. *Langmuir* **2009**, 26, 2227-2230.

[125] Brugarolas, T.; Park, B. J.; Lee, M. H.; Lee, D., Generation of Amphiphilic Janus Bubbles and Their Behavior at an Air–Water Interface. *Adv. Funct. Mater.* **2011**, 21, 3924-3931.

[126] Wan, J.; Bick, A.; Sullivan, M.; Stone, H. A., Controllable Microfluidic Production of Microbubbles in Water-in-Oil Emulsions and the Formation of Porous Microparticles. *Adv. Mater.* **2008**, 20, 3314-3318.

[127] Wan, J.; Stone, H. A., Microfluidic generation of a high volume fraction of bubbles in droplets. *Soft Matter* **2010**, 6, 4677-4680.

[128] Li, W.; Liu, K.; Simms, R.; Greener, J.; Jagadeesan, D.; Pinto, S.; Günther, A.; Kumacheva, E., Microfluidic Study of Fast Gas–Liquid Reactions. *J. Am. Chem. Soc.* **2011**, 134, 3127-3132.

[129] Bauer, W.-A. C.; Kotar, J.; Cicuta, P.; Woodward, R. T.; Weaver, J. V. M.; Huck, W. T. S., Microfluidic production of monodisperse functional o/w droplets and study of their reversible pH dependent aggregation behavior. *Soft Matter* **2011**, 7, 4214-4220.

[130] Martz, T. D.; Bardin, D.; Sheeran, P. S.; Lee, A. P.; Dayton, P. A., Microfluidic Generation of Acoustically Active Nanodroplets. *Small* **2012**, 8, 1876-1879.

[131] Niu, X.; Zhang, M.; Wu, J.; Wen, W.; Sheng, P., Generation and manipulation of "smart" droplets. *Soft Matter* **2009**, 5, 576-581.

[132] Sun, C.; Zhao, X.-W.; Zhao, Y.-J.; Zhu, R.; Gu, Z.-Z., Fabrication of Colloidal Crystal Beads by a Drop-Breaking Technique and Their Application as Bioassays. *Small* 2008, 4, 592-596.

[133] Kanai, T.; Lee, D.; Shum, H. C.; Weitz, D. A., Fabrication of Tunable Spherical Colloidal Crystals Immobilized in Soft Hydrogels. *Small* **2010**, 6, 807-810.

[134] Zhu, J.; Hayward, R. C., Hierarchically Structured Microparticles Formed by Interfacial Instabilities of Emulsion Droplets Containing Amphiphilic Block Copolymers. *Angew. Chem. Int. Ed.* **2008**, 47, 2113-2116.

[135] Kuehne, A. J. C.; Weitz, D. A., Highly monodisperse conjugated polymer particles synthesized with drop-based microfluidics. *Chem. Commun.* **2011**, 47, 12379-12381.

[136] Shojaei-Zadeh, S.; Morris, J. F.; Couzis, A.; Maldarelli, C., Highly crosslinked poly(dimethylsiloxane) microbeads with uniformly dispersed quantum dot nanocrystals. *J. Colloid Interface Sci.* **2011**, 363, 25-33.

[137] Jiang, K.; Thomas, P. C.; Forry, S. P.; DeVoe, D. L.; Raghavan, S. R., Microfluidic synthesis of monodisperse PDMS microbeads as discrete oxygen sensors. *Soft Matter* **2012**, 8, 923-926.

[138] Kim, J.; Song, Y.; He, L.; Kim, H.; Lee, H.; Park, W.; Yin, Y.; Kwon, S., Real-Time Optofluidic Synthesis of Magnetochromatic Microspheres for Reversible Structural Color Patterning. *Small* **2011**, 7, 1163-1168.

[139] Sung, K. E.; Vanapalli, S. A.; Mukhija, D.; McKay, H. A.; Mirecki Millunchick, J.; Burns, M. A.; Solomon, M. J., Programmable Fluidic Production of Microparticles with Configurable Anisotropy. *J. Am. Chem. Soc.* **2008**, 130, 1335-1340.

[140] Sophia Lee, S. H.; Dawood, M. K.; Choi, W. K.; Alan Hatton, T.; Khan, S. A., Hierarchical materials synthesis at soft all-aqueous interfaces. *Soft Matter* **2012**, 8, 3924-3928.

[141] Kaufmann, T.; Gokmen, M. T.; Wendeln, C.; Schneiders, M.; Rinnen, S.; Arlinghaus, H. F.; Bon, S. A. F.; Du Prez, F. E.; Ravoo, B. J., "Sandwich" Microcontact Printing as a Mild Route Towards Monodisperse Janus Particles with Tailored Bifunctionality. *Adv. Mater.* **2011**, 23, 79-83.

[142] Prasath, R. A.; Gokmen, M. T.; Espeel, P.; Du Prez, F. E., Thiol-ene and thiol-yne chemistry in microfluidics: a straightforward method towards macroporous and nonporous functional polymer beads. *Polym. Chem.* **2010**, 1, 685-692.

[143] Gokmen, M. T.; Van Camp, W.; Colver, P. J.; Bon, S. A. F.; Du Prez, F. E., Fabrication of Porous "Clickable" Polymer Beads and Rods through Generation of High Internal Phase Emulsion (HIPE) Droplets in a Simple Microfluidic Device. *Macromolecules* **2009**, 42, 9289-9294.

[144] Lee, I.; Yoo, Y.; Cheng, Z.; Jeong, H.-K., Generation of Monodisperse Mesoporous Silica Microspheres with Controllable Size and Surface Morphology in a Microfluidic Device. *Adv. Funct. Mater.* **2008**, 18, 4014-4021.

[145] Sin, D.; Fitzpatrick, J.; Luckman, P.; Wolvetang, E. J.; Cooper-White, J. J., Fabrication of nanopatterned, porous microspheres using a glass capillary microfluidic device. *Soft Matter* **2012**, advance article.

[146] Carroll, N. J.; Rathod, S. B.; Derbins, E.; Mendez, S.; Weitz, D. A.; Petsev, D. N., Droplet-Based Microfluidics for Emulsion and Solvent Evaporation Synthesis of Monodisperse Mesoporous Silica Microspheres. *Langmuir* **2008**, 24, 658-661.

[147] Rastogi, V.; Velikov, K. P.; Velev, O. D., Microfluidic characterization of sustained solute release from porous supraparticles. *Phys. Chem. Chem. Phys.* **2010**, 12, 11975-11983.

[148] Duncanson, W. J.; Zieringer, M.; Wagner, O.; Wilking, J. N.; Abbaspourrad, A.; Haag, R.; Weitz, D. A., Microfluidic synthesis of monodisperse porous microspheres with size-tunable pores. *Soft Matter* **2012**, advance article.

[149] Abraham, S.; Park, Y. H.; Lee, J. K.; Ha, C.-S.; Kim, I., Microfluidic Synthesis of Reversibly Swelling Porous Polymeric Microcapsules with Controlled Morphology. *Adv. Mater.* **2008**, 20, 2177-2182.

[150] Shah, R. K.; Kim, J.-W.; Weitz, D. A., Janus Supraparticles by Induced Phase Separation of Nanoparticles in Droplets. *Adv. Mater.* **2009**, 21, 1949-1953.

[151] Lone, S.; Kim, S. H.; Nam, S. W.; Park, S.; Joo, J.; Cheong, I. W., Microfluidic synthesis of Janus particles by UV-directed phase separation. *Chem. Commun.* **2011**, 47, 2634-2636.

[152] Chang, E. P.; Hatton, T. A., Membrane Emulsification and Solvent Pervaporation Processes for the Continuous Synthesis of Functional Magnetic and Janus Nanobeads. *Langmuir* **2012**, 28, 9748-9758.

[153] Nisisako, T.; Torii, T., Formation of Biphasic Janus Droplets in a Microfabricated Channel for the Synthesis of Shape-Controlled Polymer Microparticles. *Adv. Mater.* **2007**, 19, 1489-1493.

[154] Shepherd, R. F.; Conrad, J. C.; Rhodes, S. K.; Link, D. R.; Marquez, M.; Weitz, D. A.; Lewis, J. A., Microfluidic Assembly of Homogeneous and Janus Colloid-Filled Hydrogel Granules. *Langmuir* **2006**, 22, 8618-8622.

[155] Nie, Z.; Li, W.; Seo, M.; Xu, S.; Kumacheva, E., Janus and Ternary Particles Generated by Microfluidic Synthesis: Design, Synthesis, and Self-Assembly. *J. Am. Chem. Soc.* **2006**, 128, 9408-9412.

[156] Kim, S.-H.; Jeon, S.-J.; Jeong, W. C.; Park, H. S.; Yang, S.-M., Optofluidic Synthesis of Electroresponsive Photonic Janus Balls with Isotropic Structural Colors. *Adv. Mater.* **2008**, 20, 4129-4134.

[157] Seiffert, S.; Romanowsky, M. B.; Weitz, D. A., Janus Microgels Produced from Functional Precursor Polymers. *Langmuir* **2010**, 26, 14842-14847.

[158] Xie, H.; She, Z.-G.; Wang, S.; Sharma, G.; Smith, J. W., One-Step Fabrication of Polymeric Janus Nanoparticles for Drug Delivery. *Langmuir* **2012**, 28, 4459-4463.

[159] Roh, K.-H.; Yoshida, M.; Lahann, J., Water-Stable Biphasic Nanocolloids with Potential Use as Anisotropic Imaging Probes. *Langmuir* **2007**, 23, 5683-5688.

[160] Chen, C.-H.; Shah, R. K.; Abate, A. R.; Weitz, D. A., Janus Particles Templated from Double Emulsion Droplets Generated Using Microfluidics. *Langmuir* **2009**, 25, 4320-4323.

[161] Suh, S. K.; Yuet, K.; Hwang, D. K.; Bong, K. W.; Doyle, P. S.; Hatton, T. A., Synthesis of Nonspherical Superparamagnetic Particles: In Situ Coprecipitation of Magnetic Nanoparticles in Microgels Prepared by Stop-Flow Lithography. *J. Am. Chem. Soc.* **2012**, 134, 7337-7343.

[162] Dendukuri, D.; Hatton, T. A.; Doyle, P. S., Synthesis and Self-Assembly of Amphiphilic Polymeric Microparticles. *Langmuir* **2006**, 23, 4669-4674.

[163] Fialkowski, M.; Bitner, A.; Grzybowski, B. A., Self-assembly of polymeric microspheres of complex internal structures. *Nat. Mater.* **2005**, 4, 93-97.

[164] Millman, J. R.; Bhatt, K. H.; Prevo, B. G.; Velev, O. D., Anisotropic particle synthesis in dielectrophoretically controlled microdroplet reactors. *Nat. Mater.* **2005**, 4, 98-102.

[165] Dendukuri, D.; Tsoi, K.; Hatton, T. A.; Doyle, P. S., Controlled Synthesis of Nonspherical Microparticles Using Microfluidics. *Langmuir* **2005**, 21, 2113-2116.

[166] Hwang, D. K.; Dendukuri, D.; Doyle, P. S., Microfluidic-based synthesis of non-spherical magnetic hydrogel microparticles. *Lab Chip* **2008**, 8, 1640-1647.

[167] Xu, S.; Nie, Z.; Seo, M.; Lewis, P.; Kumacheva, E.; Stone, H. A.; Garstecki, P.; Weibel, D. B.; Gitlin, I.; Whitesides, G. M., Generation of Monodisperse Particles by Using Microfluidics: Control over Size, Shape, and Composition. *Angew. Chem. Int. Ed.* **2005**, 44, 3799-3799.

[168] Seo, M.; Nie, Z.; Xu, S.; Lewis, P. C.; Kumacheva, E., Microfluidics: From Dynamic Lattices to Periodic Arrays of Polymer Disks. *Langmuir* **2005**, 21, 4773-4775.

[169] Bhaskar, S.; Hitt, J.; Chang, S.-W. L.; Lahann, J., Multicompartmental Microcylinders. *Angew. Chem. Int. Ed.* **2009**, 48, 4589-4593.

[170] Baah, D.; Tigner, J.; Bean, K.; Walker, N.; Britton, B.; Floyd-Smith, T., Microfluidic synthesis and post processing of non-spherical polymeric microparticles. *Microfluid. Nanofluid.* **2012**, 12, 657-662.

[171] Szymusiak, M.; Sharma, V.; Nitsche, L. C.; Liu, Y., Interaction of sedimenting drops in a miscible solution - formation of heterogeneous toroidal-spiral particles. *Soft Matter* **2012**, 8, 7556-7559.

[172] Nie, Z.; Xu, S.; Seo, M.; Lewis, P. C.; Kumacheva, E., Polymer Particles with Various Shapes and Morphologies Produced in Continuous Microfluidic Reactors. *J. Am. Chem. Soc.* **2005**, 127, 8058-8063.

[173] Studart, A. R.; Shum, H. C.; Weitz, D. A., Arrested Coalescence of Particle-coated Droplets into Nonspherical Supracolloidal Structures. *J. Phys. Chem. B* **2009**, 113, 3914-3919.

[174] Liu, S.; Deng, R.; Li, W.; Zhu, J., Polymer Microparticles with Controllable Surface Textures Generated through Interfacial Instabilities of Emulsion Droplets. *Adv. Funct. Mater.* **2012**, 22, 1692-1697.

[175] Zhang, Q.; Lin, B.; Qin, J., Synthesis of shape-controlled particles based on synergistic effect of geometry confinement, double emulsion template, and polymerization quenching. *Microfluid. Nanofluid.* **2012**, 12, 33-39.

[176] Srivastava, Y.; Rhodes, C.; Marquez, M.; Thorsen, T., Electrospinning hollow and core/sheath nanofibers using hydrodynamic fluid focusing. *Microfluid. Nanofluid.* **2008**, 5, 455-458.

[177] Viry, L.; Moulton, S. E.; Romeo, T.; Suhr, C.; Mawad, D.; Cook, M.; Wallace, G. G., Emulsion-coaxial electrospinning: designing novel architectures for sustained release of highly soluble low molecular weight drugs. *J. Mater. Chem.* **2012**, 22, 11347-11353.

[178] Bhaskar, S.; Lahann, J., Microstructured Materials Based on Multicompartmental Fibers. *J. Am. Chem. Soc.* **2009**, 131, 6650-6651.

[179] Ma, Q.; Wang, J.; Dong, X.; Yu, W.; Liu, G.; Xu, J., Electrospinning preparation and properties of magnetic-photoluminescent bifunctional coaxial nanofibers. *J. Mater. Chem.* **2012**, 22, 14438-14442.

[180] Kiriya, D.; Kawano, R.; Onoe, H.; Takeuchi, S., Microfluidic Control of the Internal Morphology in Nanofiber-based Macroscopic Cables. *Angew. Chem. Int. Ed.* **2012**, 51, 7942-7947.

[181] Lan, W.; Li, S.; Lu, Y.; Xu, J.; Luo, G., Controllable preparation of microscale tubes with multiphase co-laminar flow in a double co-axial microdevice. *Lab Chip* **2009**, 9, 3282-3288.

[182] Seiffert, S.; Weitz, D. A., Controlled fabrication of polymer microgels by polymer-analogous gelation in droplet microfluidics. *Soft Matter* **2010**, 6, 3184-3190.

[183] Chen, W.; Yang, Y.; Rinadi, C.; Zhou, D.; Shen, A. Q., Formation of supramolecular hydrogel microspheres via microfluidics. *Lab Chip* **2009**, 9, 2947-2951.

[184] Ziemecka, I.; van Steijn, V.; Koper, G. J. M.; Rosso, M.; Brizard, A. M.; van Esch, J. H.; Kreutzer, M. T., Monodisperse hydrogel microspheres by forced droplet formation in aqueous two-phase systems. *Lab Chip* **2011**, 11, 620-624.

[185] Jeong, W. J.; Kim, J. Y.; Choo, J.; Lee, E. K.; Han, C. S.; Beebe, D. J.; Seong, G. H.; Lee, S. H., Continuous Fabrication of Biocatalyst Immobilized Microparticles Using Photopolymerization and Immiscible Liquids in Microfluidic Systems. *Langmuir* **2005**, 21, 3738-3741.

[186] Lewis, C. L.; Lin, Y.; Yang, C.; Manocchi, A. K.; Yuet, K. P.; Doyle, P. S.; Yi, H., Microfluidic Fabrication of Hydrogel Microparticles Containing Functionalized Viral Nanotemplates. *Langmuir* **2010**, 26, 13436-13441.

[187] Ma, S.; Thiele, J.; Liu, X.; Bai, Y.; Abell, C.; Huck, W. T. S., Fabrication of Microgel Particles with Complex Shape via Selective Polymerization of Aqueous Two-Phase Systems. *Small* **2012**, 8, 2356-2360.

[188] Jeong, W.-W.; Kim, C., One-step method for monodisperse microbiogels by glass capillary microfluidics. *Colloids Surf.* **2011**, 384, 268-273.

[189] Rondeau, E.; Cooper-White, J. J., Biopolymer Microparticle and Nanoparticle Formation within a Microfluidic Device. *Langmuir* **2008**, 24, 6937-6945.

[190] Rossow, T.; Heyman, J. A.; Ehrlicher, A. J.; Langhoff, A.; Weitz, D. A.; Haag, R.; Seiffert, S., Controlled Synthesis of Cell-Laden Microgels by Radical-Free Gelation in Droplet Microfluidics. *J. Am. Chem. Soc.* **2012**, 134, 4983-4989.

[191] Kesselman, L. R. B.; Shinwary, S.; Selvaganapathy, P. R.; Hoare, T., Synthesis of Monodisperse, Covalently Cross-Linked, Degradable "Smart" Microgels Using Microfluidics. *Small* **2012**, 8, 1092-1098.

[192] De Geest, B. G.; Urbanski, J. P.; Thorsen, T.; Demeester, J.; De Smedt, S. C., Synthesis of Monodisperse Biodegradable Microgels in Microfluidic Devices. *Langmuir* **2005**, 21, 10275-10279.

[193] Xu, Q.; Hashimoto, M.; Dang, T. T.; Hoare, T.; Kohane, D. S.; Whitesides, G. M.; Langer, R.; Anderson, D. G., Preparation of Monodisperse Biodegradable Polymer Microparticles Using a Microfluidic Flow-Focusing Device for Controlled Drug Delivery. *Small* **2009**, 5, 1575-1581.

[194] Um, E.; Lee, D.-S.; Pyo, H.-B.; Park, J.-K., Continuous generation of hydrogel beads and encapsulation of biological materials using a microfluidic droplet-merging channel. *Microfluid. Nanofluid.* **2008**, 5, 541-549.

[195] Seo, M.; Nie, Z.; Xu, S.; Mok, M.; Lewis, P. C.; Graham, R.; Kumacheva, E., Continuous Microfluidic Reactors for Polymer Particles. *Langmuir* **2005**, 21, 11614-11622.

[196] Li, W.; Pham, H. H.; Nie, Z.; MacDonald, B.; Güenther, A.; Kumacheva, E., Multi-Step Microfluidic Polymerization Reactions Conducted in Droplets: The Internal Trigger Approach. *J. Am. Chem. Soc.* **2008**, 130, 9935-9941.

[197] Wacker, J. B.; Parashar, V. K.; Gijs, M. A. M., Grafting submicron titania particles with gold nanoparticles using droplet microfluidics. *RSC Adv.* **2012**, 2, 3599-3601.

[198] Schunk, D.; Hardt, S.; Wiggers, H.; Marlow, F., Monodisperse titania microspheres via controlled nanoparticle aggregation. *Phys. Chem. Chem. Phys.* **2012**.

[199] Hutter, T.; Bauer, W.-A. C.; Elliott, S. R.; Huck, W. T. S., Formation of Spherical and Non-Spherical Eutectic Gallium-Indium Liquid-Metal Microdroplets in Microfluidic Channels at Room Temperature. *Adv. Funct. Mater.* **2012**, 22, 2624-2631.

[200] Tadmouri, R.; Romano, M.; Guillemot, L.; Mondain-Monval, O.; Wunenburger, R.; Leng, J., Millifluidic production of metallic microparticles. *Soft Matter* **2012**, advance article.

[201] Hung, L.-H.; Choi, K. M.; Tseng, W.-Y.; Tan, Y.-C.; Shea, K. J.; Lee, A. P., Alternating droplet generation and controlled dynamic droplet fusion in microfluidic device for CdS nanoparticle synthesis. *Lab Chip* **2006**, 6, 174-178.

[202] Shestopalov, I.; Tice, J. D.; Ismagilov, R. F., Multi-step synthesis of nanoparticles performed on millisecond time scale in a microfluidic droplet-based system. *Lab Chip* **2004**, 4, 316-321.

[203] Jung, J. H.; Park, T. J.; Lee, S. Y.; Seo, T. S., Homogeneous Biogenic Paramagnetic Nanoparticle Synthesis Based on a Microfluidic Droplet Generator. *Angew. Chem. Int. Ed.* **2012**, 51, 5634-5637.

[204] Zhang, Y.; Jiang, W.; Wang, L., Microfluidic synthesis of copper nanofluids. *Microfluid. Nanofluid.* **2010**, 9, 727-735.

[205] Zhang, J.; Coulston, R. J.; Jones, S. T.; Geng, J.; Scherman, O. A.; Abell, C., One-Step Fabrication of Supramolecular Microcapsules from Microfluidic Droplets. *Science* **2012**, 335, 690-694.

[206] Abraham, S.; Jeong, E. H.; Arakawa, T.; Shoji, S.; Kim, K. C.; Kim, I.; Go, J. S., Microfluidics assisted synthesis of well-defined spherical polymeric microcapsules and their utilization as potential encapsulants. *Lab Chip* **2006**, 6, 752-756.

[207] Choi, C.-H.; Jung, J.-H.; Kim, D.-W.; Chung, Y.-M.; Lee, C.-S., Novel one-pot route to monodisperse thermosensitive hollow microcapsules in a microfluidic system. *Lab Chip* **2008**, 8, 1544-1551.

[208] Priest, C.; Quinn, A.; Postma, A.; Zelikin, A. N.; Ralston, J.; Caruso, F., Microfluidic polymer multilayer adsorption on liquid crystal droplets for microcapsule synthesis. *Lab Chip* **2008**, 8, 2182-2187.

[209] Gokmen, M. T.; De Geest, B. G.; Hennink, W. E.; Du Prez, F. E., "Giant" Hollow Multilayer Capsules by Microfluidic Templating. *ACS Appl. Mater. Interfaces* **2009**, 1, 1196-1202.

[210] Tu, F.; Lee, D., Controlling the Stability and Size of Double-Emulsion-Templated Poly(lactic-co-glycolic) Acid Microcapsules. *Langmuir* **2012**, 28, 9944-9952.

[211] Abate, A. R.; Thiele, J.; Weitz, D. A., One-step formation of multiple emulsions in microfluidics. *Lab Chip* **2011**, 11, 253-258.

[212] Hennequin, Y.; Pannacci, N.; de Torres, C. n. P.; Tetradis-Meris, G.; Chapuliot, S.; Bouchaud, E.; Tabeling, P., Synthesizing Microcapsules with Controlled Geometrical and Mechanical Properties with Microfluidic Double Emulsion Technology. *Langmuir* **2009**, 25, 7857-7861.

[213] Ziemecka, I.; van Steijn, V.; Koper, G. J. M.; Kreutzer, M. T.; van Esch, J. H., All-aqueous core-shell droplets produced in a microfluidic device. *Soft Matter* **2011**, 7, 9878-9880.

[214] Kanai, T.; Lee, D.; Shum, H. C.; Shah, R. K.; Weitz, D. A., Gel-Immobilized Colloidal Crystal Shell with Enhanced Thermal Sensitivity at Photonic Wavelengths. *Adv. Mater.* **2010**, 22, 4998-5002.

[215] Kim, J.-W.; Utada, A. S.; Fernández-Nieves, A.; Hu, Z.; Weitz, D. A., Fabrication of Monodisperse Gel Shells and Functional Microgels in Microfluidic Devices. *Angew. Chem. Int. Ed.* **2007**, 46, 1819-1822.

[216] Liu, L.; Yang, J.-P.; Ju, X.-J.; Xie, R.; Yang, L.; Liang, B.; Chu, L.-Y., Microfluidic preparation of monodisperse ethyl cellulose hollow microcapsules with non-toxic solvent. *J. Colloid Interface Sci.* **2009**, 336, 100-106.

[217] Ren, P.-W.; Ju, X.-J.; Xie, R.; Chu, L.-Y., Monodisperse alginate microcapsules with oil core generated from a microfluidic device. *J. Colloid Interface Sci.* **2010**, 343, 392-395.

[218] Miesch, C.; Kosif, I.; Lee, E.; Kim, J.-K.; Russell, T. P.; Hayward, R. C.; Emrick, T., Nanoparticle-Stabilized Double Emulsions and Compressed Droplets. *Angew. Chem. Int. Ed.* **2012**, 51, 145-149.

[219] Lee, M. H.; Hribar, K. C.; Brugarolas, T.; Kamat, N. P.; Burdick, J. A.; Lee, D., Harnessing Interfacial Phenomena to Program the Release Properties of Hollow Microcapsules. *Adv. Funct. Mater.* **2012**, 22, 131-138.

[220] Seiffert, S.; Thiele, J.; Abate, A. R.; Weitz, D. A., Smart Microgel Capsules from Macromolecular Precursors. *J. Am. Chem. Soc.* **2010**, 132, 6606-6609.

[221] Chu, L.-Y.; Utada, A. S.; Shah, R. K.; Kim, J.-W.; Weitz, D. A., Controllable Monodisperse Multiple Emulsions. *Angew. Chem. Int. Ed.* **2007**, 46, 8970-8974.

[222] Wang, W.; Xie, R.; Ju, X.-J.; Luo, T.; Liu, L.; Weitz, D. A.; Chu, L.-Y., Controllable microfluidic production of multicomponent multiple emulsions. *Lab Chip* **2011**, 11, 1587-1592.

[223] Kim, S.-H.; Hwang, H.; Lim, C. H.; Shim, J. W.; Yang, S.-M., Packing of Emulsion Droplets: Structural and Functional Motifs for Multi-Cored Microcapsules. *Adv. Funct. Mater.* **2011**, 21, 1608-1615.

[224] Thiele, J.; Seiffert, S., Double emulsions with controlled morphology by microgel scaffolding. *Lab Chip* **2011**, 11, 3188-3192.

[225] Huang, K.-S.; Lai, T.-H.; Lin, Y.-C., Manipulating the generation of Ca-alginate microspheres using microfluidic channels as a carrier of gold nanoparticles. *Lab Chip* **2006**, 6, 954-957.

[226] Abalde-Cela, S.; Auguie, B.; Fischlechner, M.; Huck, W. T. S.; Alvarez-Puebla, R. A.; Liz-Marzan, L. M.; Abell, C., Microdroplet fabrication of silver-agarose nanocomposite beads for SERS optical accumulation. *Soft Matter* **2011**, 7, 1321-1325.

[227] Chabert, M.; Viovy, J.-L., Microfluidic high-throughput encapsulation and hydrodynamic self-sorting of single cells. *Proc. Natl. Acad.* **2008**, 105, 3191-3196.

[228] Kumachev, A.; Greener, J.; Tumarkin, E.; Eiser, E.; Zandstra, P. W.; Kumacheva, E., High-throughput generation of hydrogel microbeads with varying elasticity for cell encapsulation. *Biomaterials* **2011**, 32, 1477-1483.

[229] Koster, S.; Angile, F. E.; Duan, H.; Agresti, J. J.; Wintner, A.; Schmitz, C.; Rowat, A. C.; Merten, C. A.; Pisignano, D.; Griffiths, A. D.; Weitz, D. A., Drop-based microfluidic devices for encapsulation of single cells. *Lab Chip* **2008**, 8, 1110-1115.

[230] Liu, K.; Deng, Y.; Zhang, N.; Li, S.; Ding, H.; Guo, F.; Liu, W.; Guo, S.; Zhao, X.-Z., Generation of disk-like hydrogel beads for cell encapsulation and manipulation using a droplet-based microfluidic device. *Microfluid. Nanofluid.* **2012**, 1-7.

[231] Jongin Hong and Andrew, J. d. a. S. N. J., Bio-electrospraying and droplet-based microfluidics: control of cell numbers within living residues. *Biomed. Mater.* **2010**, 5, 021001-021007.

[232] Stachowiak, J. C.; Richmond, D. L.; Li, T. H.; Liu, A. P.; Parekh, S. H.; Fletcher, D. A., Unilamellar vesicle formation and encapsulation by microfluidic jetting. *Proc. Natl. Acad.* **2008**, 105, 4697-4702.

[233] Richmond, D. L.; Schmid, E. M.; Martens, S.; Stachowiak, J. C.; Liska, N.; Fletcher, D. A., Forming giant vesicles with controlled membrane composition, asymmetry, and contents. *Proc. Natl. Acad.* **2011**, 108, 9431-9436.

[234] Kamat, N. P.; Lee, M. H.; Lee, D.; Hammer, D. A., Micropipette aspiration of double emulsion-templated polymersomes. *Soft Matter* **2011**, 7, 9863-9866.

[235] Shum, H. C.; Kim, J.-W.; Weitz, D. A., Microfluidic Fabrication of Monodisperse Biocompatible and Biodegradable Polymersomes with Controlled Permeability. *J. Am. Chem. Soc.* **2008**, 130, 9543-9549.

[236] Nishimura, K.; Suzuki, H.; Toyota, T.; Yomo, T., Size control of giant unilamellar vesicles prepared from inverted emulsion droplets. *J. Colloid Interface Sci.* **2012**, 376, 119-125.

[237] Brown, L.; McArthur, S. L.; Wright, P. C.; Lewis, A.; Battaglia, G., Polymersome production on a microfluidic platform using pH sensitive block copolymers. *Lab Chip* **2010**, 10, 1922-1928.

[238] Sugiura, S.; Kuroiwa, T.; Kagota, T.; Nakajima, M.; Sato, S.; Mukataka, S.; Walde, P.; Ichikawa, S., Novel Method for Obtaining Homogeneous Giant Vesicles from a Monodisperse Water-in-Oil Emulsion Prepared with a Microfluidic Device. *Langmuir* **2008**, 24, 4581-4588.

[239] Kuroiwa, T.; Kiuchi, H.; Noda, K.; Kobayashi, I.; Nakajima, M.; Uemura, K.; Sato, S.; Mukataka, S.; Ichikawa, S., Controlled preparation of giant vesicles from uniform water droplets obtained by microchannel emulsification with bilayer-forming lipids as emulsifiers. *Microfluid. Nanofluid.* **2009**, 6, 811-821.

[240] Mabrouk, E.; Cuvelier, D.; Pontani, L.-L.; Xu, B.; Levy, D.; Keller, P.; Brochard-Wyart, F.; Nassoy, P.; Li, M.-H., Formation and material properties of giant liquid crystal polymersomes. *Soft Matter* **2009**, 5, 1870-1878.

[241] Ota, S.; Yoshizawa, S.; Takeuchi, S., Microfluidic Formation of Monodisperse, Cell-Sized, and Unilamellar Vesicles. *Angew. Chem. Int. Ed.* **2009**, 48, 6533-6537.

[242] Lorenceau, E.; Utada, A. S.; Link, D. R.; Cristobal, G.; Joanicot, M.; Weitz, D. A., Generation of Polymerosomes from Double-Emulsions. *Langmuir* **2005**, 21, 9183-9186.

[243] Foster, T.; Dorfman, K. D.; Ted Davis, H., Giant biocompatible and biodegradable PEG–PMCL vesicles and microcapsules by solvent evaporation from double emulsion droplets. *J. Colloid Interface Sci.* **2010**, 351, 140-150.

[244] Thiele, J.; Abate, A. R.; Shum, H. C.; Bachtler, S.; Förster, S.; Weitz, D. A., Fabrication of Polymersomes using Double-Emulsion Templates in Glass-Coated Stamped Microfluidic Devices. *Small* **2010**, 6, 1723-1727.

[245] Hettiarachchi, K.; Lee, A. P., Polymer–lipid microbubbles for biosensing and the formation of porous structures. *J. Colloid Interface Sci.* **2010**, 344, 521-527.

[246] Shum, H. C.; Lee, D.; Yoon, I.; Kodger, T.; Weitz, D. A., Double Emulsion Templated Monodisperse Phospholipid Vesicles. *Langmuir* **2008**, 24, 7651-7653.

[247] Kim, S.-H.; Shum, H. C.; Kim, J. W.; Cho, J.-C.; Weitz, D. A., Multiple Polymersomes for Programmed Release of Multiple Components. *J. Am. Chem. Soc.* **2011**, 133, 15165-15171.

[248] Thiam, A. R.; Bremond, N.; Bibette, J., From Stability to Permeability of Adhesive Emulsion Bilayers. *Langmuir* **2012**, 28, 6291-6298.

[249] Shum, H. C.; Zhao, Y.-j.; Kim, S.-H.; Weitz, D. A., Multicompartment Polymersomes from Double Emulsions. *Angew. Chem. Int. Ed.* **2011**, 50, 1648-1651.

[250] Perro, A.; Nicolet, C. l.; Angly, J.; Lecommandoux, S. b.; Le Meins, J.-F. o.; Colin, A., Mastering a Double Emulsion in a Simple Co-Flow Microfluidic to Generate Complex Polymersomes. *Langmuir* **2010**, 27, 9034-9042.

[251] Hayward, R. C.; Utada, A. S.; Dan, N.; Weitz, D. A., Dewetting Instability during the Formation of Polymersomes from Block-Copolymer-Stabilized Double Emulsions. *Langmuir* **2006**, 22, 4457-4461.

[252] Shum, H. C.; Santanach-Carreras, E.; Kim, J.-W.; Ehrlicher, A.; Bibette, J.; Weitz, D. A., Dewetting-Induced Membrane Formation by Adhesion of Amphiphile-Laden Interfaces. *J. Am. Chem. Soc.* **2011**, 133, 4420-4426.

CHAPTER II

Materials and Experimental Methods

In this chapter we describe chemical syntheses, microfluidic device manufacturing procedures and computational fluid dynamics modeling employed in the thesis. The first part describes materials and supplies used to implement our experiments. The second part describes in detail experimental methods used in the each chapter.

II.1 Materials and equipment

II.1.1 Materials

Table II-1. Chemicals and additional supplies used in this thesis.

Name	Description	Purity	Supplier
1-octadecene	$CH_3(CH_2)_{15}CH=CH_2$	90%	Sigma-Aldrich
1-decanol	$CH_3(CH_2)_9OH$	99%	Sigma-Aldrich
1,6 hexanedioldiacrylate	$[H_2C=CHCO_2(CH_2)_3-]_2$	80%	Sigma-Aldrich
2-hydroxyethyl methacrylate	$CH_2=C(CH_3)COOCH_2CH_2OH$	97%	Sigma-Aldrich
2-(dimethylamino) ethyl methacrylate	$C_7H_{15}O_2N$	98%	Sigma-Aldrich
2,2-dimethoxy-2-phenylacetophenone	$C_6H_5COC(OCH_3)_2C_6H_5$	99%	Sigma-Aldrich
2,2'-azobis(2-methylbutyronitrile)	$C_{10}H_{16}N_4$	≥98%	Sigma-Aldrich
Ammonium hydroxide	NH_4OH	35 vol%	Fisher
Aluminium oxide	Al_2O_3	98%	Sigma-Aldrich
Acetone	C_3H_6O	≥99%	VMR
Araldite-80805 epoxy adhesive	−	−	Wilkinson
Butyl methacrylate	$CH_2=C(CH_3)COO(CH_2)_3CH_3$	99%	Sigma-Aldrich
Copper (I) bromide	CuBr	≥98%	Sigma-Aldrich
ChromaZone® pigments	−	−	TMC Ltd.
Dibutyl phthalate	C_6H_4-1,2-$[CO_2(CH_2)_3CH_3]_2$	99%	Sigma-Aldrich
D-(+)-Glucose	$C_6H_{12}O_6$	≥99%	Sigma-Aldrich
Ethanol absolute	C_2H_6O	≥99.7%	VMR
Ethyl α-bromoisobutyrate	$(CH_3)_2CBrCOOC_2H_5$	98%	Sigma-Aldrich

Ethylene glycol dimethacrylate	$[CH_2=C(CH_3)COOCH_2-]_2$	98.0%	Sigma-Aldrich
Glycidyl methacrylate	$C_7H_{10}O_3$	97.0%	Sigma-Aldrich
Hydrogen peroxide	H_2O_2	30 wt%	Sigma-Aldrich
Iron (II) chloride tetrahydrate	$FeCl_2•4H_2O$	≥99%	Fluka
Iron (III) chloride hexahydrate	$FeCl_3•6H_2O$	≥99%	Acros
Isobornyl acrylate	$C_{13}H_{20}O_2$	t.g*	Sigma-Aldrich
Methyl methacrylate	$CH_2=CCOOCH_3$	99%	Sigma-Aldrich
Manganese oxide	MnO_2	≈85%	Sigma-Aldrich
Nitric acid	HNO_3	1M	Fisher
N-(*n*-propyl)-2-pyridylmethanimine	$C_{11}H_{19}N_2$	95%	Prepared[1]
Oleoresin paprika	–	–	Kalsec UK
Oleic acid	$C_{18}H_{34}O_2$	90%	Sigma-Aldrich
Poly(vinyl alcohol)	$[-CH_2CHOH-]_n$	87-89%	Sigma-Aldrich
Poly(dimethylsiloxane) 200 fluid	$(CH_3)_3SiOSi(CH_3)_3$	≥99%	Sigma-Aldrich
Polyvinylpirrolidone K90	$(C_6H_9NO)_n$	–	Fluka
Styrene	C_8H_8	≥99%	Sigma-Aldrich
Sodium 4-vinylbenzenesulfonate	$C_8H_7NaO_3S$	≥90%	Sigma-Aldrich
Sodium nitrate	$NaNO_3$	≥97%	Sigma-Aldrich
Silver nitrate	$AgNO_3$	≥99%	Sigma-Aldrich
Standard wall borosilicate capillaries	OD 1.0mm, ID 0.58mm	Harvard Apparatus	
Standard wall borosilicate capillaries	OD 3.0 mm, ID 1.62 mm	Harvard Apparatus	
Transparent C-FLEX® tubing	1/32" ID × 3/32" OD	Cole-Parmer	
32 gauge dispensing needles	ID 0.1 mm	Farnell UK	

UV LED diodes	200mcd, 405nm	Farnell UK

*t.g. – technical grade

II.1.2 Equipment

All procedures requiring mixing and/or heating were carried out using IKA WERKA magnetic stirrers. Glass capillaries were processed using a diamond scribe, mini drill kit (Farnell UK) and a P-2000 Laser Capillary Puller (Sutter Instruments). All sonication experiments were implemented using a Branson 450W digital sonifier with Ultra-Sonic probe at 70% amplitude. The fluid transfer and control over flow rates were performed by PHD2000 Harvard Apparatus precision pumps. Polymerization in capillary channels was induced using UV LED diodes and further continued in a 36 kW UV-light reactor. Surface tension measurements were performed using a Kruss DSA100 drop shape analysis machine. Optical micrographs were taken using a LEICA DM2500 microscope with Leica oil immersed lenses and attached Nikon® D5100 DSLR or Phantom® V7.3 high-speed cameras. Scanning electron microscopy with energy dispersive X-ray spectroscopy (EDAX) was performed on a Zeiss Supra® 55VP FEG/SEM. The models of the devices were drawn and rendered in Autodesk® AutoCAD® software programme. Fluid flow simulations were made using ANSYS Fluent® CFD software. All measurements on micrographs were performed using ImageJ software.

II.2 Experimental methods

II.2.1 Chapter III experimental

II.2.1.1 Synthesis of magnetic polymerisable colloidal suspension

Methyl methacrylate containing magnetic iron oxide (Fe_3O_4) nanoparticles coated with a surfactant were prepared by the method previously reported by Wooding *et al.*[2] and further developed by Shen *et al.*[3] and Maity *et al.*[4] is based on precipitation of Fe(II) and Fe(III) salts by NH_4OH in aqueous medium and consequent coating with oleic acid. $FeCl_3$•$6H_2O$ (2.35 g) and $FeCl_2$•$4H_2O$ (0.86 g) were dissolved in 40 mL of deionized water and once dissolved degassed with N_2 for 30 min. The solution was heated to 90 °C and vigorously stirred for 1h. Subsequently NH_4OH (5 mL) was added to the heated solution followed by oleic acid (1 mL). The mixture was stirred for another 30 min. After cooling to room temperature magnetite nanoparticles were flocculated by addition of acetone (200 mL) and isolated by magnetic decantation. The precipitate was washed ten times with ethanol/acetone mixture (1:1 vol. ratio) to remove excess of oleic acid and dried at 60 °C for 8h. 0.05 g (5 wt% of the yield) of the obtained magnetic nanoparticles was dispersed in MMA (10 g) by Branson 450 sonifier (1h, 70% amplitude). During the sonication the monomer vial was placed into the ice bath to avoid the heat induced polymerization. The synthesised colloidal particles were stable in the monomer for at least one year.

II.2.1.2 Preparation of solutions for silver deposition

Silver nanoparticles which can selectively cover the hydrophilic surface were produced by silver reduction[5] of a blend of two solutions. Solution A was prepared as

follows. $AgNO_3$ (0.075g) was dissolved in 2.5 mL of H_2O, after that NH_4OH (3.5 wt%, 1 mL) was added dropwise until a black precipitate was dissolved. Subsequently, 10 mL of NaOH (1 wt%) was added which led to the formation of precipitate, followed by 1.5 mL of NH_4OH in order to dissolve it. Solution B consisted of glucose (0.26g) dissolved in 5 mL of H_2O of deionized water and 0.05 mL of HNO_3, which was heated to 90 °C and cooled to room temperature before usage. Both components were mixed in 10:1 ratio respectively in order to induce silver particles synthesis.

$$2Ag^{+} + 2NH_4^{-} + OH^{-} \rightarrow 2[Ag(NH_3)_2]OH \qquad \textbf{Solution A}$$

Silver reduction:

$$R{-}CH{=}O + 2[Ag(NH_3)_2]OH \rightarrow RCOONH_4 + 2Ag\downarrow + 3NH_3 + H_20$$

II.2.1.3 Polymer "microbuckets" fabrication

In Table III-1 the compositions of dispersed monomer(s)/silicone oil mixtures used to fabrication of above noted types of "microbuckets" are shown.

Table II-1. The composition of blends used to fabricate "microbuckets" with lids and without.

Number/Chemical	MMA, mL	Styrene, mL	HEMA, mL	HDDA, mL	PDMS, mL
1 (lid)	0.9	x	x	x	0.1
2 (lid)	0.8	x	x	x	0.2
3 (lid)	0.7	x	x	x	0.3
4 (no lid)	0.5	0.35	x	0.05	0.1
5 (no lid)	0.45	0.35	0.05	0.05	0.1

"Microbuckets" with Lids. PMMA buckets in which the internal volume was closed were synthesized by the following procedure. Three polymerisable blends were prepared in the following ratios: 90 vol% of MMA and 10 vol% of PDMS, 80 vol% of MMA and 20 vol% of PDMS, 70 vol% of MMA and 30 vol% of PDMS. 2,2-dimethoxy-2-phenylacetophenone (0.035g) was dissolved in the MMA/PDMS mixture (1 mL) and dispersed in the continuous phase utilizing the above noted droplet generator. An aqueous PVA solution (1 wt%) was used to provide colloidal stability and prevent coalescence of the MMA/PDMS droplets. Typical flow rates of 0.2 mL min^{-1} and 0.015 mL min^{-1} were used for the continuous and the dispersed phases. MMA/PDMS droplets were collected into the vial and polymerized in a UV-reactor for 15 min.

Lidless "Microbuckets" Fabrication. In order to prevent the formation of the lid, the following modifications were implemented. The dispersed phase consisted of 50 vol% of MMA, 35 vol% of styrene, 5 vol% of HDDA and 10 vol% of PDMS (1 mL) with dissolved 0.035g of the photoinitiator. The continuous phase (PVA, 1 wt%) was pumped into the device at 0.2 mL min^{-1} flow rate, while dispersed at 0.015 ml min^{-1}. The droplets were collected into the vial and subsequently exposed to the UV light for 45 min to form the lidless "microbuckets".

Chemical Functionalisation of "Microbuckets". The magnetic amphiphilic "microbuckets" were synthesized by the following procedure. The oil phase consisted of 40 vol% of MMA, 5 vol% of the magnetic MMA, 35 vol% of styrene, 5 vol% of HEMA, 5 vol% of HDDA, 10vol% of PDMS (1 mL) and the photoinitiator (0.035 g) was dispersed in the aqueous PVA (1 wt%) solution *via* microfluidic droplet generator. Typical flow rates were 0.2 ml min^{-1} and 0.015 mL $min^{-1}$for the continuous and

dispersed phases respectively. The subsequent exposure of the droplets to the 36 kW UV-light lead to formation of "microbuckets" (see Figure II-1).

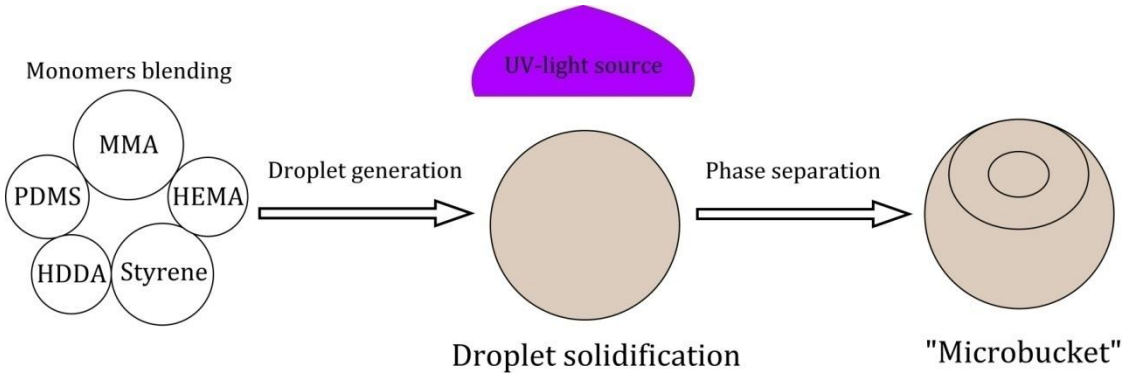

Figure II-1. Schematic synthesis of amphiphilic "microbuckets. The process consists of three stages: preparation of monomers/silicone mixture; dispersion using microfluidic droplet generator; UV irradiation of droplets.

II.2.1.4 Surface tension measurements

The value of surface tension at the air/liquid interface of each compound was measured employing the pendant drop method. Surface tensions at the aqueous PVA/monomer mixture were calculated using Antonov's rule.[6,7] Prior to the measurement a syringe filled with required mixture was fixed in the Kruss DSA100 machine, so that the needle tip was visible to its camera. 7 µL of liquid was pushed out from the syringe forming a hanging drop on the needle tip. Each droplet was kept in one position for 1 min to reach hydromechanical equilibrium before the start of calculation. After this calculations carried out by machine's software were run. We used the most accurate Young-Laplace fitting method,[8] which considers the value of the surface tension using following equation:

$$\Delta\rho = \sigma\left(\frac{1}{r_1} + \frac{1}{r_2}\right) \qquad \textbf{Equation II-1}$$

Where Δρ represents a difference in Laplace pressure, σ– surface tension,r_1 and r_2– principal radii of a curvature.

Method Explanation: For a pendant drop which is rotationally symmetrical in the z-direction then, based on Equation II-1, it is possible to give an analytically accurate geometric description of the principal radii of curvature. The tangent at the intersection of the z-axis with the apex of the drop forms the x-axis. The drop profile is given by pairs of values (x,z) in the x-z-plane.

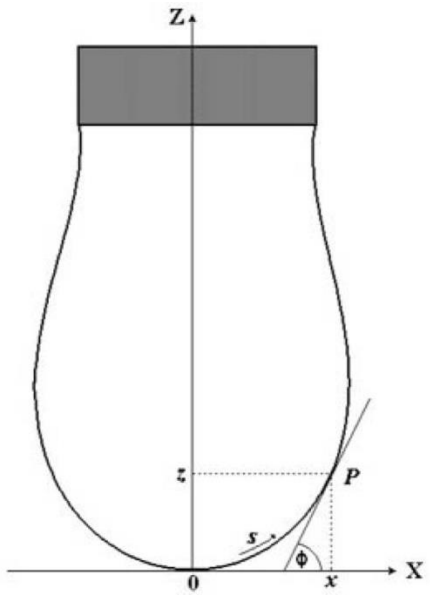

Figure II-2. Geometry of the pendant drop. Reproduced from the reference [8].

In hydromechanical equilibrium the following relationship applies:

$$\Delta p_{apex} - \Delta p_P = z \Delta p g \qquad \textbf{Equation II-2}$$

Where $\Delta\rho_{apex}$ – pressure difference at apex, $\Delta\rho_P$ – pressure difference at point P (x, z axis), $\Delta\rho$ – difference in pressure the drop liquid and surroundings, g – acceleration due to the gravity.

With principal curvatures k (reciprocal value of principal curvature radius r) and the Young-Laplace equation (Equation II-1) we obtain:

$$\Delta p_{apex} = \sigma(k_{apex,1} + k_{apex,2}) \qquad \textbf{Equation II-3}$$

$$\Delta p_P = \sigma(k_{P,1} + k_{P,2}) \qquad \textbf{Equation II-4}$$

where $k_{apex,1(2)}$– principal curvatures at apex, $k_{p,1(2)}$ – principal curvatures at point P.

Because the axial symmetry of the drop, the principal curvatures at the apex are the same in all directions (→k_{apex}). From differential geometry the analytical expressions for the curvatures of the principal normal sections at the point P (x, z) are known:

$$k_{P,1} = \frac{d\varphi}{ds} = \frac{d^2z}{dx^2}\left(1 + \left(\frac{dz}{dx}\right)^2\right)^{-3/2} \qquad \textbf{Equation II-5}$$

$$k_{P,2} = \frac{sin\varphi}{x} = \left(\frac{dz}{dx}\right)\frac{1}{x}\left(1 + \left(\frac{dz}{dx}\right)^2\right)^{-1/2} \qquad \textbf{Equation II-6}$$

From the Equations II-5 and 6 we obtain:

$$\frac{d\varphi}{ds} = 2k_{apex} - \frac{z\Delta pg}{\sigma} - \frac{sin\varphi}{x} \qquad \textbf{Equation II-7}$$

where S – length of arc along the drop profile, φ – angle between the tangents at point P(x, z) and x-axis.

Equation II-7 describes the profile of a pendant drop in hydromechanical equilibrium. The Equation is converted into a dimensionless form to solve it. The following definitions are used:

$$X = \frac{x}{a};\ Z = \frac{z}{a};\ S = \frac{s}{a};\ B = \frac{1}{ak_{apex}};\ a = \sqrt{\frac{\sigma}{\Delta\rho g}};$$

where B – dimensionless parameter of the drop, a – capillary constant.

With these definitions Equitation II-7 can also be expressed in the following way:

$$\frac{d\varphi}{dS} = \frac{2}{B} - Z - \frac{sin\varphi}{X};\ \frac{dX}{dS} = \cos\varphi;\ \frac{dZ}{dS} = \sin\varphi; \qquad \textbf{Equation II-8}$$

At the apex limiting conditions apply X=Z=S=φ=0 apply. This results in:

$$\frac{sin\varphi}{X} = \frac{1}{B} \qquad \textbf{Equation II-9}$$

B is only parameter to determine the shape of the drop profile. It is therefore known as the form parameter. In addition, it can be seen that the surface tension can be calculated for a known difference in density Δρ if the relative size ratio of a measured drop can be determined for the corresponding theoretical drop profile.

Equation II-9 is, together with the limiting conditions from Equation II-8, known as the fundamental equation for a pendant drop.

By varying the form parameter B it is possible to calculate theoretical drop profiles after carrying out a numerical integration method. If the theoretical drop profile corresponds to the measured drop profile then the surface tension can be calculated. The problem in measuring the interfacial tension therefore consists in determining the correct theoretical drop profile for a measured drop exactly and rapidly.

The Young-Laplace fitting method explanation was reproduced from the reference [8].

II.2.1.5 Microfluidic droplet generator manufacture

The concept of the microfluidic device was based on work by Quevedo *et al.*,[9] however several modifications were made. A standard wall borosilicate capillary was narrowed by heating and pulling on a P-2000 Laser Capillary Puller (Sutter Instruments) and used as the main channel. The dispersed phase was delivered to the droplet formation section via the 32 gauge needle which was bent and inserted in the main capillary through a hole made with a diamond scribe. The needle tip was placed in the

narrowed area of the main channel in order to focus the flow and decrease the size of the droplets. Another end of the needle was fixed in the standard borosilicate capillary by epoxy glue and both channels were attached on the glass slide (see Figure II-3). The device was connected to the precision pumps (PHD2000, purchased from Harvard Apparatus) with flexible PVC tubing.

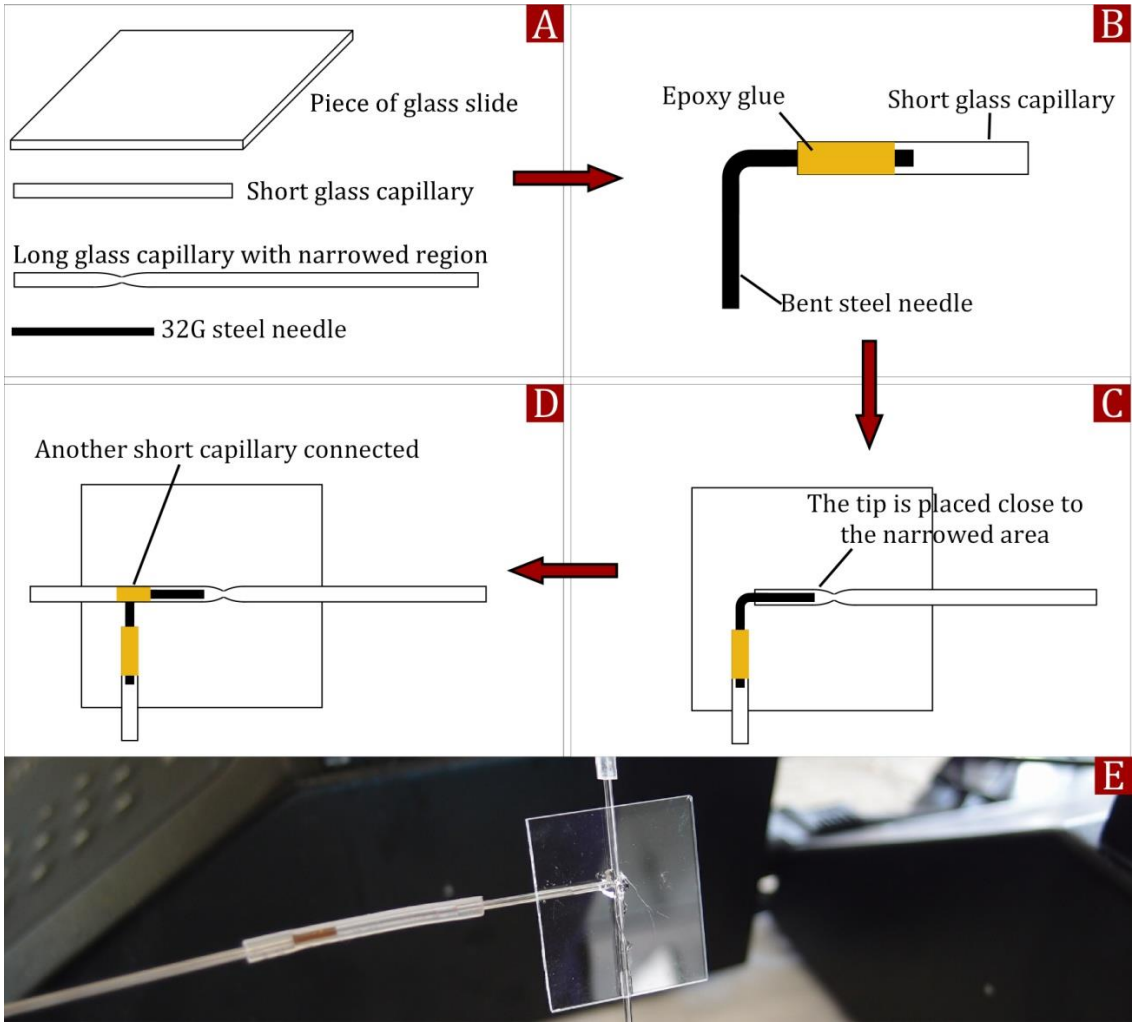

Figure II-3. Microfluidic device fabrication procedure. (A) Required components: 32G needle, rectangular piece of microscopy slide, narrowed and standard wall borosilicate capillaries. (B) The short capillary needs to be cut for two pieces. The needle then is fixed in one piece of the short capillary by epoxy glue. (C) Loose end of the needle tip is placed in the narrowed area of the long capillary forming the flow-focusing droplet formation region. (D) Another piece of the short capillary is connected to the long forming the inlet channel for the continuous phase. The fracture is blanked off with epoxy glue and all capillaries are glued on the glass slide. (E) The microfluidic device in action.

II.2.2 Chapter IV experimental

In the Chapter IV we used magnetic polymerisable colloidal suspension. The method of preparation is described in the paragraph **II.2.1.1**.

II.2.2.1 Fabrication of Janus particles

In the above of the microfluidics device that two separate flows of the reagent mixtures should be pumped into the dispersing channel to form a Janus droplet after injection into the continuous phase. In order to form a Janus droplet the phases should not mix after the contact, which implies the use of two immiscible liquids. The immiscibility can be natural or achieved specially for a particular application by increasing viscosity of the liquids. The following sections describe preparation of viscous mixtures and their use in the synthesis of Janus particles.

Hydrophilic/hydrophobic Janus particles. 0.025 g of the 2,2-dimethoxy-2-phenylacetophenone photoinitiator was dissolved in MMA (10 g), after which the solution was UV irradiated in a 36 kW reactor for 45 minutes. Further, MMA (5.0 g) was mixed with prepolymer in order to reduce viscosity. The obtained prepolymer solution was used as the hydrophobic phase. 0.025g of the photoinitiator was dissolved in the mixture of MMA (8.5 g) and HEMA (1.5 g) followed by exposure to the UV-light for 25 minutes in the same reactor. The synthesized prepolymer liquid was diluted with MMA (5.0 g) and used as the hydrophilic phase. Before dispersion 1 mL of each phase was mixed with 0.01g of the photoinitiator in order to initiate further solidification. The continuous phase consisted of 1:1 mixture of glycerol and aqueous PVA solution (1.0 wt%) in order to increase the viscosity and stabilize droplets of the dispersed phase. Both double T-junction and co-flow Janus droplet generators were

used to make biphasic droplets. Typical flow rates were 0.01 mL min^{-1} for the each dispersed phase and 0.125 mL min^{-1} for the continuous phase. The droplets were collected into vial, and solidified in the UV reactor for 60 minutes.

Magnetic/non-magnetic Janus particles. 0.025 g of the photoinitiator was dissolved in MMA (10.0 g) followed by 45 minutes irradiation with UV light in the reactor to prepolymerize. After this, a magnetic suspension of iron oxide nanoparticles in MMA (5.0 g with 1.0 wt% of nanoparticles) was added in order to reduce the viscosity. This mixture was used as the "magnetic phase" of the Janus particles. A non-magnetic phase was prepared by the same procedure as the above with the difference that no iron oxide particles were added upon dilution. Before dispersion, 1 mL of each of these two phases was mixed with 0.01g of the photoinitiator. Both liquids were dispersed in the continuous phase using the microfluidic devices. The continuous phase consisted of 1:1 mixture of glycerol and aqueous PVA solution (1 wt%). Typical flow rates were 0.01 mL min^{-1} for each of the dispersed phases and 0.125 mL min^{-1} for the continuous phase. The generated Janus droplets were collected into a vial and post-cured in the UV reactor for 60 minutes.

Solid/porous Janus particles. A prepolymerized PMMA solution as prepared above was used to form the solid hemisphere of the Janus particles. This phase contained 1.0 wt% of 2,2-dimethoxy-2-phenylacetophenone photoinitiator. We used two types of blends to make the porous part of the particles tuning it from mesoporous to macroporous. Both mixtures consisted of ethylene glycol dimethacrylate (16 vol%) and glycidyl methacrylate (24 vol%), but differed in the concentration of the porogen (60 vol%), which was dibutyl ether or 1-decanol for mesoporous and macroporous structures, respectively. 2,2-dimethoxy-2-phenylacetophenone photoinitiator (4.0 wt%) was employed in both cases. As continuous phase a 1:1 mixture of glycerol and aqueous

PVA solution (1 wt%) was employed. A typical flow rate of the continuous phase was 0.125 mL min^{-1}, while both dispersed flows were pumped in the channels at 0.01 mL min^{-1}. The particles were collected into a vial and placed in the UV reactor for 45 minutes. The obtained polymer "Janus" particles were washed in a ethanol/cyclohexane mixture (1:1 vol. ratio) in order to wash out the porogen.

II.2.2.2 Fluid flow simulations

The geometry consists of the fluid domain within the microfluidic and the details of the injection needles are preserved to study the hydrodynamic changes of the main flow streams. A 0.56 mm diameter of the columnar fluid domain was used for the simulation and the injection needles are represented as solid rods (D = 0.15 mm) within the fluid domain. Different arrangements of the injection needles within the fluid domain were simulated. The length of the geometry is 10 mm and the point of impact, i.e. the position of the injection needle, is placed at the length of 5 mm for most cases. Preliminary simulation results showed that fully developed flow profiles were always obtained before reaching the point of impact. The minimum orthogonal qualities of the geometries' meshes were controlled to be bigger than 0.2, which is good enough for ANSYS Fluent® CFD simulation.

II.2.2.3 Fabrication of microfluidic "Janus" droplet generators

Double T-junction layout. Two 32 gauge needles were fixed in standard borosilicate capillary pieces (OD 1.0 mm, ID 0.58 mm, Harvard Apparatus) by epoxy glue. Capillaries were 3D aligned leaving 0.2 mm between the needle tips by using optical microscope and glued to a piece of a glass slide. Subsequently, two pieces of

capillaries were attached on the glass slide so that they formed a perpendicular channel to capillaries with needles. Further, the junction was sealed with a fast-curing transparent epoxy glue. After these steps the device was connected to the PHD2000 pumps using C-FLEX® flexible PVC tubing (1/32"ID x 3/32"OD) and used for synthesis of Janus particles (see Figure II-4).

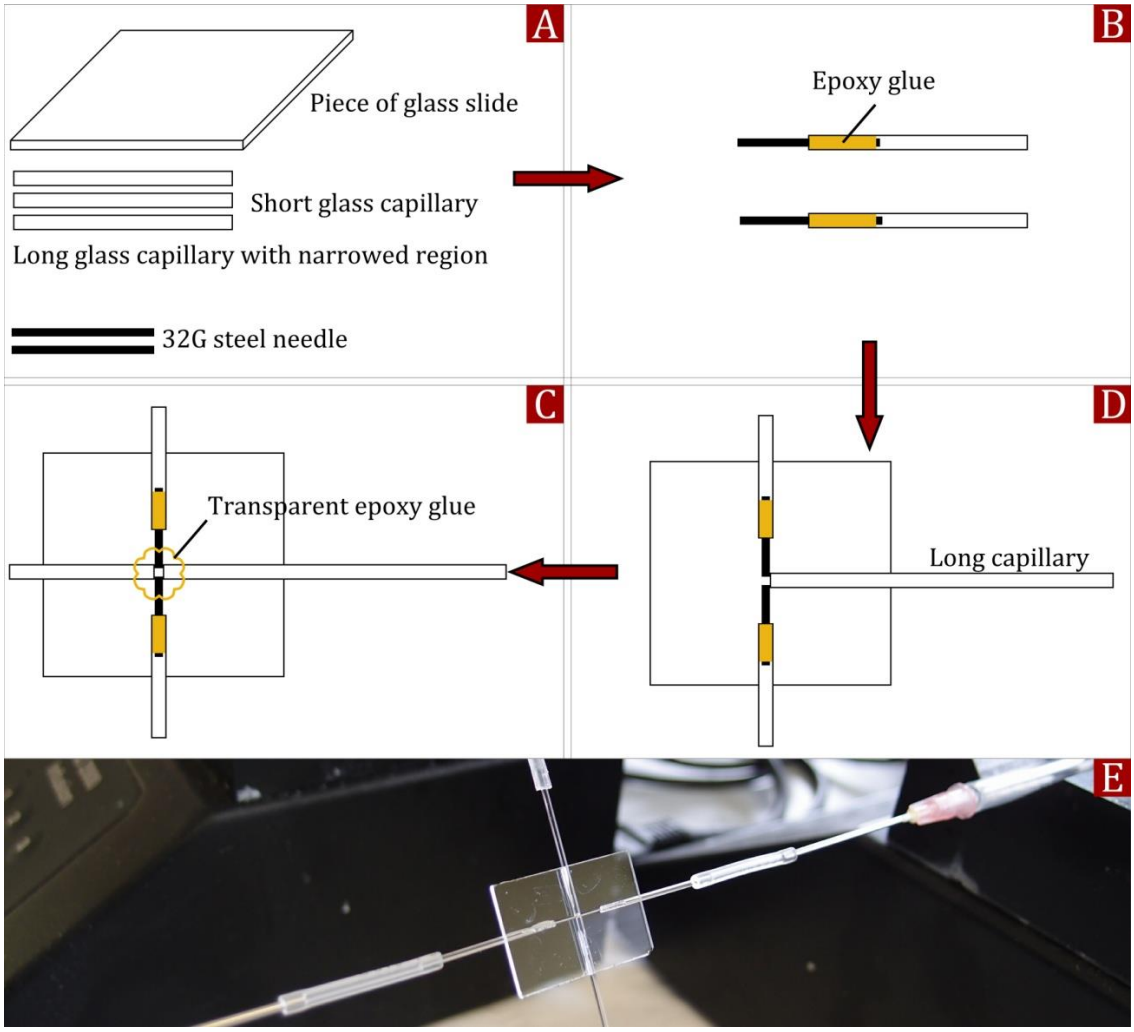

Figure II-4. Double T-junction device manufacture. (A) Materials required: two 32 gauge needles, glass slide, three short and one long borosilicate capillaries. (B) Short capillaries with attached needles. (C, D) Connection of two the short and long capillaries formed the orthogonal channel and imbedded the joint of needles into it.(E) The device in operation connected to syringe pumps.

Co-flow layout. Two 32 gauge needles were bent at 90° angle and connected to each other by epoxy glue so that tips were fixed on one line. The glass segments

deployed from each other at 180° angle, while paired needles were inserted into a capillary (OD 1.0 mm, ID 0.58 mm) forming a unit of the dispersed phases injection, followed by attaching it on a glass slide. The width of the double needle unit (~450 µm) allowed to place inside the main channel (~580 µm) leaving a sufficient distance to the walls in order to avoid potential wetting issues. A piece of capillary was placed at the junction forming an extension of the main channel, after which the joint was sealed with epoxy adhesive. C-FLEX® flexible PVC tubing (1/32"ID x 3/32"OD) was used to connect the device to the PHD2000 pumps and perform the fabrication procedure (see Figure II-5).

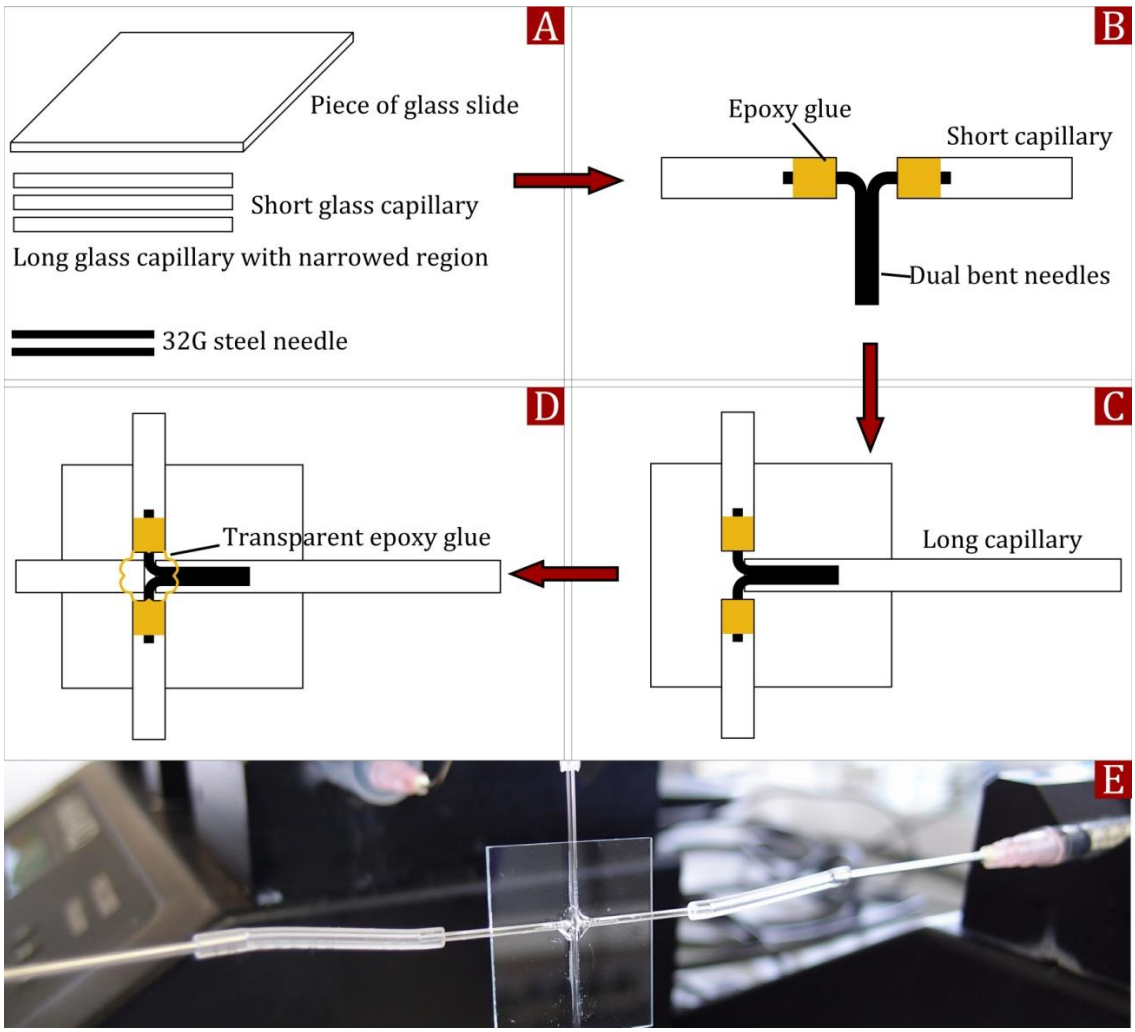

Figure II-5. Co-flow device assembly. (A) Materials required. (B) Paired needles formed the dispersed phase injector. (C, D) The injector was inserted into the capillary which formed the main channel after attaching another piece of the capillary and sealing the fracture. (E) The device in action connected to the pumps.

II.2.2.4 Nitrogen sorption porosimetry

Porosimetry samples were prepared by degassing to 15 µm Hg for 120 minutes, followed by a heating programme to 70 °C at a ramp rate of 10 °C per minute, and held for 120 minutes. Samples were backfilled with nitrogen prior to analysis. BJH measurements (HK method) were performed on Micromeritics ASAP 2020 using nitrogen at cryogenic temperature (77 °K), between a relative pressure of 0.50 and 0.99.

II.2.3 Chapter V experimental

In the Chapter V we studied fluid dynamics within the T-junction microfluidic device using ANSYS Fluent® CFD software. The method is described in the paragraph **II.2.2.2**.

II.2.3.1 Synthesis of waterborne ferrofluids

Iron oxide (Fe_3O_4) nanoparticles coated with a double layer of surfactant were synthesized by the technique first reported by Wooding *et al.*[2] and further developed by Shen *et al.*[3] and Maity *et al.*[4] which is based on the precipitation of Fe (II) and Fe (III) salts dissolved in distilled water by ammonium hydroxide (NH_4OH).The magnetite nanoparticles were obtained by dissolving $FeCl_3 \cdot 6H_2O$ (2.35 g) and $FeCl_2 \cdot 4H_2O$ (0.86 g) in 40 mL of deionised water under vigorous stirring while purging with nitrogen gas. The solution was heated to 90 °C and stirred for 1h. Subsequently NH_4OH (5 mL) was added followed by oleic acid (1 mL). The mixture was vigorously stirred for 30 min at 90 °C. After cooling to room temperature, acetone (200 mL) was added. This lead to flocculation of the Fe_3O_4 nanoparticles which were isolated by magnetic decantation. The precipitate was washed with a mixture of acetone and ethanol (1:1 volume ratio) ten

times to remove excess of oleic acid. The obtained Fe_3O_4nanoparticles which were coated with oleic acid were suspended in purified water (20 mL) and the slurry was heated to 80 °C under vigorous stirring. A solution of 10% (w/v) of ammonium salt of oleic acid was prepared separately by mixing 20 mL of water, 2 mL of oleic acid and 30 drops of NH_4OH. This solution was added dropwise to the slurry (typical amount is 5 mL) until a stable dispersion was obtained (see Figure II-6).

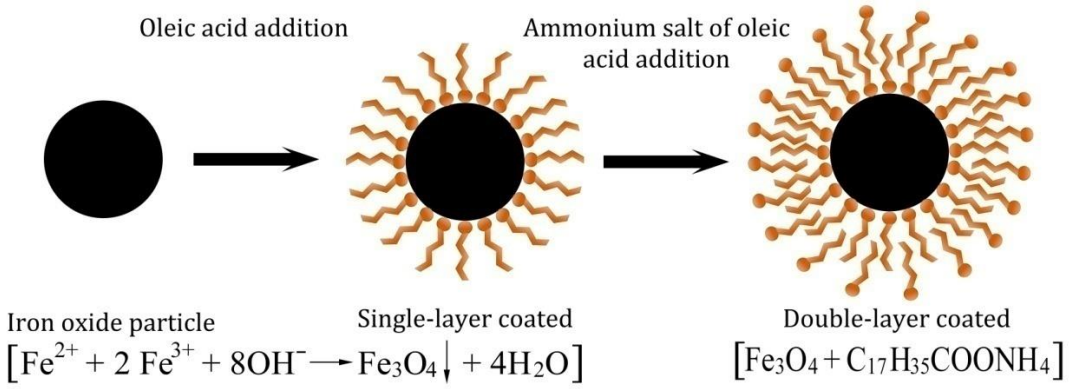

Figure II-6. Schematic representation of aqueous ferrofluid synthesis. Fe_3O_4 magnetite particles first coated with a single layer of surfactant. In the second stage single-layered magnetite particles were treated with ammonium salt of fatty acid and double-layered Fe_3O_4 particles were obtained.

II.2.3.2 Preparation of poly(isobornyl acrylate)capsules containing waterborne ferrofluid or ChromaZone® pigment

Typically 1 mL of ferrofluid as prepared was mixed with 2 mL of purified water and used as the inner dispersed phase (infused via the needle). The middle dispersed phase was isobornyl acrylate with 0.5 wt% of 2,2-dimethoxy-2-phenylacetophenone (infused via the PVC tubing). An aqueous 5 wt% PVA solution was used as outer continuous phase (infused via the larger glass capillary). Various flow rates were applied for the inner, middle and outer phase; typical values were 0.01 mL min^{-1}, 0.05 mL min^{-1} and 0.1 mL min^{-1} respectively. The obtained ferrofluid-in-IBA-in-water droplets were collected and irradiated with UV light for a few minutes in order to polymerize IBA and fabricate the polymer microcapsule. In the case of the waterborne

ChromaZone® pigment dispersion (inner dispersed phase) the flow rate of the inner phase was increased to 0.04 mL min^{-1}; the amount of photoinitiator was increased to 1 wt% in order to solidify the middle phase faster.

II.2.3.3 Fabrication of a simplified microfluidic device

A 100 mm length borosilicate glass capillary (OD 3.0 mm, ID 1.62 mm, Harvard Apparatus) and a 50 mm length borosilicate glass capillary (OD 1.0 mm, ID 0.58 mm Harvard Apparatus) were connected orthogonally by epoxy glue. A hole was made in the middle of the thicker capillary with a diamond scribe and the thinner capillary was inserted and fixed with epoxy glue. We found through fluid flow simulations and experiments that the optimal depth of penetration of the tip of the thinner capillary was at half the ID of the larger capillary. Transparent C-FLEX® flexible PVC tubing (1/32"ID x 3/32"OD) was connected to the inserted capillary and a 30 gauge needle which was bent at a 90° angle was perforated into the tubing so that the needle's tip was in the middle of the capillary and parallel to it (see Figure II-7). Fabrication of our device is obviously limited to the availability of capillaries and needles of small inner diameter. In general this means that droplets formed with commercially available materials typically are of the length scale of 0.1 mm.

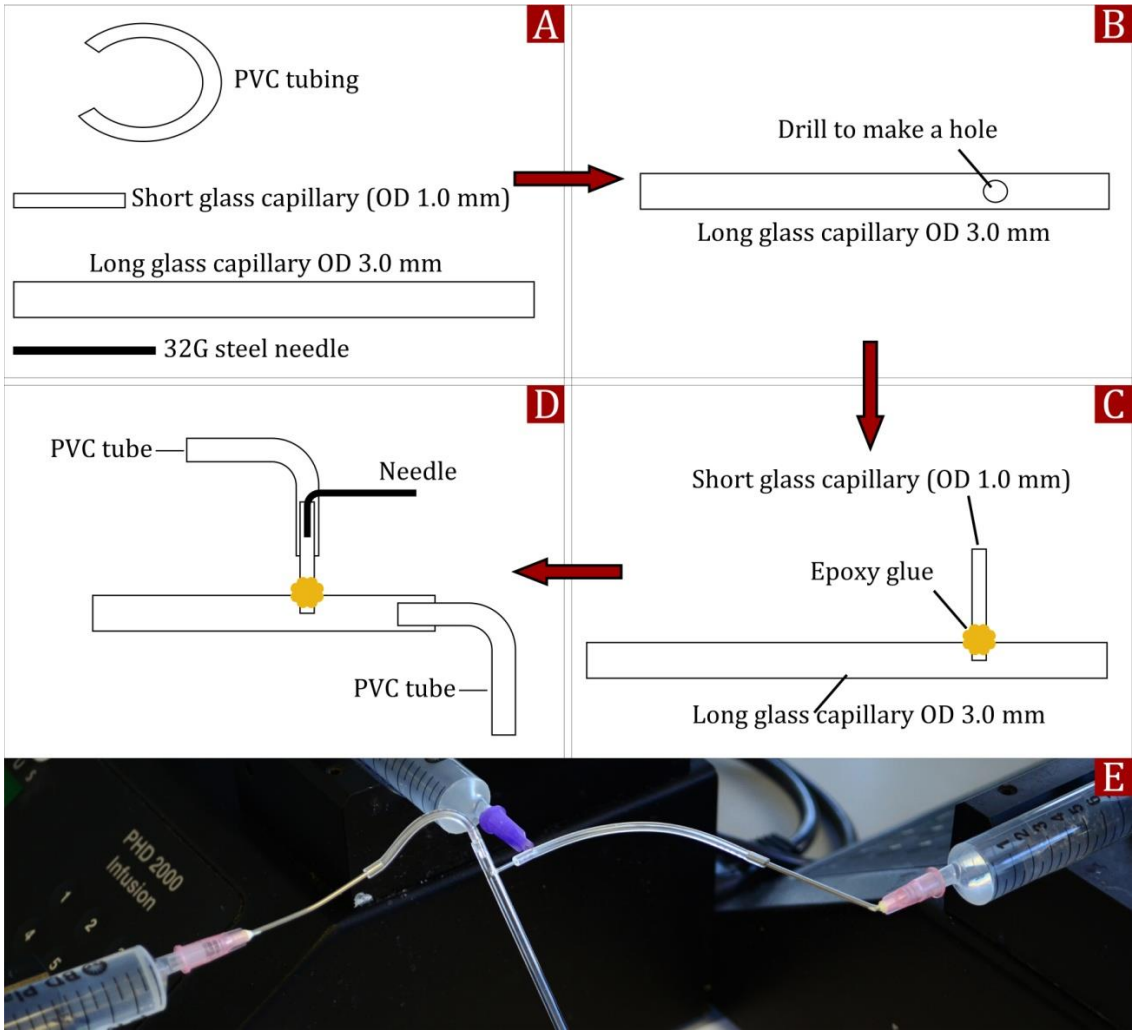

Figure II-7. The step-by-step fabrication of the microfluidic device. (A) Materials and equipment required: PVC tubing, 32G needle, short and long capillaries different in diameter. (B) A hole in the main capillary made by drilling using the mini drill kit or manually with scribe. (C) The short thinner capillary orthogonally inserted through the hole and sealed with glue. The penetration depth adjusted by using an optical microscope. (D) PVC tubing connected to the capillaries. (E) The device in action connected to the pumps.

II.2.4 Chapter VI experimental

In the Chapter VI we employed magnetic iron oxide nanoparticles. The synthetic procedures are described in the paragraph **II.2.1.1**. The method is identical, but obtained nanoparticles were not dispersed in the monomer to form the colloidal suspension.

II.2.4.1 Synthesis of poly(n-butyl methacrylate)-block-poly(2-(dimethylamino) ethyl methacrylate) (PBMA-block-PDMAEMA) by atomic transfer radical polymerisation(ATRP)

In a typical ATRP procedure, a Schlenk tube was charged with solvent, purified monomer, the initiator, and the Cu (I) catalyst such as CuBr. The mixture was de-aerated by three freeze-pump-thaw cycles, placed under a nitrogen gas atmosphere, and subsequently immersed into a preheated oil bath of 90°C. Next the ligand, PPMI was injected into the system by syringe to start the reaction. After the polymerization, the tube was rapidly cooled and exposed to air. The polymer was purified by precipitation in methanol at -30°C and further dried under vacuum. To synthesize PBMA, 10g of toluene, BMA (10g, 70mmol), Ethyl α-bromoisobutyrate (0.185g, 0.95mmol), CuBr (0.138g, 0.96mmol) were charged in the Schlenk tube. After the system reached 90°C, PPMI (0.3 mL, 1.94mmol) was injected and the solution turned to dark brown. The reaction was performed for four hours before quenching with cold water. $M_n$calc = 10000 Da. M_n (GPC) = 11605. PDI (GPC) = 1.14. To synthesize the block copolymer, the same protocol was applied except using the PBMA product as macroinitiator and DMAEMA as monomer. $M_n$calc = 15000 Da. M_n(GPC) = 14748. PDI (GPC) = 1.10.

II.2.4.2 Synthesis of highly cross-linked polystyrene particles covered with platinum nanoparticles

All syntheses of polystyrene particles were based on procedures reported by Winnik and co-workers[10] and El-Aasser and collegues.[11]

Highly cross-linked polystyrene particles: The reaction carried out in three stages. First of all, PVP K90 (1.0 g), Brij® 35 (0.35 g) and AMBN (0.25 g) were dissolved in styrene (6.25 g) and ethanol (18.75 g) in 250 mL round bottom flask. After

homogenization the solution was deoxygenated with N_2 for at least 30 minutes. Then the flask was placed into a 70 °C oil bath and stirred at 100 rpm under the nitrogen atmosphere in order to start the reaction. Secondly, 1 h after the start of the reaction a portion of styrene (6.25 g) and ethanol (18.75 g) was added into the flask to provide a growth of particles. Finally, 2 h after the addition of the second portion of styrene, a mixture of EGDMA (3 mL) and styrene (3 mL) was added in parts (0.6 mL) every 45 minutes into the flask. Then the reaction was run for another 16 hours. Obtained particles were separated by centrifugation and redispersed in ethanol in order to washout an excess of PVP. The cycle was repeated five times, after which particles dried at the room temperature for 24 h.

***Deposition of platinum nanoparticles on the polystyrene microbeads*:** Monodisperse highly cross-linked particles were covered with platinum nanoparticles by following procedure. A propylene centrifuge tube was filled with 20 mL of methanol in which0.01 g of highly cross-linked polystyrene particles was dispersed in 20 mL of methanol using sonication bath. The microscopy glass slide was placed into the tube so that half of it was under the liquid level. After that the centrifuge was placed into the oven and kept inside for 48 h at 60 °C to convectively assemble polystyrene particles on the glass slide. The glass slide was then placed into the sputter coater chamber used to prepare SEM samples and was subjected to platinum deposition for 3 cycles (metal evaporation time = 15 s). Obtained particles were washed from the glass with methanol before dispersion.

II.2.4.3 Fabrication of polymer vesicles using the simplified device

Double distilled deionized water was used as the inner phase. PBMA-block-PDMAEMA polymer was dissolved in the mixture of toluene (50%) and chloroform

(50%), so that final concentration was 5 g L^{-1}, and used as the middle phase. Aqueous PVA solution (1 wt%) employed as the outer phase. Typical flow rates used were 0.007 mL min^{-1}, 0.013 mL min^{-1} and 0.15 mL min^{-1} respectively. The solutions were pumped into the device by following order: outer → middle → inner in order to avoid any wetting issues. In all experiments on plating polymer vesicles with a colloidal armor solid content in the middle phase was 0.001 g mL^{-1}. The obtained double-emulsion droplets were collected into a vial which further was left on the table rotor to prevent agglutination while the middle phase solvent evaporates. The droplets were kept in the rotating vial until the all solvent evaporated and they transformed into polymer vesicles.

II.2.4.4 Double emulsion droplet generator assembly

A flow focussing area on the main channel was made on P-2000 machine. The machine heats the capillary with laser pulses and simultaneously pulls it, which results in the formation of two pieces of micropipettes. However, if the cycle is interrupted the capillary stays unbroken with a bottleneck-like area. We used the following machine settings: heat = 550 °K, filament = 4, velocity = 10, delay = 121, pull = 12. The cycle was stopped after three pulses of the laser. Further, at the distance of 15 mm from the thinnest part of the flow focussing area a hole was made by gentle scratching. A 40 mm long standard capillary was attached to the hole by epoxy adhesive forming the connected side channel at 90° angle. Thereafter, a 32 gauge needle was inserted inside the main channel placing the tip in the centre of the bottleneck area and fixed by epoxy glue. Simultaneously, adhesive blocked the capillary from the edge of the needle penetration making it an exclusive continuation of the channel. After this, a short capillary was drilled and divided so that cut line was in the centre of the perforated hole. The protrusive end of the needle was inserted in one of these pieces and fixed by epoxy

glue forming a new separated segment of the main channel. Another 32 gauge needle was bent at 90° angle and fixed in the piece of capillary with one end, while the other was aligned with the first needle's tip at a distance of 0.5 mm by means of the optical microscopy. Then the second part of the bisected capillary was connected with the first, seizing the needle inside, and forming the second orthogonal channel on the opposite side of the main channel, followed by sealing the hole with a fast curing epoxy glue. After these steps, the obtained device was attached to the microscopy glass slide in order to increase its structural strength (see Figure II-8).

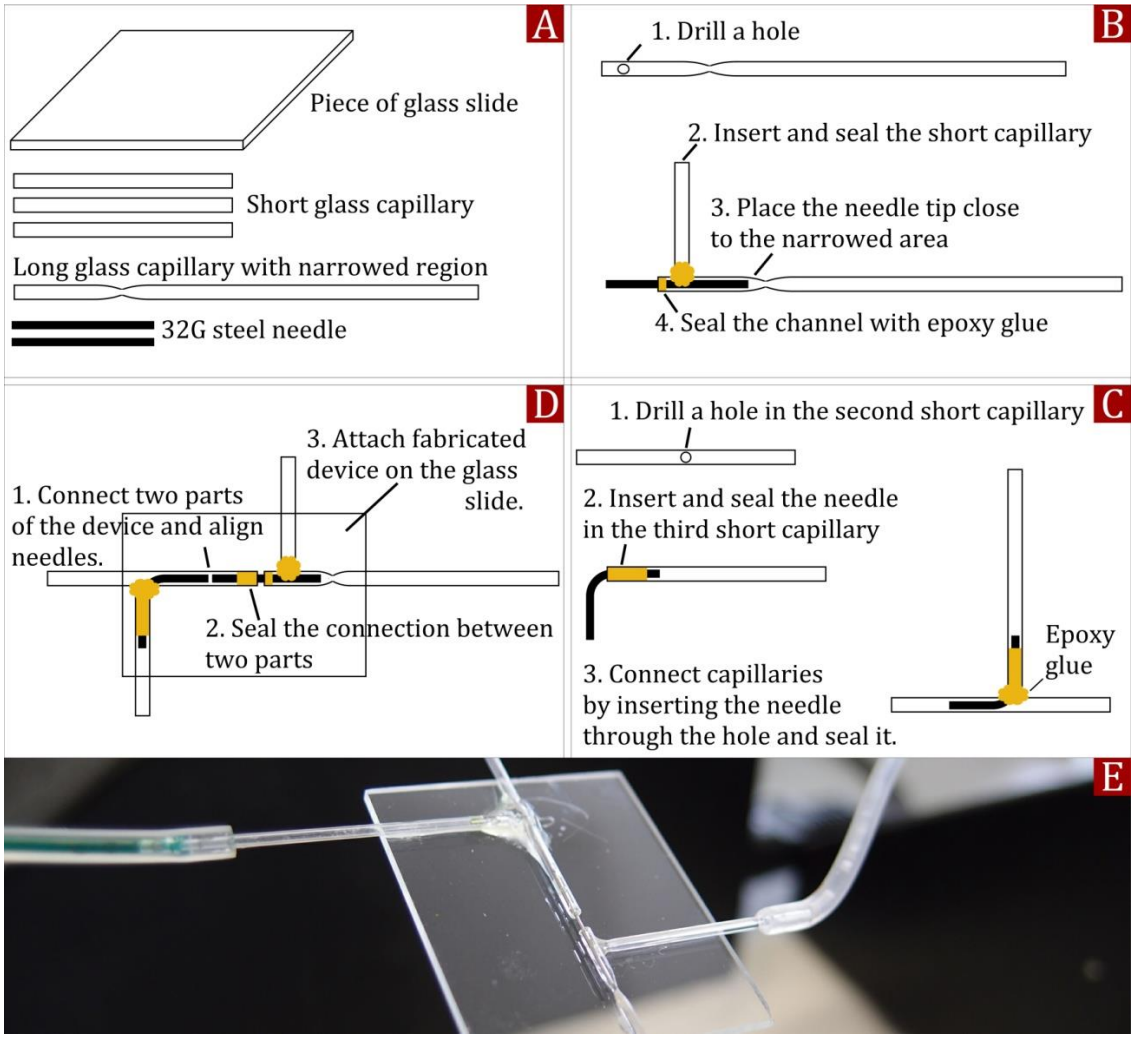

Figure II-8. Schematic illustration of the manufacturing process of the simplified co-flow double emulsion droplet generator.

II.3 References

[1] Haddleton, D. M.; Crossman, M. C.; Dana, B. H.; Duncalf, D. J.; Heming, A. M.; Kukulj, D.; Shooter, A. J., Atom Transfer Polymerization of Methyl Methacrylate Mediated by Alkylpyridylmethanimine Type Ligands, Copper(I) Bromide, and Alkyl Halides in Hydrocarbon Solution. *Macromolecules* **1999**, 32, 2110-2119.

[2] Wooding, A.; Kilner, M.; Lambrick, D. B., Studies of the double surfactant layer stabilization of water-based magnetic fluids. *J. Colloid Interface Sci.* **1991**, 144, 236-242.

[3] Shen, L.; Laibinis, P. E.; Hatton, T. A., Bilayer Surfactant Stabilized Magnetic Fluids: Synthesis and Interactions at Interfaces. *Langmuir* **1998**, 15, 447-453.

[4] Maity, D.; Agrawal, D. C., Synthesis of iron oxide nanoparticles under oxidizing environment and their stabilization in aqueous and non-aqueous media. *J. Magn. Magn. Mater.* **2007**, 308, 46-55.

[5] Yin, Y.; Li, Z.-Y.; Zhong, Z.; Gates, B.; Xia, Y.; Venkateswaran, S., Synthesis and characterization of stable aqueous dispersions of silver nanoparticles through the Tollens process. *J. Mater. Chem.* **2002**, 12, 522-527.

[6] Cahn, J. W., Critical point wetting. *J. Chem. Phys.* **1977**, 66, 3667-3672.

[7] Robledo, A.; Varea, C.; Indekeu, J. O., Wetting transition for the contact line and Antonov's rule for the line tension. *Physical Review A* **1992**, 45, 2423-2427.

[8] Kruss GmbH, Measurement contact angle. http://www.kruss.de/en/theory/measurements/contact-angle/measurement-contact-angle.html (accessed **15 December 2012**).

[9] Quevedo, E.; Steinbacher, J.; McQuade, D. T., Interfacial Polymerization within a Simplified Microfluidic Device: Capturing Capsules. *J. Am. Chem. Soc.* **2005**, 127, 10498-10499.

[10] Song, J.-S.; Winnik, M. A., Cross-Linked, Monodisperse, Micron-Sized Polystyrene Particles by Two-Stage Dispersion Polymerization. *Macromolecules* **2005**, 38, 8300-8307.

[11] Wang, D.; Dimonie, V. L.; Sudol, E. D.; El-Aasser, M. S., Seeded dispersion polymerization. *J. Appl. Polym. Sci.* **2002**, 84, 2710-2720.

CHAPTER III

Synthesis of Anisotropically-shaped Amphiphilic Microparticles

In this chapter we show that induced internal phase separation can transform the microfluidically generated droplets into multifunctional anisotropic polymer-based structures. An application of the microfluidic device gives a control over the size and monodispersity of synthesized objects. A blend of non-polymerisable oil with hydrophilic and hydrophobic monomers allows formation of amphiphilic "microbuckets" with an outer hydrophilic surface and an inner hydrophobic cavity. We provide experimental evidence of the surface amphiphilicity by exposing our "microbuckets" to selective hydrophilic-hydrophobic interactions. Finally we demonstrate that magnetic microbuckets can be used to capture oil droplets dispersed in water.

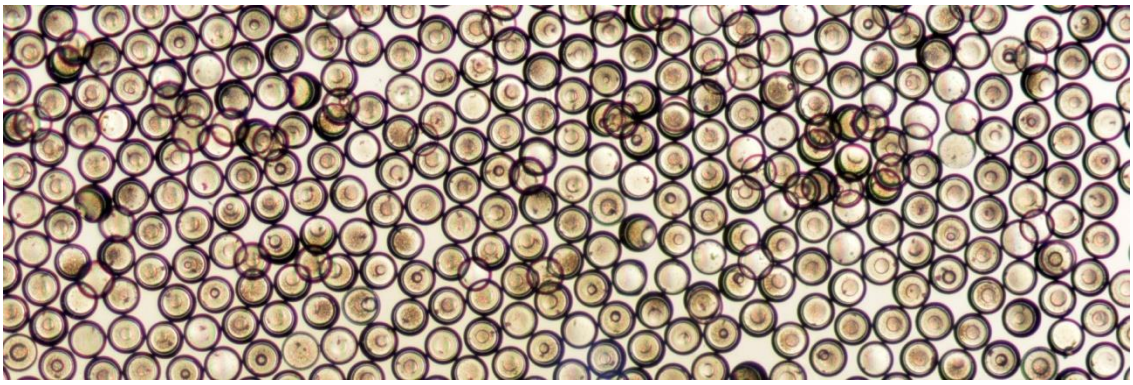

[Graphical abstract]

III.1 Introduction

Recent progress in synthetic routes towards anisotropic microparticles provided a wealth of opportunities to fabricate anisotropic materials of various patterns, shapes, compositions and functionalities.[1] Where anisotropy is imparted through shape, the resulting colloids show radically different behaviour at interfaces.[2,3] Where the chemical nature of the colloid is heterogeneous, particles have been demonstrated to work efficiently in electrophoretic display technologies,[4] as bifunctional biological receptors[5] and have the ability to self-assemble under particular conditions.[6,7] Exploitation of both chemical and shape inhomogeneity allows for an immense range of structures with a variety of applications. Amphiphilic particles with a peanut type morphology for example, have the ability to self-assemble into supracolloidal structures similar to those formed by amphiphilic molecules, the assembly process driven by hydrophobic attractive forces and governed by a geometric packing parameter.[8]These biphasic type particles can be produced by a multitude of methods including seeded polymerization of monomer swollen crosslinked particles,[9] continuous-flow lithography[10] and by phase separation of emulsion droplets upon evaporation of a volatile solvent.[11-15]

One fabrication technique which has played, and continues to play, a prominent role in this revolution in synthetic methodology, is droplet based microfluidics. The versatility of microfluidics has allowed synthesis of diverse complex microstructures,[16] for instance non-spherical particles,[17-21] multiphase "Janus" particles,[22-25] porous structures,[26-32] giant polymer vesicles[33-38] and microgels.[39-42] Such diversity of the synthesized particles is achieved, in many respects, by virtue of the performance of microfluidic devices which can be very simple[43] or complex setups,[44, 45] requiring complex technologies, for instance lithography or glass capillary pulling. The finite

structure of the particles defines the type of the device which is employed in the process: simple single emulsion generators are suitable for non-hollow particles, while capsule-like microstructures demand utilization of more complex multiple emulsion units.

We were inspired by the possibilities to create intricate functional microstructures by combining the phenomenon of internal phase separation and microfluidic techniques. Taking as a basis of inspiration internal phase separation studies presented by Vincent *et al.* who synthesized oil core-polymer shell microcapsules for controlled release,[46-48] and freezing/warming method of toluene swollen polystyrene beads which led to formation of "bucket-like" polymer colloids by Xia and coworkers,[49] we set ourselves the goal to develop a method of fabrication of polymer "microbuckets" using induced phase separation as a tool to create hollow shapes. We used a simple approach to make monodisperse biphasic microparticles that does not rely heavily on complex microfluidic device geometry, but rather on interfacial tension of the selected fluids. We set a requirement that the outer surface of our microbuckets had to be hydrophilic to optimize wettability with water and the inner surface of its cavity had to be hydrophobic, so that the microbuckets would have the ability to take up and store oil. Our intention was to design and employ a microfluidic device which can be manufactured with affordable materials (see Figure II-3) which generates droplets of ~100 microns in diameter or less to be in range which microfluidics supposed to provide. To fabricate our microbuckets an emulsified droplet containing acrylic monomer and silicone oil is polymerized to induce phase separation, producing a solid-liquid Janus particle. The use of a hydrophilic, surface active monomer (2-hydroxyethyl methacrylate) imparted amphiphilic surface properties on the “microbucket” particle.

III.2 Results and discussion

III.2.1 Device performance and droplet formation parameters

As we have seen in Figures II-1C and D the needle tip is adjacent to the narrowest section of the capillary. The distance from the centre of that section to the droplet formation area is crucial. Placing the needle tip too far depreciates the flow-focusing effect, which allows for significant droplet size reduction, while placing it too close increases the local outer flow velocity too much, resulting in droplet formation instabilities. We manufactured three types of devices with different distances between the needle tip and the narrowed sections (see Figure III-1). Each device was tested using a 0.2 mL min^{-1} flow rate for the continuous phase and 0.015 mL min^{-1} for the dispersed phase. We found that 0.35-0.85 mm distance provides robust generation of monodisperse droplets, 0.2-0.35 mm retains stability and allows for decreasing the size of the droplets. When the distance was less than 0.2 mm the generated droplets were polydisperse. Aside from the distance between the tip and narrowest point, the diameter of the last is critical. Too small diameter significantly increases the local flow velocity resulting in the jetting regime of droplet formation, which in turn reduces the stability of whole process. We found that the diameter of the narrowest point should be equal to the outer diameter of the needle or 1.5 times larger to provide the best performance. Figures III-1A and B show that diameter of the narrowed area is equal to the diameter of the needle or slightly higher. These diameters of the narrowed region provided the monodisperse droplet generation (see Figures III-1D and E), while the smaller diameter led to the formation of polydisperse particles (see Figure III-1C and F). Lower values increase the polydispersity of the generated droplets, while higher the size.

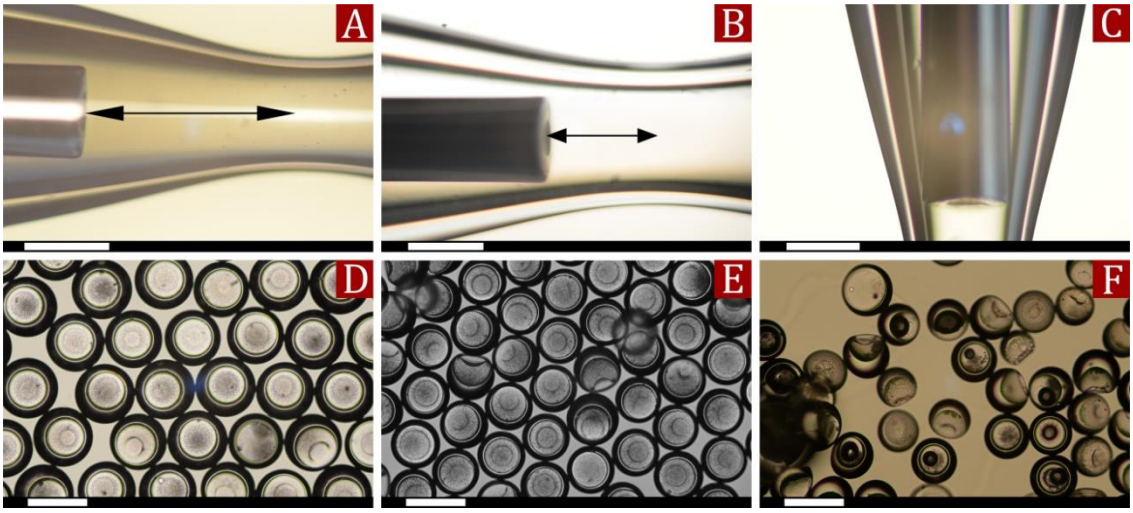

Figure III-1. Different distances of the needle tip to the narrowed area and particles fabricated using these devices. (A) The distance is 750 µm. (B) 250µm. (C) 125 µm. Scale bars are 250 µm(A-C) and 150 µm (D-F).

Having the experimental evidence of the device layout validity, we determined the regimes of droplet formation as a derivative of Capillary and Weber numbers in order to provide a higher monodispersity and stability. The sum of the Ca and We numbers defines whether the regime is dripping, and droplets are monodisperse, or jetting and droplets are polydisperse.[50] However, Clanet *et al.*[51] demonstrated that droplets generated by jetting regime are not necessarily polydisperse. Rather it is a factor influencing droplet formation stability, while the dripping regime provides stable droplet generation, and thus preferable. If the sum of Ca and We numbers is greater than 1, the regime is jetting, but if it is less than 1, the regime is dripping. Hence, tuning of Weber and/or Capillary numbers offers a clear view on the droplet formation process under various conditions. To calculate Ca and We numbers a value of interfacial tension at the monomer/aqueous PVA interface should be known (see Equations I-2 and II-3). Since a value of surface tension is unknown for both continuous and dispersed phases, direct measurement of the interfacial tension is complicated. The main reason is that the drop-shape analyser machine requires a full list of physical properties for each

solution to run the direct measurement. We decided to measure the value of the surface tension at the air/liquid interface for each mixture and then employ Antonov's rule[52, 53] to calculate a value of interfacial tension at liquid/liquid interface.

Antonov's rule:

$$\sigma_{12} = \sigma_1 - \sigma_2$$

Figure III-2 illustrates the hanging droplets during the measurement on a Kruss DSA-100 machine. As it can be seen on the images, the shapes of the droplets are not the same, which in turn means a difference in radii of curvature allowing calculating the surface tension.

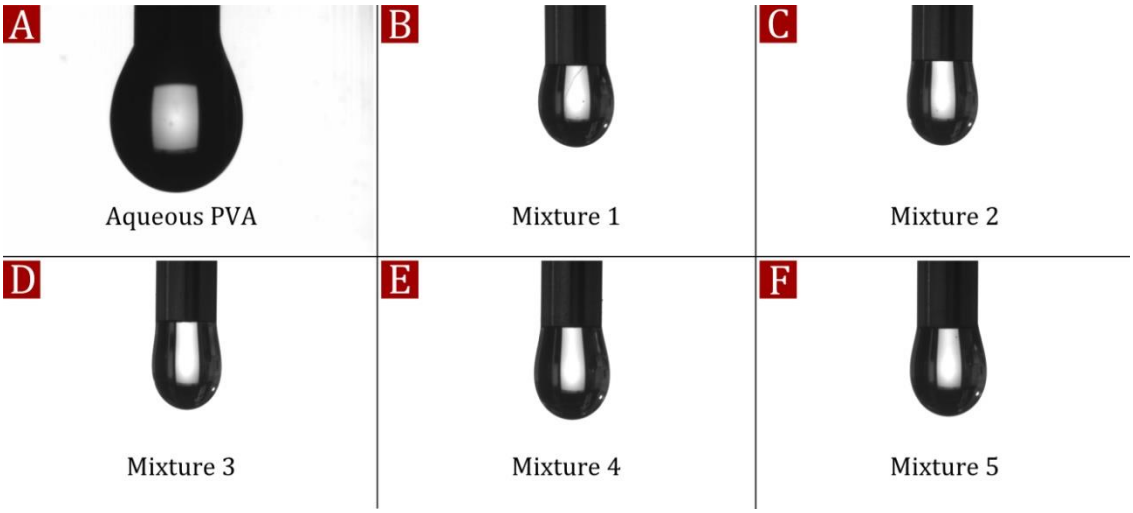

Figure III-2. Droplet shapes used to calculate values of surface tension.

Table III-1 presents the values of surface tension at the air/liquid ($\sigma_{A\text{-}L}$) and liquid/liquid ($\sigma_{L\text{-}L}$) interfaces and theoretical estimation of droplet formation regimes for each monomer/PDMS mixtures. As it arises from the shown figures the flow retains laminar and regime is classified as dripping.

Table III-1. Physical parameters of mixtures required to calculate values of surface tension using Equation III-2.

Mixture	σ_{A-L}, mN m^{-1}	σ_{L-L},mN m^{-1}	Tube D, m*	Velocity, m s^{-1}**	Ca + We***
1	22.16	28.86	$5.8\times10^{-4}/1\times10^{-4}$	$1.2\times10^{-2}/3.1\times10^{-2}$	5×10^{-3}
2	21.67	29.35	$5.8\times10^{-4}/1\times10^{-4}$	$1.2\times10^{-2}/3.1\times10^{-2}$	4.8×10^{-3}
3	15.92	35.10	$5.8\times10^{-4}/1\times10^{-4}$	$1.2\times10^{-2}/3.1\times10^{-2}$	6.8×10^{-3}
4	20.14	30.88	$5.8\times10^{-4}/1\times10^{-4}$	$1.2\times10^{-2}/3.1\times10^{-2}$	5.3×10^{-3}
5	21.58	29.44	$5.8\times10^{-4}/1\times10^{-4}$	$1.2\times10^{-2}/3.1\times10^{-2}$	4.9×10^{-3}
PVA aq.	51.02	x	x	x	x

* Outer tube diameter/inner tube diameter

** Outer flow velocity/ inner flow velocity

*** Regime dripping: Ca + We < 1

III.2.2 Microfluidics assisted synthesis of polymer "microbuckets"

After dispersion, the droplets were collected into a vial where they remained stable due to the stabilization by PVA. Upon exposure to the UV light the photoinitiator induced polymerization of the monomers and as a consequence phase separation occurred. Polymer chain growth increases viscosity and density of the mixture and changes the stability of phase equilibrium in the homogeneous monomer/oil system, transforming it into a heterogeneous polymer/oil one. The phase separation process decreases the total free energy of the system, but the PDMS molecules cannot disperse in aqueous continuous medium and thus form a "bucket"-like structure (see Figure III-3E). The prediction of the shape of the Janus particles based on volumetric ratios of monomer/PDMS reported by Nisisako *et al.*[25] is not applicable in our case. This method

implies the existence of a constant contact angle between the phases, while it changes throughout the reaction. Due to the solubility of MMA in the water (1.5 wt%) we observed polymerisation in the aqueous phase, which is undesirable. It was prevented by the presence of sodium nitrate (1 wt%) in the aqueous phase, which stopped the reaction, which was added to the aqueous phase prior to the polymerisation.

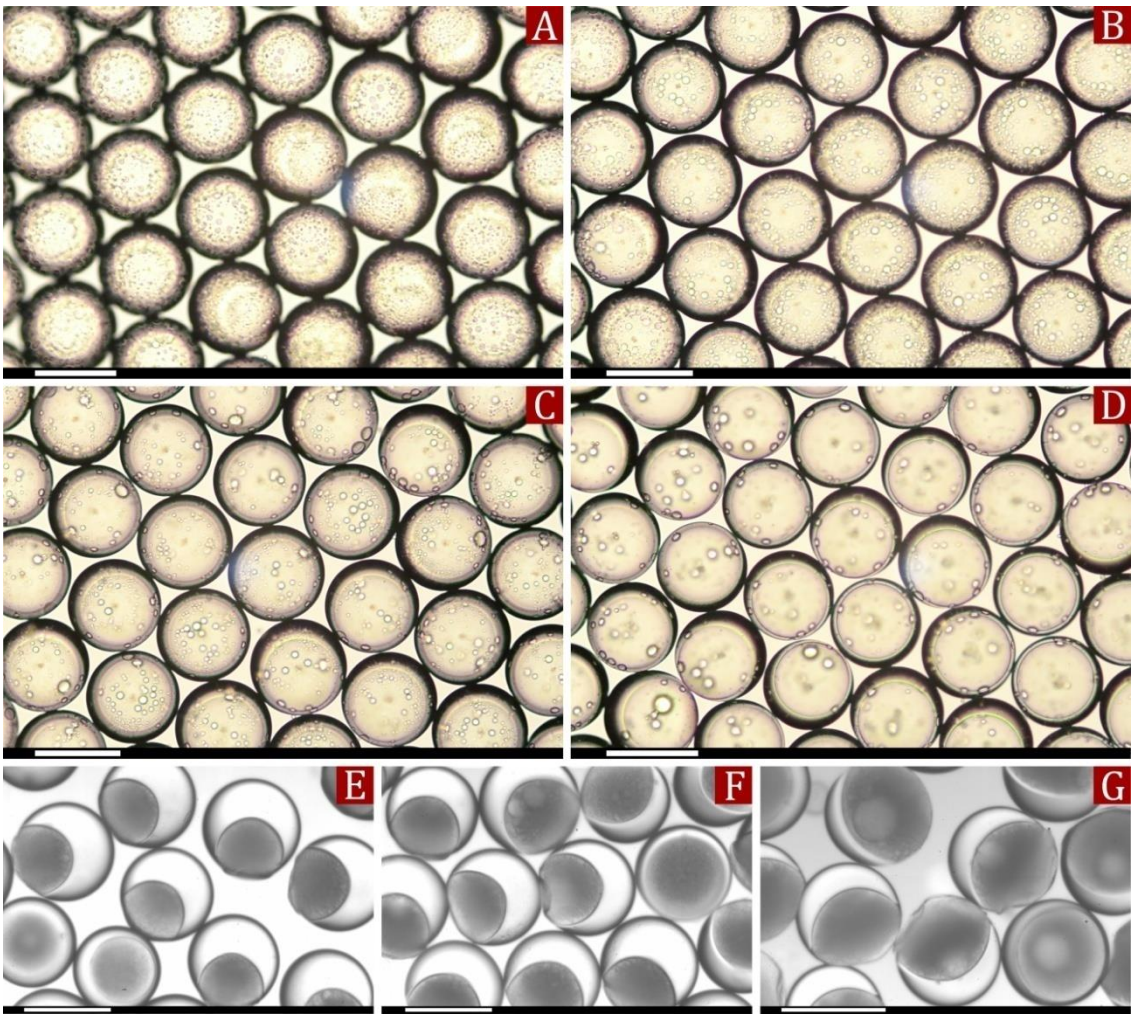

Figure III-3. The stop-frame illustration of the internal phase separation and types of "microbuckets" with lids. (A) Image was taken 3 minutes ftera the start of the reaction. (B) 5 minutes. (C) 10 minutes. (D) 25 minutes. (E) Dry particles on glass, monomer/oil ratio is 9:1. (F) Dry particles on glass, ratio is 8:2. (G) Dry particles on glass, ratio is 7:3. Images A-D were taken from the top in the vial, and the Janus structure is not clear. The particles on images E-G were taken after polymerisation, when particles were dry and placed to the glass slide to observe the Janus structure. All scale bars are 100 µm.

However, not all molecules of the monomer can separate from the oil and polymerize within it, forming a suspension which can be recognized as the dark part of

the "buckets" (see Figure III-3E). Along with solubility of MMA in water, this affects the volume of the cavity which increases, because a smaller amount of monomer takes part in the shell formation. This explains the discrepancy between the actual volume and the theoretical, which is a function of the initial volume ratios of the monomer and non-polymerisable oil. Initially, our polymerisable blend consisted only of methyl methacrylate and silicone oil in different ratios. This combination did not allow producing the “bucket”-like thermodynamic shape, because a silicone oil compartment was covered with a thin layer of the polymer, in essence forming capsules. A general explanation includes two reasons: a relative hydrophilicity of MMA in comparison to the silicone oil and high polymerisation rate of the monomer. Being between the aqueous medium and the highly hydrophobic PDMS a thin layer of monomer corresponds to the position of energy minima, while continuous exposure to UV-light rapidly polymerises it. The volumetric amount of silicone oil in the mixture affected morphology of both, the polymer and oil parts of the capsules, increasing one and reducing another. Despite this, the "bucket"-like particles can be formed from the capsules by cracking the shell and washing out the silicone oil. We sonicated our particles and afterwards removed the contents of the cavity which led to the formation of the "bucket"-like particle (see Figure III-4).

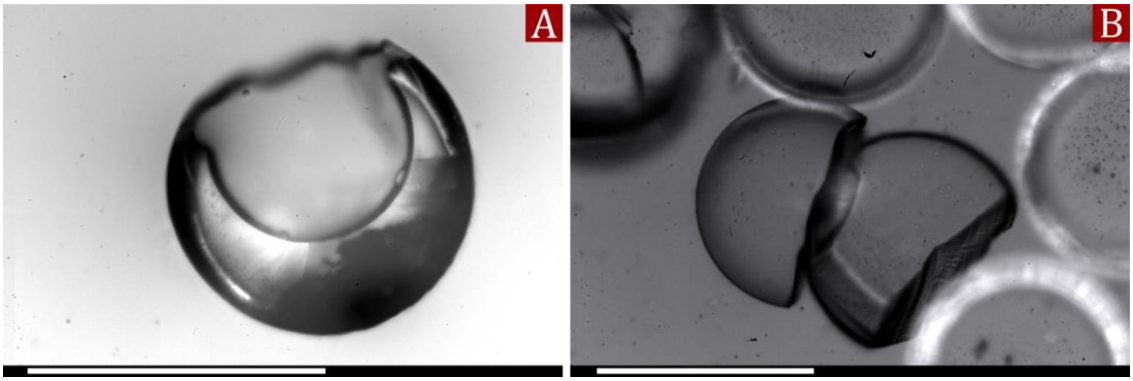

Figure III-4. Results of the "microbuckets" sonication. (A) Proper "bucket"-like shaped microparticle. (B) Longer sonication caused the destruction of thin walls and transformation buckets into hemispherical particles. All scale bars are 100 µm.

III.2.3 "Microbuckets" with amphiphilic surface behaviour

In order to synthesize the "microbuckets" without lids, we experimented with various monomer blends. We found that using a methyl methacrylate/styrene mixture improved the phase separation dynamics providing a hole formation in the shell through which the PDMS rich phase could be washed out easily. According to Beuermann and colleagues,[54] the propagation rate coefficient (k_p) for MMA homopolymerisation at 25 °C using 2,2-dimethoxy-2-phenylacetophenone as the initiator is 372 L mol^{-1} s^{-1}, while Buback and co-workers[55] employing the same temperature and initiator found that k_p for styrene is 95L mol^{-1} s^{-1}.The difference is significant and impacts on the k_p of MMA/styrene copolymerisation, which is 104 L mol^{-1} s^{-1} with reference to Olaj *et al*.[56] Besides, solubility of styrene in water is lower (<1 wt%) than MMA's, which makes the monomer mixture more hydrophobic. This in turn means that the interfacial energy minimum is achievable without a thin layer of monomer over the silicone oil compartment. Hence, an addition of styrene drastically affected the reasons of the "lid" formation, allowing deeper phase separation and as a result formation of the "bucket"-like particles (see Figure III-5). Nevertheless, if pure methyl methacrylate cures within 20 minutes, styrene blends require several hours, which is an unfortunate side effect. In order to reduce the reaction time and retain "microbuckets" formation we introduced a new variable: a cross-linker. The presence of 1,6-hexanediol diacrylate significantly increased the rate of the reaction by virtue of autoacceleration[57] also known as Trommsdorff-Norrish/Gel effect. The essence of the phenomenon is that a cross-linker locally increases viscosity of the reacting mass, slowing termination of the radicals, which results in a faster polymer chain growth. This avoids the disadvantage, and retains the benefit of styrene addition.

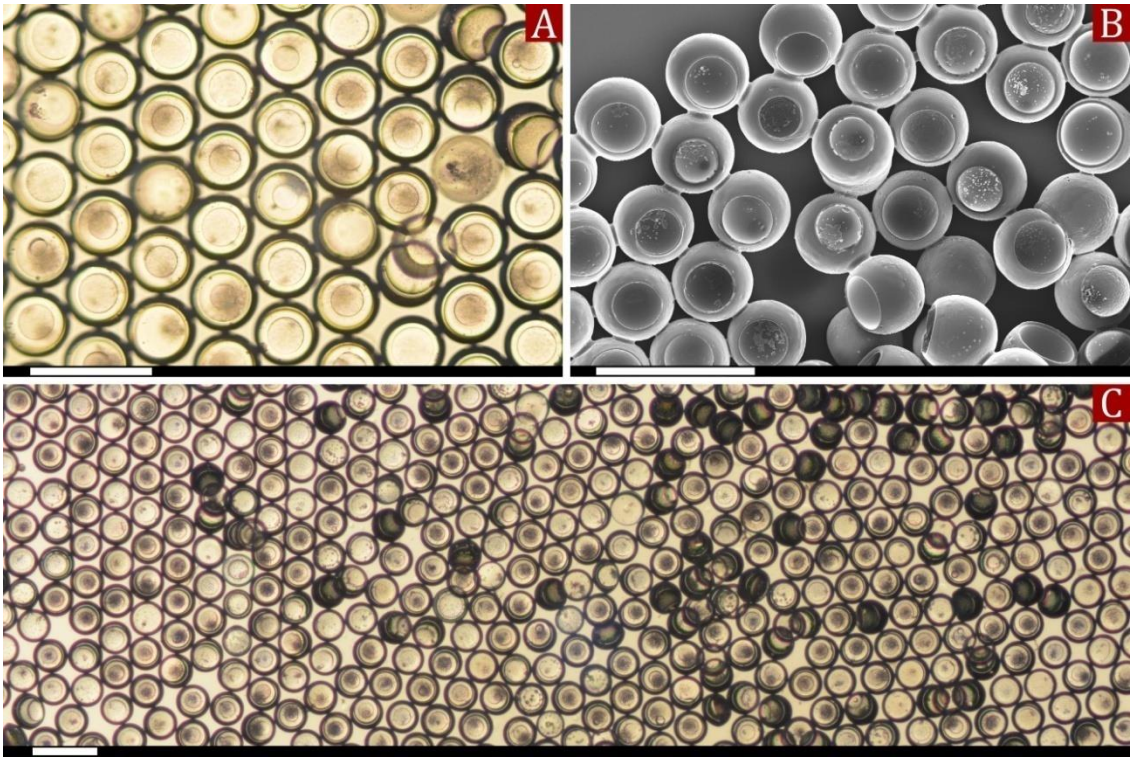

Figure III-5. Lidless "microbuckets" fabrication by tuning the monomer mixture. (A) Optical micrograph shows the hole on the top of the particles allowing washing out the cavity contents. (B) Scanning electron microscopy image of the "microbuckets". (C) Predicted dripping regime of the droplet formation resulted in highly monodisperse "microbuckets". All scale bars are 200 µm.

The polymer "microbuckets" have shape anisotropy, yet still did not have an amphiphilic surface where the outer surface is hydrophilic and the cavity is hydrophobic. This property would have to appear as a hydrophilic outer surface of the "microbuckets" and a hydrophobic surface of the cavity. The formation of a hydrophobic surface in the cavity is a self-evident process, as minimization of interfacial tension between the polymer phase and the PDMS liquid. However, formation of hydrophilic outer surface of the microbuckets, required an additional modification. Since the outer surface forms in constant interaction with the continuous aqueous medium, the hydrophilicity could be tuned as a result of an interfacial phenomenon.

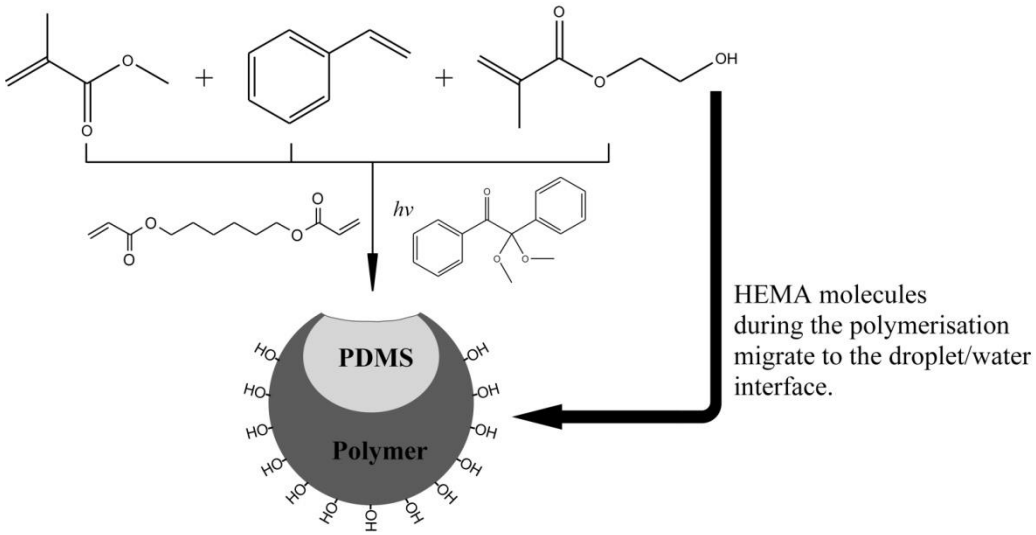

Figure III-6. Scheme of the surface hydrophilisation. Due to amphiphilic structure molecules of 2-hydrxyethyl methacrylate modify the outer surface of "microbuckets", forming a hydrophilic layer.

An addition of hydrophilic 2-hydroxyethyl methacrylate to the monomer blend allowed a straightforward hydrophilisation of the "microbuckets" exterior. The mechanism of the process can be described as follows. Possessing both the hydrophilic and hydrophobic parts, 2-hydroxyethyl methacrylate molecules diffuse and enrich themselves towards the water/monomer interface and taking the position of the free energy minimum when the hydroxyl group was converted to water, while the other part remained in the monomer. The subsequent curing led to the formation of the hydrophilic outer surface.

The amphiphilicity of the surface was verified by three methods: confocal laser scanning microscopy, colloidal silver deposition on a hydrophilic surface and vigorous stirring of "microbuckets" in oil-in-water emulsion which led to withdrawal of oil droplets from aqueous medium into the internal volume of "microbuckets". First of all, we used an oil-soluble dye (nile red) to observe the surface amphiphilicity. Dissolved in the oil, it should mark the hydrophobic surface of the cavity. Figure III-7E shows that cavity has an intensive red colour which means that the oil containing dye selectively

wetted it. The second method is based on the reduction of silver ions in aqueous medium leading to the formation of silver colloidal particles which can precipitate solely on the hydrophilic surface and also known as a "silver mirror test". Such behaviour is attributable to wettability of the polymer “microbuckets” surface by the aqueous medium containing dissolved silver ions. If the surface is hydrophobic, Ag^+ ions cannot reach it, thus reducing primarily in the aqueous medium, whereas the hydrophilic surface is completely wetted allowing the reduced silver nanoparticles to be deposited on it.[58-61] In our case this phenomenon should appear as an exterior covered with silver particles and an intact cavity surface. Prior to the silver reduction, “microbuckets” were cleaned and filled with “Solution A” (see paragraph II.2.1.2). The reaction was carried out in a polypropylene vial to prevent silver deposition on the reaction vessel. Therefore, the only surface theoretically capable of depositing silver particles was the exterior of the "microbuckets". The third method demonstrates the amphiphilic nature of "microbuckets" more clearly and will be discussed in the next section. Figure III-7 shows the experimental validity of our assumptions, because silver particles selectively covered the outer surface while the inside surface remained intact.

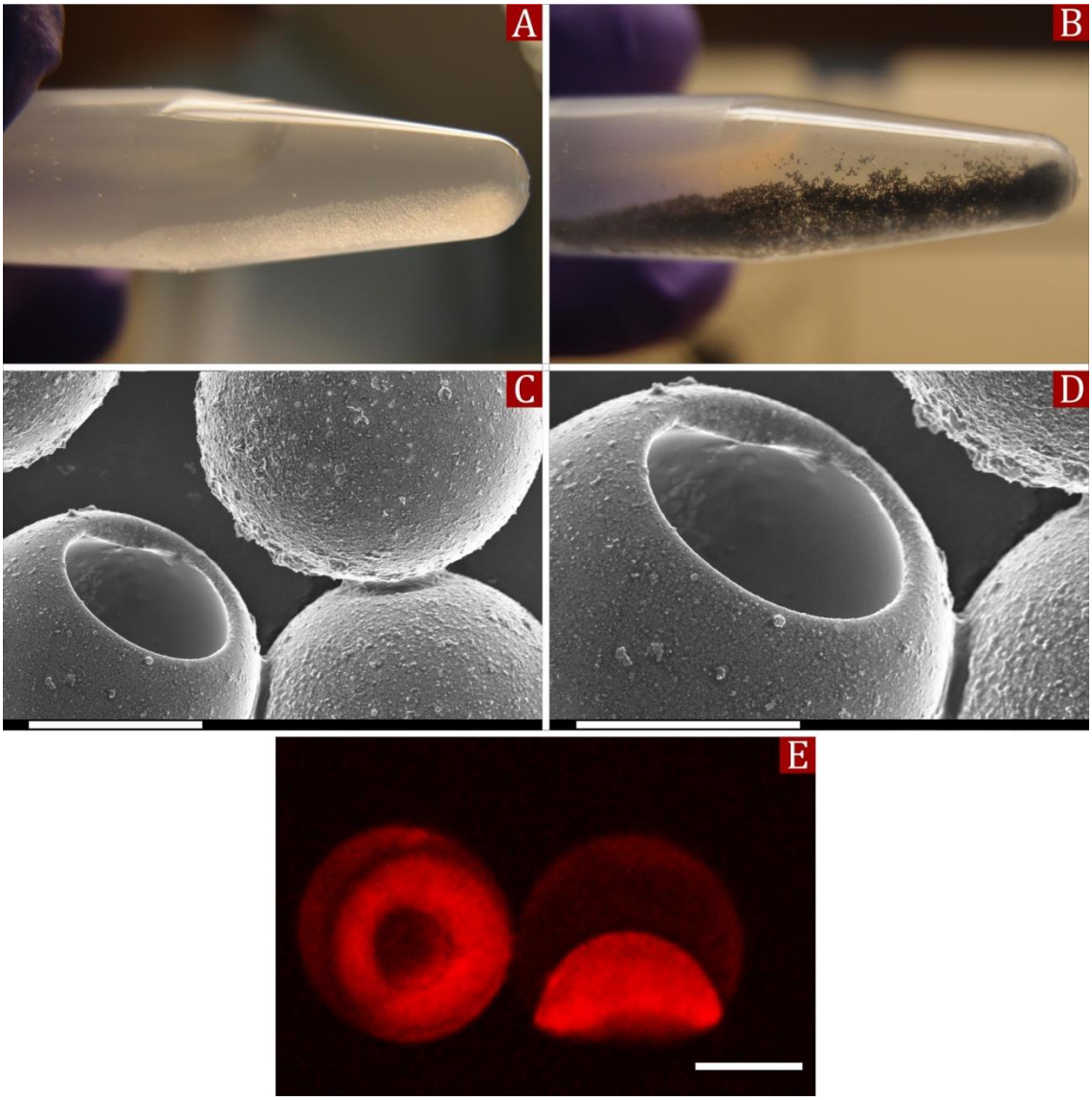

Figure III-7. Optical and SEM images of the selective silver deposition on the hydrophilic surface.(A) "Microbuckets" before silver ions reduction. (B) After the reaction. (C)The exterior surface covered with silver particles, whilst the inner retained intact. (B) Close view to the internal surface. (E) Confocal microscopy image of amphiphilic particles. All scale bars are 50 μm.

We performed elemental analysis using energy-dispersive X-ray spectroscopy (EDAX) to prove the existence of Ag on microbuckets. Figure III-8 shows EDAX spectrum, where Ag peak is shown. Besides, there is Si peak, which suggests that a part of PDMS oil grafted on the inner surface of microbuckets providing hydrophobicity.

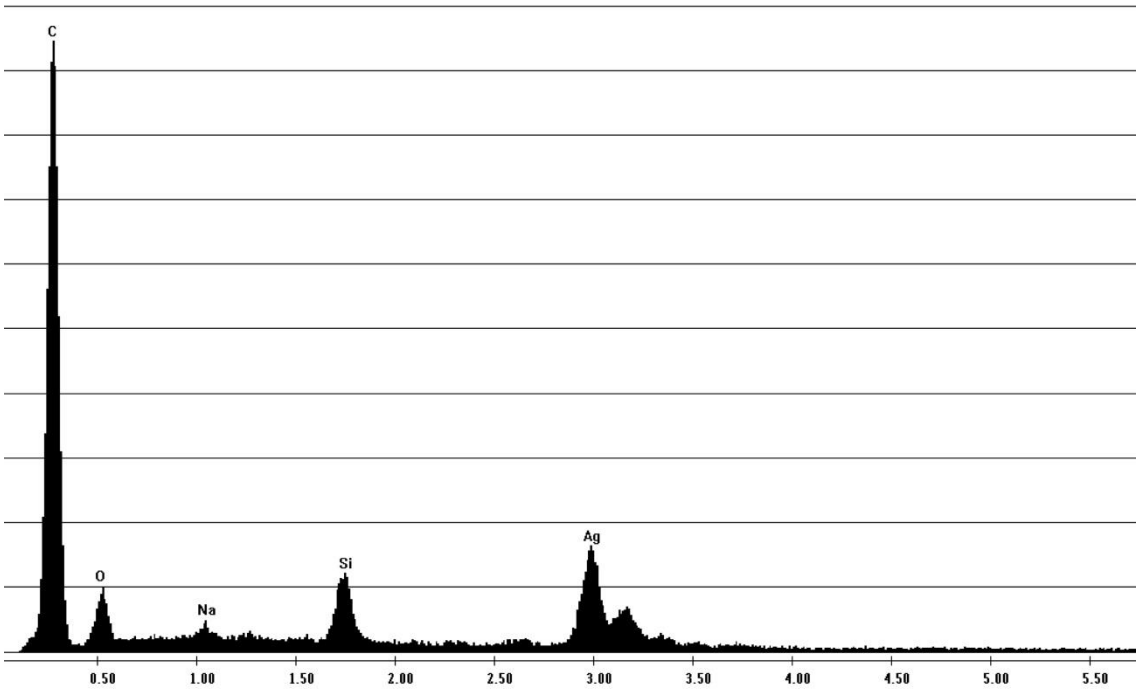

Figure III-8. EDAX spectrum of microbuckets.

III.2.4 Magnetically propelled oil carriers

With such the amphiphilic structure the "microbuckets" could be potentially used as oil tanks for the capture, storage, transportation or delivery of oil droplets in aqueous environments on the micro scale. However, this step required another modification of the synthesis procedure in order to make the "microbuckets" sensitive to external forces which could actuate them. We therefore decided to incorporate hydrophobic magnetic iron oxide nanoparticles, which were dispersed in the monomer blend. Using a relatively large amount of Fe_3O_4 particles (0.5 wt%) in the monomer blend led to several complications. Upon mixing with silicone oil the iron oxide sol lost stability, which caused formation of magnetically heterogeneous "microbuckets". If we would be able to control this aggregation process and confine the magnetic nanoparticles to one specific zone, this could act as a locomotive control zone allowing precise directing of "microbucket" movement. In practice, magnetic clusters settled spontaneously in a

random fashion from particle to particle without giving any advantage (see Figure III-8). Additionally, the relatively high concentration of nanoparticles blocked UV penetration slowing the polymerization reaction, which is an undesirable effect. We therefore gradually decreased the concentration of Fe_3O_4 nanoparticles from 0.5 wt% to 0.005 wt% to explore the optimal conditions. We found that a monomer blend containing 0.01 wt% did not affect the morphology and amphiphilicity of the "microbuckets", allowed keeping the curing times equal to the non-magnetic one, but did add the desired high magnetic responsiveness. Our attempts to compartmentalize magnetic particles in a controlled manner, for instance by putting a magnet under the vial during polymerisation, were unavailing. Partly it is explained by a high colloidal stability of the Fe_3O_4 particles, partly in virtue of the short solidification time of the monomer phase. Figure III-9 shows that Fe_3O_4 particles are randomly distributed in the polymer.

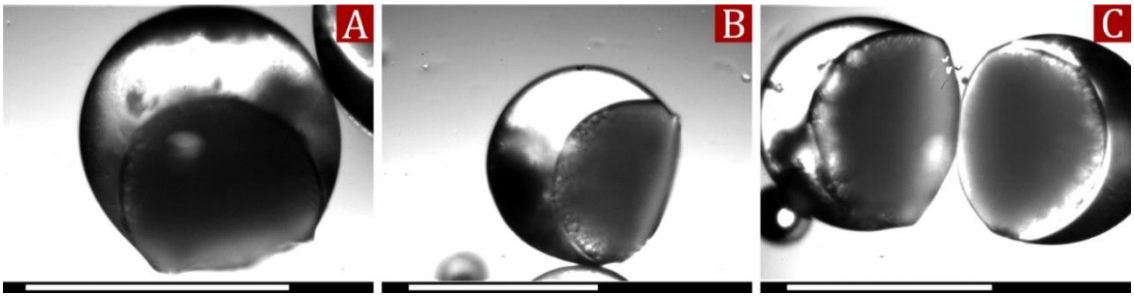

Figure III-9. "Microbuckets" with magnetic contaminations (dark areas). (A) Monomer/oil ratio is 9:1, most iron oxide particles localized on the bottom. (B) Ratio is 8:2, magnetic particles are on the side. (C) Ratio is 7:3, particles are concentrated on the side (left) or distributed (right). All scale bars are 100 µm.

In order to perform oil seizure by the hydrophobic cavities of the "microbuckets" we ran the following experiments. First of all, we tried to fill the emptied “microbuckets” with polar and non-polar solutions to illustrate an ability to fill the cavity with a specific substance. We washed out all cavity contents and sonicated “microbuckets” to make the inner and outer surface clean and dried them for 1 h at 60

°C. After that we placed them into water and ethanol. In the first case water could not replace air inside the cavity due to hydrophobic repulsion by the inner surface of the “microbuckets”, while ethanol quickly filled the cavity by virtue of affinity to the hydrophobic surfaces (see Figure III-10B and C). Secondly, we placed the freshly prepared “microbuckets” into ethanol for a short while (10 s), which caused partial diffusion of the silicone oil into the medium. After that we quickly replaced ethanol with deionised water, which in turn “arrested” the remaining amount of PDMS in the cavity, which wetted the hydrophobic inner surface (see Figure III-10D).All further attempts to remove the remaining silicone oil by shaking or sonication failed due to robust locking by interaction of the two hydrophobic surfaces. Thirdly, we tried to perform actual capturing of oil droplets by “microbuckets”. We prepared a 15% oil-in-water emulsion where the dispersed phase was a mixture of 1-octadecene and oleoresin paprika and blended our emptied "microbuckets" with it by stirring for 15 min. After that we isolated "microbuckets" with centrifugation and analysed them on an optical microscope (see Figure III-10E). As seen in the image the hydrophobic interior surface easily intakes oil from the medium and reliably locks it within the cavity. Magnetic responsiveness allows to manipulate oil-filled "microbuckets" moving them to the desired location, for instance to change the medium to release cavity contents.

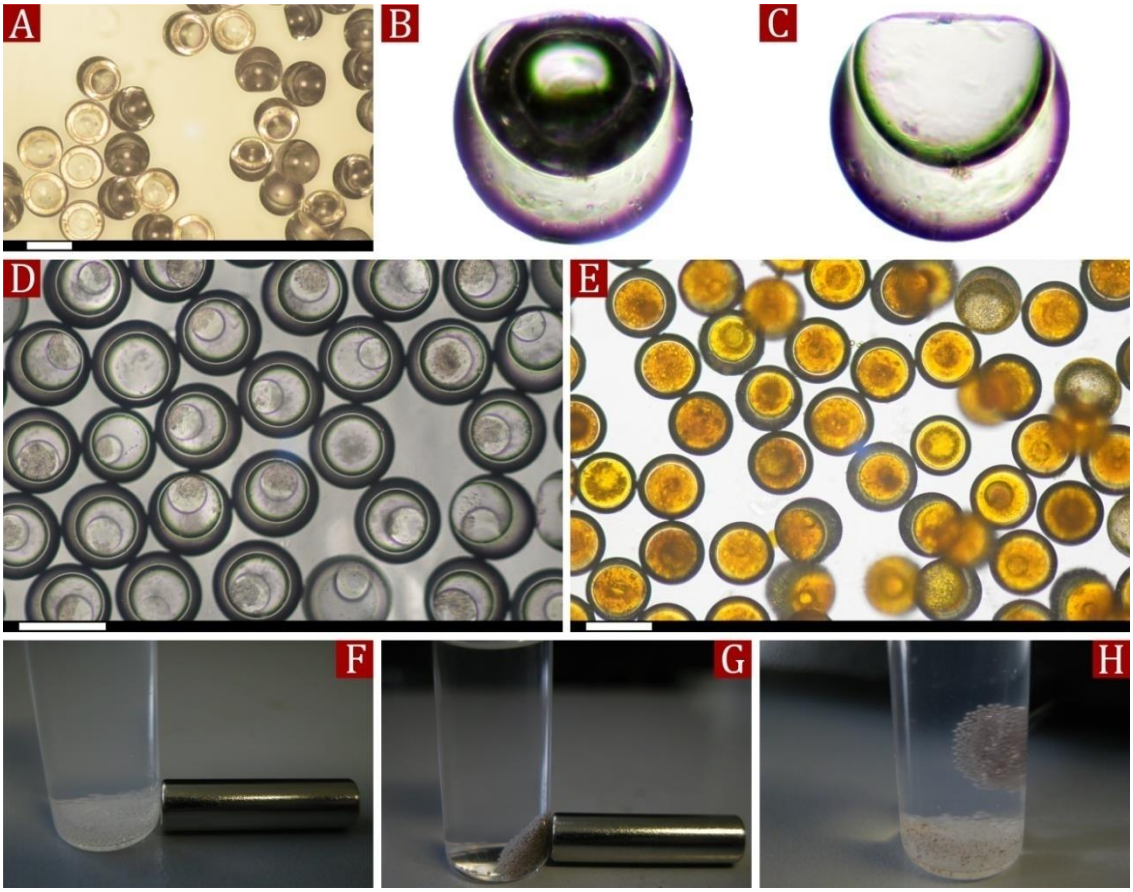

Figure III-10. The hydrophobic and magnetic properties of the "microbuckets". (A) Cleaned and dried “microbuckets” on the glass slide. (B) In the aqueous medium the air bubble inside the cavity (dark region) is locked. (C) While ethanol replaced it and filled the cavity. (D) Optical micrograph of silicone oil droplets in cavities. (E) Coloured 1-octadecene filled the internal volume. (F) Non-magnetic "microbuckets". (G) Magnetic behaviour of the particles under external field. (H) Mixture of magnetic and non-magnetic "microbuckets" and selective attraction of the first ones. All scale bars are 100 μm.

III.3 Conclusions

In conclusion, we have developed a microfluidic-based method for the synthesis of amphiphilic polymer "microbuckets" which have a hydrophilic outer surface and a hydrophobic inner cavity, which can be propelled by an external magnetic field and thus act like oil carriers which can be easily washed out by acetone. The amphiphilic nature was achieved by employment of different types of monomers, whilst addition of

colloidal iron oxide nanoparticles assured the magnetic properties. We proved selective self-sorption and locking properties of our "microbuckets". We also suggested a cheap and reliable route for assembly of microfluidic droplet generators which does not require special equipment or skills.

III.4 References

[1] Glotzer, S. C.; Solomon, M. J., Anisotropy of building blocks and their assembly into complex structures. *Nat. Mater.* **2007**, 6, 557-562.

[2] Ballard, N.; Bon, S. A. F., Hybrid biological spores wrapped in a mesh composed of interpenetrating polymer nanoparticles as "patchy" Pickering stabilizers. *Polym. Chem.* **2011**, 2, 823-827.

[3] Binks, B. P.; Clint, J. H.; Mackenzie, G.; Simcock, C.; Whitby, C. P., Naturally occurring spore particles at planar fluid interfaces and in emulsions. *Langmuir* **2005**, 21, 8161-8167.

[4] Chen, Y.; Au, J.; Kazlas, P.; Ritenour, A.; Gates, H.; McCreary, M., Flexible active-matrix electronic ink display. *Nature* **2003**, 423, 136-136.

[5] Kaufmann, T.; Gokmen, M. T.; Wendeln, C.; Schneiders, M.; Rinnen, S.; Arlinghaus, H. F.; Bon, S. A. F.; Du Prez, F. E.; Ravoo, B. J., "Sandwich" Microcontact Printing as a Mild Route Towards Monodisperse Janus Particles with Tailored Bifunctionality. *Adv. Mater.* **2011**, 23, 79-89.

[6] Chen, Q.; Bae, S. C.; Granick, S., Directed self-assembly of a colloidal kagome lattice. *Nature* **2011**, 469, 381-384.

[7] Chen, Q.; Whitmer, J. K.; Jiang, S.; Bae, S. C.; Luijten, E.; Granick, S., Supracolloidal Reaction Kinetics of Janus Spheres. *Science* **2011**, 331, 199-202.

[8] Whitelam, S.; Bon, S. A. F., Self-assembly of amphiphilic peanut-shaped nanoparticles. *J. Chem. Phys.* **2010**, 132, 074901-074908 .

[9] Sheu, H. R.; Elaasser, M. S.; Vanderhoff, J. W., Phase separation in polystyrene latex interpenetrating polymer networks. *J. Polym. Sci., Part A: Polym. Chem.* **1990**, 28, 629-651.

[10] Pregibon, D. C.; Toner, M.; Doyle, P. S., Multifunctional encoded particles for high-throughput biomolecule analysis. *Science* **2007**, 315, 1393-1396.

[11] Yow, H. N.; Routh, A. F., Colloidal buckets formed via internal phase separation. *Soft Matter* **2008**, 4, 2080-2085.

[12] Wang, Y.; Guo, B. H.; Wan, X.; Xu, J.; Wang, X.; Zhang, Y. P., Janus-like polymer particles prepared via internal phase separation from emulsified polymer/oil droplets. *Polymer* **2009**, 50, 3361-3369.

[13] Tanaka, T.; Okayama, M.; Kitayama, Y.; Kagawa, Y.; Okubo, M., Preparation of “Mushroom-like” Janus Particles by Site-Selective Surface-Initiated Atom Transfer Radical Polymerization in Aqueous Dispersed Systems. *Langmuir* **2010**, 26, 7843-7847.

[14] Tanaka, T.; Komatsu, Y.; Fujibayashi, T.; Minami, H.; Okubo, M., A Novel Approach for Preparation of Micrometer-sized, Monodisperse Dimple and Hemispherical Polystyrene Particles. *Langmuir* **2009**, 26, 3848-3853.

[15] Liu, S.; Deng, R.; Li, W.; Zhu, J., Polymer Microparticles with Controllable Surface Textures Generated through Interfacial Instabilities of Emulsion Droplets. *Adv. Funct. Mater.***2012**, 22, 1692-1697.

[16] Whitesides, G. M., The origins and the future of microfluidics. *Nature* **2006**, 442, 368-373.

[17] Nie, Z.; Xu, S.; Seo, M.; Lewis, P. C.; Kumacheva, E., Polymer Particles with Various Shapes and Morphologies Produced in Continuous Microfluidic Reactors. *J. Am. Chem. Soc.* **2005**, 127, 8058-8063.

[18] Dendukuri, D.; Tsoi, K.; Hatton, T. A.; Doyle, P. S., Controlled Synthesis of Nonspherical Microparticles Using Microfluidics. *Langmuir* **2005**, 21, 2113-2116.

[19] Nisisako, T.; Hatsuzawa, T., A microfluidic cross-flowing emulsion generator for producing biphasic droplets and anisotropically shaped polymer particles. *Microfluid. Nanofluid.* **2010**, 9, 427-437.

[20] Studart, A. R.; Shum, H. C.; Weitz, D. A., Arrested Coalescence of Particle-coated Droplets into Nonspherical Supracolloidal Structures. *J. Phys. Chem. B* **2009**, 113, 3914-3919.

[21] Bon, S. A. F.; Mookhoek, S. D.; Colver, P. J.; Fischer, H. R.; van der Zwaag, S., Route to stable non-spherical emulsion droplets. *Eur. Polym. J.* **2007**, 43, 4839-4842.

[22] Chen, C.-H.; Shah, R. K.; Abate, A. R.; Weitz, D. A., Janus Particles Templated from Double Emulsion Droplets Generated Using Microfluidics. *Langmuir* **2009**, 25, 4320-4323.

[23] Nie, Z.; Li, W.; Seo, M.; Xu, S.; Kumacheva, E., Janus and Ternary Particles Generated by Microfluidic Synthesis: Design, Synthesis, and Self-Assembly. *J. Am. Chem. Soc.* **2006**, 128, 9408-9412.

[24] Nisisako, T.; Torii, T.; Takahashi, T.; Takizawa, Y., Synthesis of Monodisperse Bicolored Janus Particles with Electrical Anisotropy Using a Microfluidic Co-Flow System. *Adv. Mater.* **2006**, 18, 1152-1156.

[25] Nisisako, T.; Torii, T., Formation of Biphasic Janus Droplets in a Microfabricated Channel for the Synthesis of Shape-Controlled Polymer Microparticles. *Adv. Mater.* **2007**, 19, 1489-1493.

[26] Dubinsky, S.; Zhang, H.; Nie, Z.; Gourevich, I.; Voicu, D.; Deetz, M.; Kumacheva, E., Microfluidic Synthesis of Macroporous Copolymer Particles. *Macromolecules* **2008**, 41, 3555-3561.

[27] Dubinsky, S.; Park, J. I.; Gourevich, I.; Chan, C.; Deetz, M.; Kumacheva, E., Toward Controlling the Surface Morphology of Macroporous Copolymer Particles. *Macromolecules* **2009**, 42, 1990-1994.

[28] Dubinsky, S.; Petukhova, A.; Gourevich, I.; Kumacheva, E., Hybrid porous material produced by polymerization-induced phase separation. *Chem. Commun.* **2010**, 46, 2578-2580.

[29] Duncanson, W. J.; Zieringer, M.; Wagner, O.; Wilking, J. N.; Abbaspourrad, A.; Haag, R.; Weitz, D. A., Microfluidic synthesis of monodisperse porous microspheres with size-tunable pores. *Soft Matter* **2012**, advance article.

[30] Lee, I.; Yoo, Y.; Cheng, Z.; Jeong, H.-K., Generation of Monodisperse Mesoporous Silica Microspheres with Controllable Size and Surface Morphology in a Microfluidic Device. *Adv. Funct. Mater.* **2008**, 18, 4014-4021.

[31] Prasath, R. A.; Gokmen, M. T.; Espeel, P.; Du Prez, F. E., Thiol-ene and thiol-yne chemistry in microfluidics: a straightforward method towards macroporous and nonporous functional polymer beads. *Polym. Chem.* **2010**, 1, 685-692.

[32] Gokmen, M. T.; Van Camp, W.; Colver, P. J.; Bon, S. A. F.; Du Prez, F. E., Fabrication of Porous "Clickable" Polymer Beads and Rods through Generation of High Internal Phase Emulsion (HIPE) Droplets in a Simple Microfluidic Device. *Macromolecules* **2009**, 42, 9289-9294.

[33] Stachowiak, J. C.; Richmond, D. L.; Li, T. H.; Liu, A. P.; Parekh, S. H.; Fletcher, D. A., Unilamellar vesicle formation and encapsulation by microfluidic jetting. *Proc. Natl. Acad.* **2008**, 105, 4697-4702.

[34] Richmond, D. L.; Schmid, E. M.; Martens, S.; Stachowiak, J. C.; Liska, N.; Fletcher, D. A., Forming giant vesicles with controlled membrane composition, asymmetry, and contents. *Proc. Natl. Acad.* **2011**, 108, 9431-9436.

[35] Perro, A.; Nicolet, C. l.; Angly, J.; Lecommandoux, S. b.; Le Meins, J.-F. o.; Colin, A., Mastering a Double Emulsion in a Simple Co-Flow Microfluidic to Generate Complex Polymersomes. *Langmuir* **2010**, 27, 9034-9042.

[36] Shum, H. C.; Lee, D.; Yoon, I.; Kodger, T.; Weitz, D. A., Double Emulsion Templated Monodisperse Phospholipid Vesicles. *Langmuir* **2008**, 24, 7651-7653.

[37] Shum, H. C.; Kim, J.-W.; Weitz, D. A., Microfluidic Fabrication of Monodisperse Biocompatible and Biodegradable Polymersomes with Controlled Permeability. *J. Am. Chem. Soc.* **2008**, 130, 9543-9549.

[38] Shum, H. C.; Zhao, Y.-j.; Kim, S.-H.; Weitz, D. A., Multicompartment Polymersomes from Double Emulsions. *Angew. Chem. Int. Ed.* **2011**, 50, 1648-1651.

[39] Hwang, D. K.; Dendukuri, D.; Doyle, P. S., Microfluidic-based synthesis of non-spherical magnetic hydrogel microparticles. *Lab Chip* **2008**, 8, 1640-1647.

[40] De Geest, B. G.; Urbanski, J. P.; Thorsen, T.; Demeester, J.; De Smedt, S. C., Synthesis of Monodisperse Biodegradable Microgels in Microfluidic Devices. *Langmuir* **2005**, 21, 10275-10279.

[41] Seiffert, S.; Weitz, D. A., Controlled fabrication of polymer microgels by polymer-analogous gelation in droplet microfluidics. *Soft Matter* **2010**, 6, 3184-3190.

[42] Seiffert, S.; Romanowsky, M. B.; Weitz, D. A., Janus Microgels Produced from Functional Precursor Polymers. *Langmuir* **2010**, 26, 14842-14847.

[43] Quevedo, E.; Steinbacher, J.; McQuade, D. T., Interfacial Polymerization within a Simplified Microfluidic Device: Capturing Capsules. *J. Am. Chem. Soc.* **2005**, 127, 10498-10499.

[44] Utada, A. S.; Lorenceau, E.; Link, D. R.; Kaplan, P. D.; Stone, H. A.; Weitz, D. A., Monodisperse Double Emulsions Generated from a Microcapillary Device. *Science* **2005**, 308, 537-541.

[45] Abate, A. R.; Weitz, D. A., High-Order Multiple Emulsions Formed in Poly(dimethylsiloxane) Microfluidics. *Small* **2009**, 5, 2030-2032.

[46] Dowding, P. J.; Atkin, R.; Vincent, B.; Bouillot, P., Oil core/polymer shell microcapsules by internal phase separation from emulsion droplets. II: Controlling the release profile of active molecules. *Langmuir* **2005**, 21, 5278-5284.

[47] Dowding, P. J.; Atkin, R.; Vincent, B.; Bouillot, P., Oil core-polymer shell microcapsules prepared by internal phase separation from emulsion droplets. I. Characterization and release rates for microcapsules with polystyrene shells. *Langmuir* **2004**, 20, 11374-11379.

[48] Loxley, A.; Vincent, B., Preparation of poly(methylmethacrylate) microcapsules with liquid cores. *J. Colloid Interface Sci.* **1998**, 208, 49-62.

[49] Hyuk Im, S.; Jeong, U.; Xia, Y., Polymer hollow particles with controllable holes in their surfaces. *Nat. Mater.* **2005**, 4, 671-675.

[50] Utada, A. S.; Fernandez-Nieves, A.; Stone, H. A.; Weitz, D. A., Dripping to Jetting Transitions in Coflowing Liquid Streams. *Phys. Rev. Lett.* **2007**, 99, 094502.

[51] Clanet, C.; Lasheras, J. C., Transition from dripping to jetting. *J. Fluid Mech.* **1999**, 383, 307-326.

[52] Cahn, J. W., Critical point wetting. *J. Chem. Phys.* **1977**, 66, 3667-3672.

[53] Robledo, A.; Varea, C.; Indekeu, J. O., Wetting transition for the contact line and Antonov's rule for the line tension. *Physical Review A* **1992**, 45, 2423-2427.

[54] Beuermann, S.; Buback, M.; Davis, T. P.; Gilbert, R. G.; Hutchinson, R. A.; Olaj, O. F.; Russell, G. T.; Schweer, J.; van Herk, A. M., Critically evaluated

rate coefficients for free-radical polymerization, 2.. Propagation rate coefficients for methyl methacrylate. *Macromol. Chem. Phys.* **1997**, 198, 1545-1560.

[55] Buback, M.; Gilbert, R. G.; Hutchinson, R. A.; Klumperman, B.; Kuchta, F.-D.; Manders, B. G.; O'Driscoll, K. F.; Russell, G. T.; Schweer, J., Critically evaluated rate coefficients for free-radical polymerization, 1. Propagation rate coefficient for styrene. *Macromol. Chem. Phys.* **1995**, 196, 3267-3280.

[56] Olaj, O. F.; Schnöll-Bitai, I.; Kremminger, P., Evaluation of individual rate constants from the chain-length distribution of polymer samples prepared by intermittent (rotating sector) photopolymerization—2. The copolymerization system styrene-methyl methacrylate. *Eur. Polym. J.* **1989**, 25, 535-541.

[57] Lee, H. B.; Turner, D. T., Autoacceleration of Free-Radical Polymerization. 2. Methyl Methacrylate. *Macromolecules* **1977**, 10, 226-231.

[58] Vázquez, B.; Ginebra, M. P.; Gil, X.; Planell, J. A.; San Román, J., Acrylic bone cements modified with -TCP particles encapsulated with poly(ethylene glycol). *Biomaterials* **2005**, 26, 4309-4316.

[59] Pol, V. G.; Grisaru, H.; Gedanken, A., Coating Noble Metal Nanocrystals (Ag, Au, Pd, and Pt) on Polystyrene Spheres via Ultrasound Irradiation. *Langmuir* **2005**, 21, 3635-3640.

[60] Kotlyar, A.; Perkas, N.; Amiryan, G.; Meyer, M.; Zimmermann, W.; Gedanken, A., Coating silver nanoparticles on poly(methyl methacrylate) chips and spheres via ultrasound irradiation. *J. Appl. Polym. Sci.* **2007**, 104, 2868-2876.

[61] Irzh, A.; Perkas, N.; Gedanken, A., Microwave-Assisted Coating of PMMA Beads by Silver Nanoparticles. *Langmuir* **2007**, 23, 9891-9897.

CHAPTER IV

Microfluidic Synthesis of Janus Polymer Particles

In this chapter we report the microfluidic fabrication of biphasic polymer particles, also known as Janus particles. Using readily available materials we manufactured an effective microfluidic device which generates Janus droplets convertible into the particles. We studied performance of these devices applying computational fluid dynamics methods. Viscous prepolymer solutions of methyl methacrylate containing magnetic iron oxide nanoparticles and 2-hydroxyethyl methacrylate were employed to synthesize anisotropic magnetic and hydrophilic Janus particles. We also employed a mixture of functional monomer with a porogen to produce “clickable” porous/solid biphasic structures.

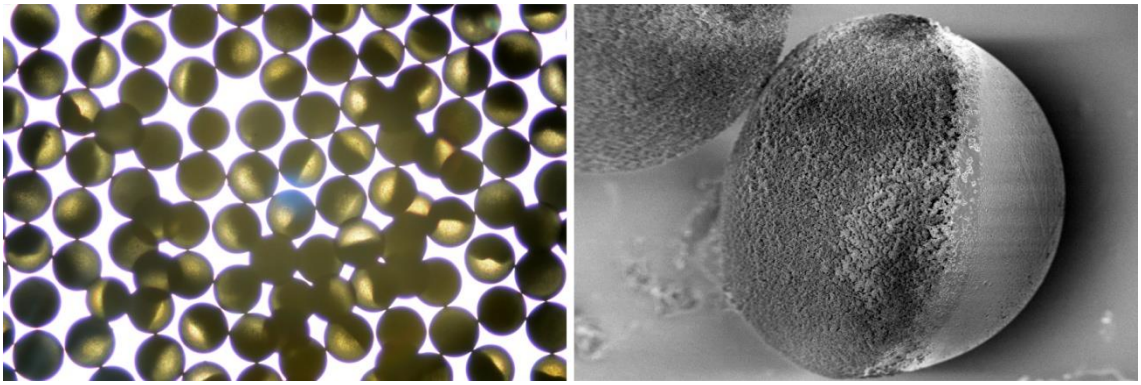

[Graphical abstract]

IV.1 Introduction

We were intrigued by the concept of using simple devices introduced in 2005 by Quevedo *et al.*[1] who used a needle in combination with plastic tubing as a droplet generator, along with the possibilities of microfluidic chips presented by Nisisako and co-workers[2] which allowed robust and continuous fabrication of biphasic Janus particles. Wishing to extend the application boundaries of the droplet-based microfluidics we set ourselves the goal of developing an entry-level microfluidic device, which would incorporate the simplicity of the first, and performance of the second for fabrication of advanced colloidal microparticles.

In this chapter we report that by using affordable expendable materials like standard wall borosilicate capillaries, dispensing needles, PVC tubing and epoxy adhesive such a microfluidic device can be easily manufactured enabling synthesis of anisotropic "Janus" particles (see Figure II-4). We illustrate performance of our device by fabrication of a variety of biphasic particles with tunable porosity, magnetism and surface behaviour.

IV.2 Results and discussion

IV.2.1 Performance of the Janus droplet generators

We studied fabrication parameters of the double T-junction microfluidic device (see Figure II-4). Geometrical peculiarities of the dispersing channels arrangement (aligned at 180°) hindered straightforward Janus droplet generation. Because the channels are separated, instead of one biphasic droplet we noticed the formation of two

independent droplets of the dispersed phase. Due to the use of PVA surfactant and high viscosities of the dispersed phases the two droplets did not coalesce in the main channel after they were formed. A potential solution was to increase the flow rates of the dispersed phases. Usually, the flow rate of the continuous phase is noticeably higher, but this device required equal values for the dispersed and the continuous phases in order to perform Janus droplet generation. In order to investigate this further we ran fluid flow simulations on the continuous phase. Figure IV-1 represents the geometry of the devices used in our modelling experiments.

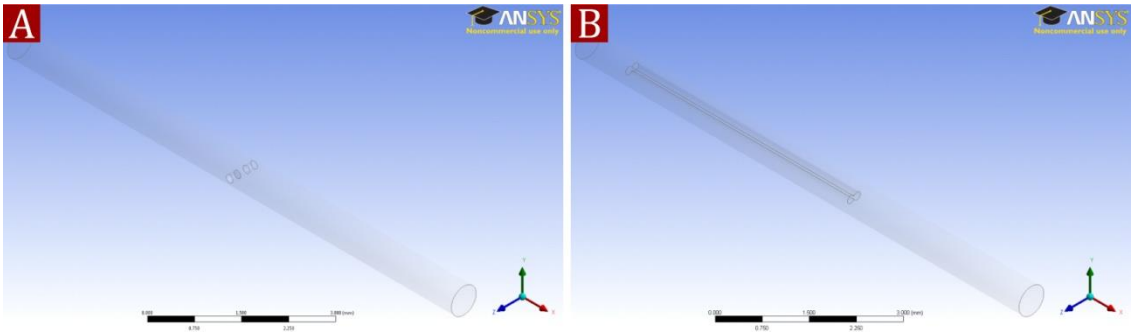

Figure IV-1. Geometry of the devices used in the simulation. (A) Double T-junction device. (B) Paired co-flow device. All scale bars are 3 mm.

The CFD simulations showed that cross-channels obstruct the flow of the continuous phase hereby squeezing the flow as a result of a decrease in the hydrodynamic diameter. This significantly increases the flow velocity of the continuous phase within the droplet formation area. Thus, the maximum lamellar velocity of the fluid before it reaches the needle tips is 5.26×10^{-4} m s^{-1}, whilst in the area between the tips it increases to 7.5×10^{-4} m s^{-1}. Such an enhancement of the velocity of the continuous phase impedes merging of the generated droplets and prevents Janus droplet formation.

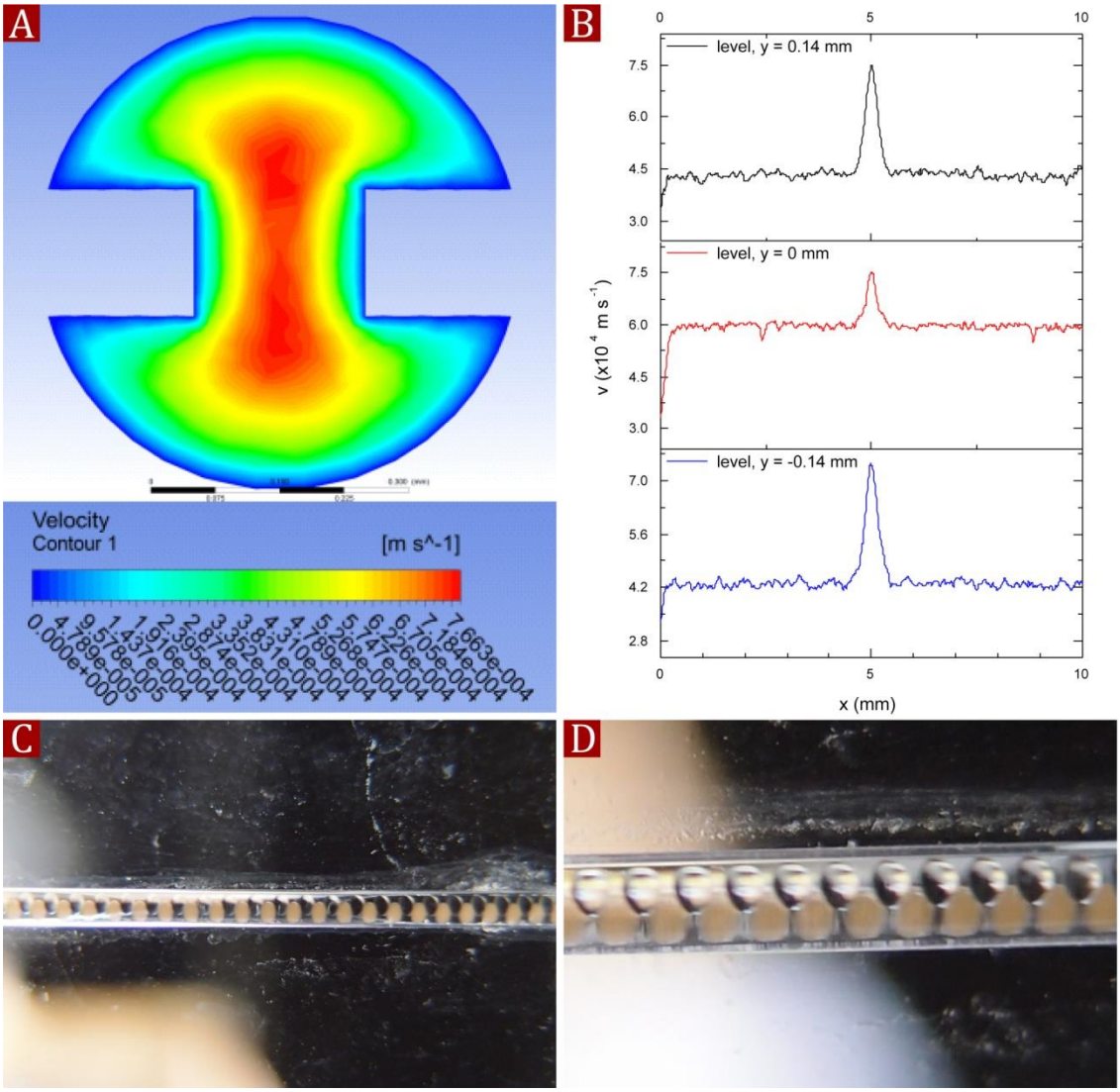

Figure IV-2. The CFD study of the double T-junction device. (A) Contour plots of the velocity within the fluid domain on y-z cross-sectional plane. (B) Velocity distribution along the lines for three y-axis levels: y = 0.14 mm, y = 0 mm and y = -0.14 mm(x = 0 - 10 mm, z = 0 mm), which corresponds to the area between the side channels. (C, D) Simultaneous generation of two types of droplets.

It explains that the relative flow rates of the dispersed phases need to be increased to promote droplet collision and fusion. Despite the fact that this device layout can be used to generate Janus droplets under such conditions, we found its operation to be unstable. For example, the dispersed phases often mixed forming a droplet with many heterogenic layers rather than a proper Janus structure. Nonetheless, a stable generation of two

qualitatively different droplets allows employing it for synthesis of complex droplet-based materials (see Figure IV-2C and D).

Secondly, we investigated performance of the paired co-flow device layout (see Figure II-5). In spite of parallel arrangement of the needle tips, the dispersed phases also tended to be introduced into the continuous phase independently. As well as in the case with the double T-junction device, this phenomenon is due to the geometry of the dispersing channels. We studied a 3D model of our paired co-flow device using computational methods in order to find appropriate methods to avoid a parallel generation of the two phases and fabricate Janus droplets. Figure IV-3 shows the continuous flow inside the main channel. From Figure IV-3A it can be observed that the two jets with the increased flow velocities are generated above and below the paired channels.

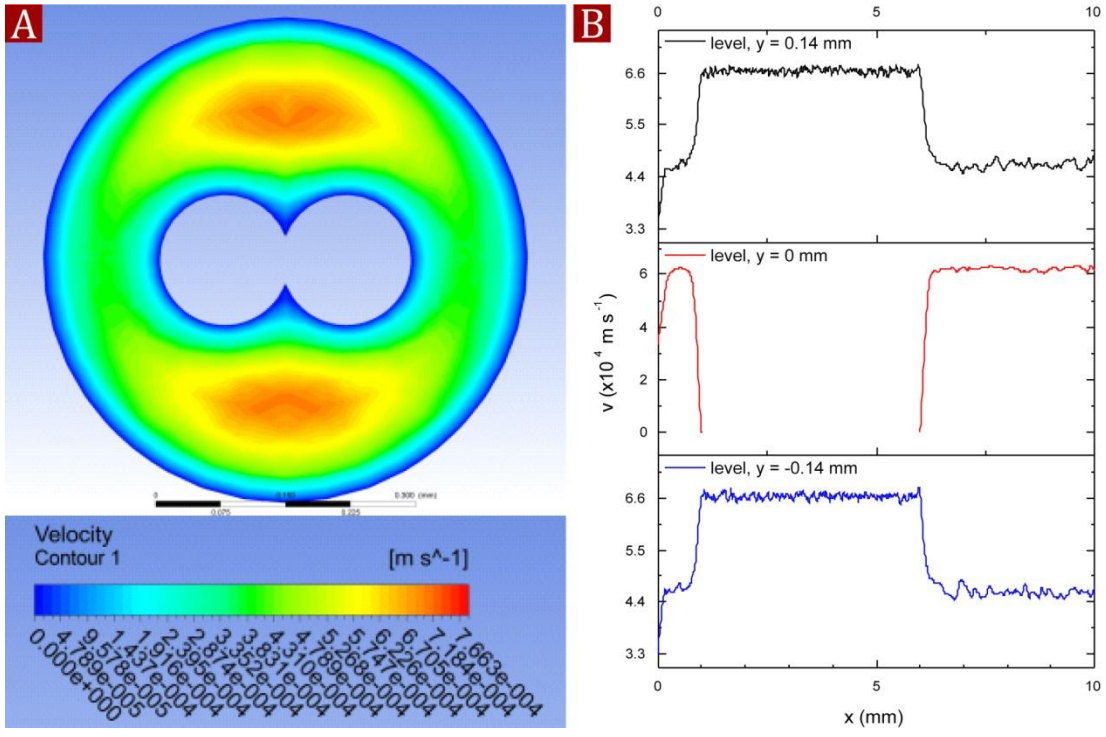

Figure IV-3. The CFD study of the paired co-flow device. (A) Contour plots of the velocity within the fluid domain on y-z cross-sectional plane. (B) Velocity distribution along the lines for three y-axis levels: y = 0.14 mm, y = 0 mm and y = -0.14 mm(x = 0 - 10 mm, z = 0 mm), which corresponds to the inner channel tip area.

From Figure IV-3B it is clear that at the end point of the paired channels the two jet streams align into the centre. This squeezing effect hinders Janus droplet formation. In addition, due to the reduced hydrodynamic diameter of the continuous phase, the actual flow velocity within the droplet generation area is significantly higher than initial value. Immediately prior to the contact between the two phases the flow velocity of the continuous phase is 6.6 m s^{-1}, while the pumping is constant at the rate of 4.31×10^{-4} m s^{-1}. In order to overcome this effect we found experimentally that the flow rates of each dispersed phase should be two times less than the value of flow of the continuous phase. Under these conditions the droplets did merge. Once this was established the continuous phase could slowly be increased to control the overall diameter of the Janus droplets. We started with 0.03 mL min^{-1} and 0.015 mL min^{-1} for the continuous and the dispersed phases respectively. After the dispersed phases merged we increased the continuous phase flow rate by 0.03 mL min^{-1} every minute until it reached a value of 0.15 mL min^{-1}. Figure IV-4 illustrates the use of typical flow rate ratios resulting in the formation of two independent droplets which can be overcome by reducing the continuous phase flow rate.

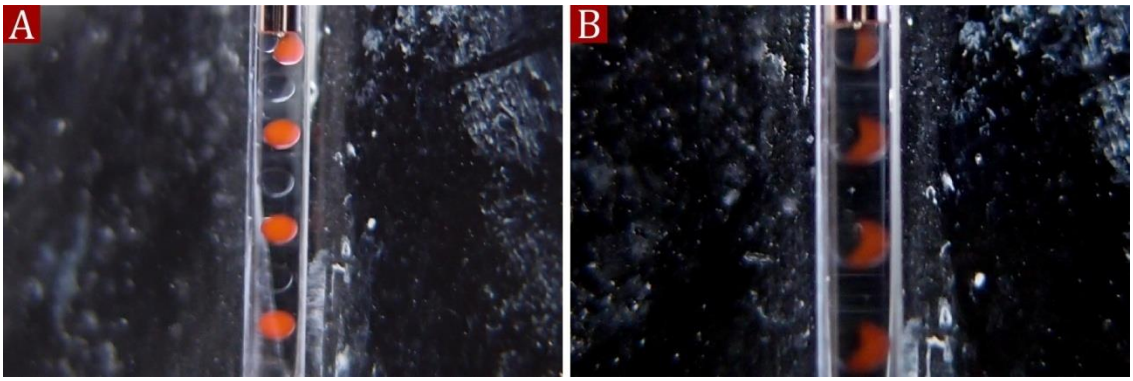

Figure IV-4. Split and merged dispersed phases at the moment of droplet formation. (A) Pink and transparent droplets of two dispersed phases. (B) Tuning the flow rate allows merging before conglobation.

It also should be emphasised that the paired co-flow device can operate in two regimes: dripping and jetting. In the case of a dripping regime (as studied above) we can use the same principles as we noted in Chapter I to describe it; the jetting regime has a different nature. The essential difference is that the dispersed flow elongates forming a jet before a droplet forms. Essentially this regime happens at relatively higher flow rates for the dispersed phase and, thus, a lower flow rate for the continuous phase. Due to the use of viscous liquids instead of bigger droplet formation, the continuous flow rate reduction leads to a slow dragging of the dispersed phase. This result in the parallel flow of two phases before the interfacial phenomena conglobates the dispersed one. An obvious negative effect is that longer contact time between the two components of the biphasic dispersed flow can cause mixing, which perturbs the integrity of Janus droplets. Figure IV-5 displays behaviour of the flows typical to dripping and jetting regimes in our paired co-flow device.

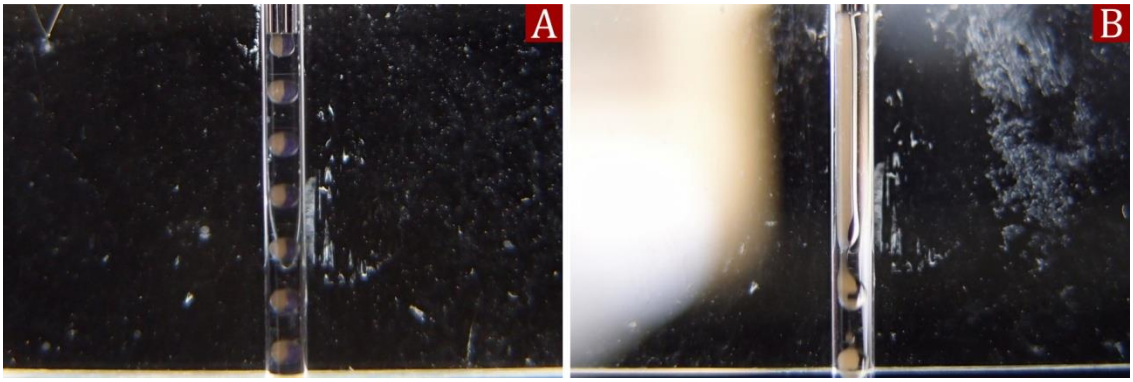

Figure IV-5. The regimes of the Janus droplets generation. (A) Dripping regime of Janus droplet formation. (B) Jetting regime leading to unstable biphasic droplet generation.

Our study showed us that the paired co-flow device layout is preferable for Janus droplet fabrication, as it allows achieving a more stable performance and tune such important parameter as droplet size.

IV.2.2 Preparation of monomers with desired viscosity

Due to a limited choice of immiscible polymerisable compounds which can add a functionality to the particles the viscosity is the main tool to achieve this goal. For example, Nisisako used ethylene glycol dimethacrylate or 1.6-hexanediol diacrylate with silicone oil to form biphasic droplets.[2, 3] We found that benzyl methacrylate can also be employed in combination with silicone oil, but ethylene glycol dimethacrylate, 1.6-hexanediol diacrylate and benzyl methacrylate are only monomers which can be used to form Janus particles with silicone oil without any modifications. In the case of application of monomers in the form of a viscous pre-polymerized solution, the choice is almost unlimited providing great synthetic opportunities. The key is to control the viscosity of the solution so that mixing time scales can be slowed down. In order to achieve it we ran several experiments tuning the amount of initiator used to synthesize a prepolymer solution. Nisisako *et al.* reported that two miscible monomers at the 20 mPa·s viscosity do not mix within a microfluidic channel allowing to generate biphasic droplets.[4] We found that in our case values below 100 mPa·s do not provide robust fabrication of Janus droplets. The difference lies in the channels geometry of the microfluidic devices used. Thus, in the case of the device reported by Nisisako,[2, 4] the geometry of dispersion channel does not affect the Janus droplet formation allowing gentle Janus droplet withdraw from its tip, while our paired co-flow layout forces the continuous phase to put more pressure on the dispersed ones before they conglobates. This in turn causes active mixing which violates Janus structure of the generated droplets. Table IV-1 shows finding of a valid concentration of the initiator and prepolymer processing before their use as the dispersed phase.

Table IV-1. The viscosity of use prepolymers as a derivative of the initiator amount.

Type	MMA, g	HEMA, g	Initiator, g	MMA addition, g	Viscosity, mPa·s
Hydrophobic	10	x	0.015	5	101
	10	x	0.020	5	134
	10	x	0.025	5	***173***
Hydrophilic	8.5	1.5	0.015	5	110
	8.5	1.5	0.020	5	152
	8.5	1.5	0.025	5	***193***
Magnetic	10	x	0.015	5	105
	10	x	0.020	5	141
	10	x	0.025	5	***178***

Mention should also be made of the amount of post-added methyl methacrylate. We tried 1, 3 and 5 mL and found that the last (5 mL) tunes the viscosity of the prepolymer to the required value of >150mPa·s. We found that if the prepolymer was used without MMA post-addition, the needle channels were often blocked after several minutes of use. We believe that hydrodynamic flow compression caused by the contraction of the dispersion channel during the transition from a glass capillary (ID 0.58 mm) into the 32 gauge needle (ID 0.1 mm) (see Figure IV-4A) rapidly increased viscosity of the dispersed phase. Such a change of physical properties of liquids under the influence of external factors, is known as jamming effect, and was studied in detail by Weitz, Coussot and Jaeger.[5-7] Mixtures used to form the porous part of the Janus particles themselves were viscous due to the nature of 1-decanol and dibutyl phthalate employed as porogens. However, the difference in viscosity between porosity imparting and

mixtures noted in Table IV-2 did not allow merging of the two phases. To overcome this issue we additionally reduced viscosity of the hydrophobic, hydrophilic and magnetic prepolymers by mixing them with pure MMA in 4:1 ratio.

It is important to consume all photoinitiator in the prepolymerisation step otherwise it can self-cure inside the microfluidic device. We found that all prepolymers did not polymerise for two weeks remaining unprotected from daylight and left at room temperature. Exposure to 36 kW UV light for 60 minutes also kept it enough liquid to avoid the blockage of the microfluidic channels. The dissolution of an additional amount of the photoinitiator allowed curing prepolymers in the UV reactor within 30 minutes by virtue of rapid achievement of the gel point by prepolymers.

In short, providing formation of the Janus droplets using the simplified devices, the viscosity demands an individual experimental study until appropriate values will be found.

III. 3.3 Formation of the biphasic structure

Depending on the flow rates of the dispersed phases the paired co-flow Janus droplet generator can produce not only spherical particles where each hemisphere has its unique properties, but torus-like particles when one phase wraps another. Figure IV-5 illustrates this phenomenon. In the first case the flow rate of the MMA prepolymer tagged with Nile red is 0.015 mL min^{-1} while the transparent one flows at 0.005 mL min^{-1} rate leading to the formation of non-hemispherical phase inequality. The photograph IV-6B shows the situation when 0.01 mL min^{-1} flow rate for both phases was used, which allows formation of a regular Janus composition of the droplets. The second type is more preferential, because the active surface of each phase is higher

while in torus-like particles this parameter is non-equal, because one phase covers another during the droplet formation.

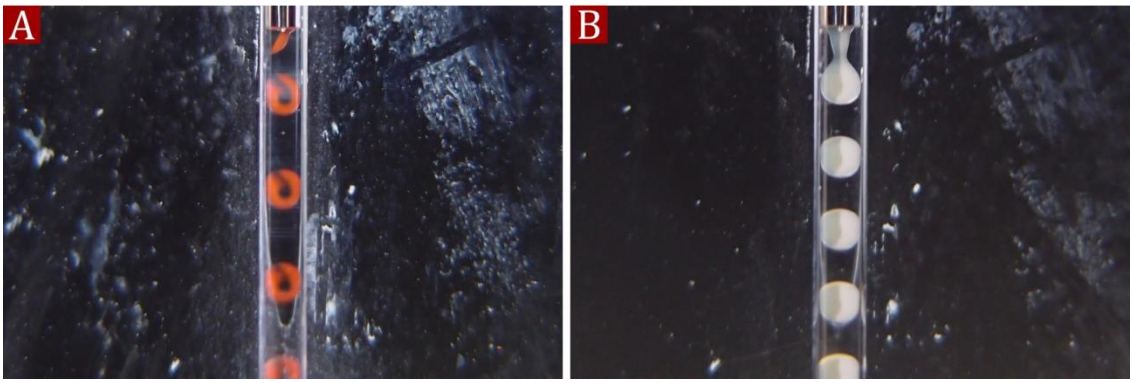

Figure IV-6. The influence of flow rates on the morphology of Janus particles. (A) The coloured phase has higher volumetric flow rate and covers the transparent one. (B) Both phases flow at the same rate forming the proper Janus structure. Nile red (red) and titanium dioxide (white) used as dyes.

The previous sections mainly considered device operation and preparation of the required viscous polymer solutions as fluid phases. Now we are going to look at anisotropic particles which can be fabricated using our paired co-flow device. First of all, we need to look at the variations of solid/solid biphasic particles in detail. The employment of magnetic iron oxide nanoparticles allows us to fabricate spherical particles which are selectively responsive to an external magnetic field by one of their hemispheres. The benefit of the "Janus" magnetism is that particles can be assembled into the colloidal structures, for instance "wires" where the magnetic parts are used as connectors. Figure IV-7 illustrates schematically formation of magnetic/non-magnetic Janus particles and represents their structure.

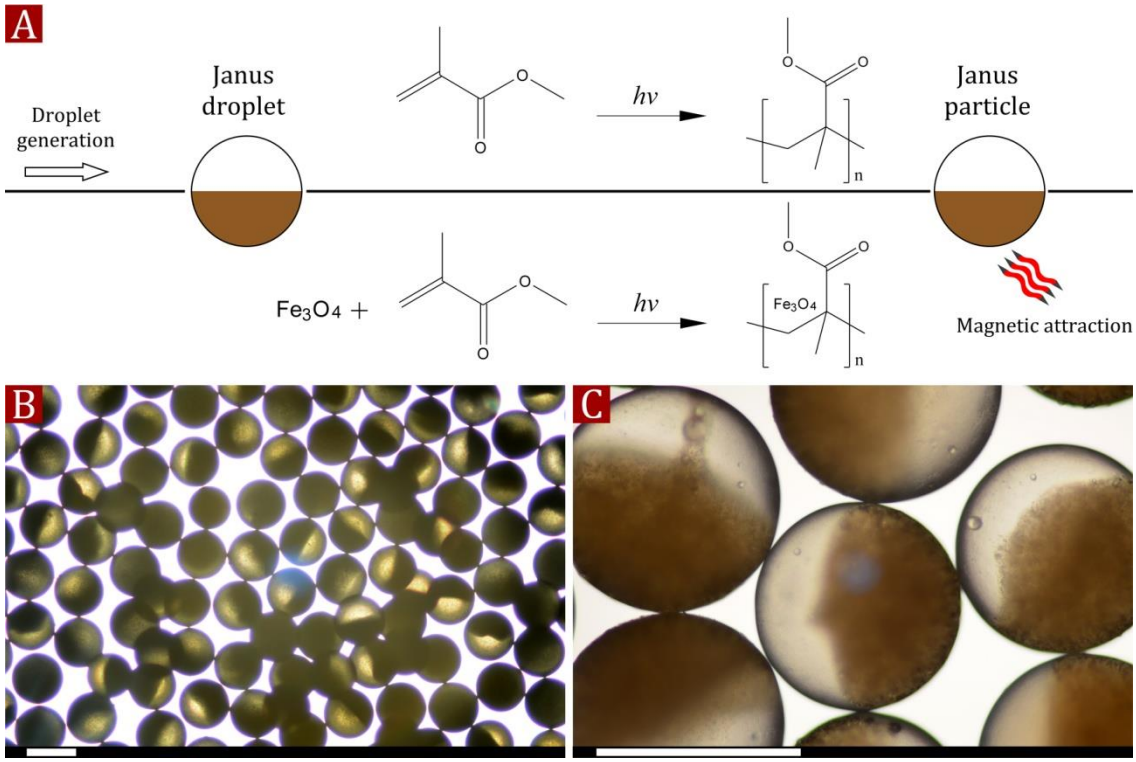

Figure IV-7. Scheme of Janus droplet solidification and micrographs of magnetic/non-magnetic particles. (A) After the droplet generation both parts were cured upon exposure to UV light which impregnated Fe_3O_4 particles into the particle structure. (B) Optical microscopy images of Janus particles. (C) Close look at the particles clearly indicates biphasic structure. All scale bars 400 µm.

Good magnetic properties of fabricated Janus particles allowed us to employ an inefficient 0.5 kg magnet to demonstrate attraction (see Figure IV-8). Such behaviour gives an opportunity to manipulate movement of the particles in a controlled manner, which in turn expands the range of potential applications.

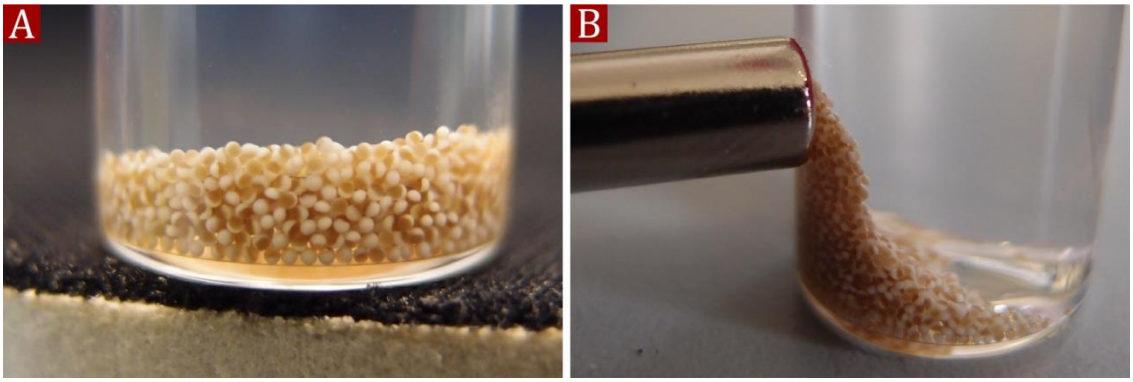

Figure IV-8. Magnetic properties of the Janus particles. (A) Particles in the vial outside the magnetic field. (B) Applying an external magnetic field provided by neodymium rod magnet attracted particles to one of its poles.

Another possibility to intricate Janus particles is hydrophilisation of one of its components resulting in a different surface behaviour. In order to introduce such properties we copolymerised MMA with 2-hydroxyethyl methacrylate, often used for fabrication hydrophilic polymer materials, for instance contact lenses. This copolymer solution was then used as one of the dispersed phases to make amphiphilic Janus particles. Figure IV-9 shows the schematic route of this approach.

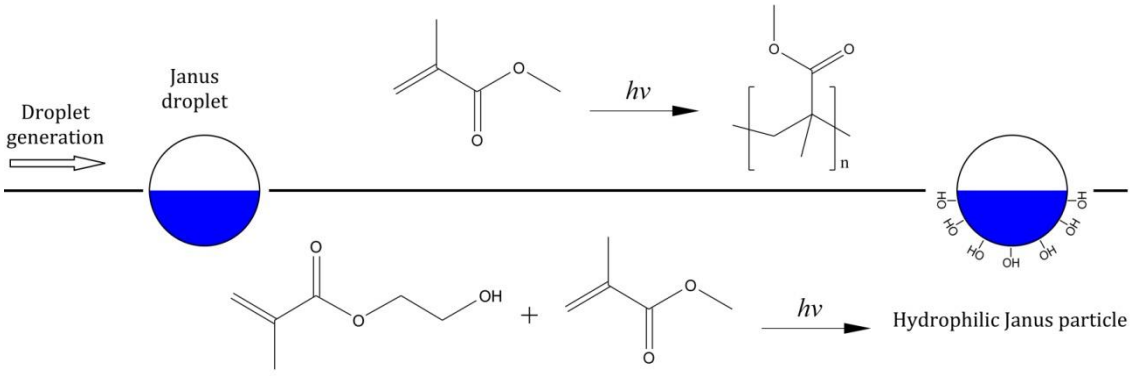

Figure IV-9. Scheme of hydrophilic/hydrophobic particle fabrication.

In practice, intention to minimize surface free energy forced the hydrophilic phase to cover the hydrophobic one with a thin wetting layer, in essence forming a capsule with a biphasic core. Photographs of the droplet generation process clearly show the Janus structure, where transparent is the hydrophilic and red are the hydrophobic parts (see

Figure IV-10). However, scanning electron microscopy showed that the surface of the particles is homogeneous, but cracks on it revealed the difference between top and bottom layers. In order to define properties of each, we ran the silver deposition experiment described in Chapter III. As it can be seen on the Figure IV-10 silver nanoparticles cover only the surface, which confirms its hydrophilicity and our assumptions about its behaviour at the prepolymer/aqueous medium interface.

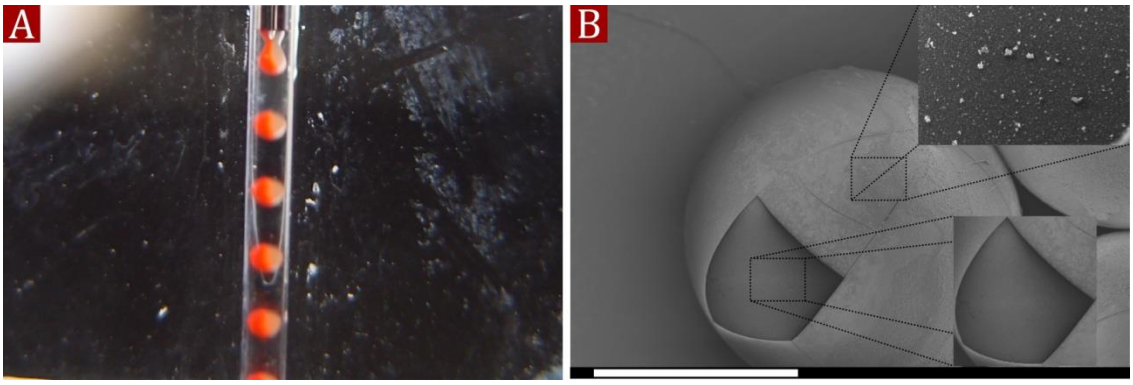

Figure IV-10. Selective silver deposition on the hydrophilic surface. (A) Photograph of Janus droplet generation where coloured flow is the hydrophobic prepolymer and another is hydrophilic. (B) SEM micrograph of the particle and its surface covered with silver particles. Scale bar is 400 µm.

Another type of Janus particles which can be obtained using our paired co-flow device are solid/porous particles. The importance of this type of particles lies in the interactions between the porous part and a medium. Thus, such particles can act like micro sponges and clean the carrier from unwanted contents by adsorption, for example oil droplets from an aqueous medium. Moreover, a seized matter can be released back to the medium in a controlled manner, which makes particles interesting for biological applications such as drug delivery or cell behaviour investigations. Along with the porous component, the solid part can also contribute to the functionality of the Janus particles. In our particular case it can be hydrophilic and reject wetting of its surface accumulating all hydrophobic compounds in the porous part. Otherwise it can be responsive to external magnetic field providing the motility to the loaded porous

component and accurate delivery of a cargo to the desired location. Besides the above described macro properties of the Janus particles, morphology of the porous component can easily be tuned by using different porogens. A mechanism of pores formation is described by the following reaction.

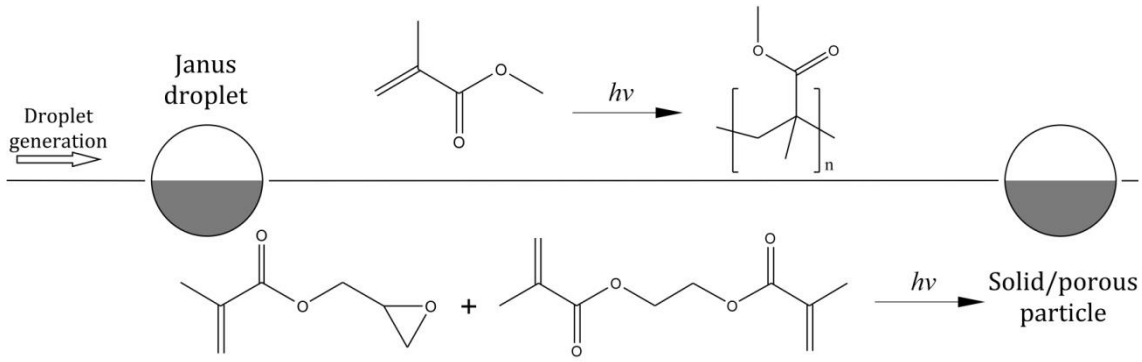

Figure IV-11. Schematic illustration of pore formation. Polymerising molecules of GMA and EGDMA form a cross-linked network which contains an unreacted porogen. Subsequent removal of a porogen results in a porous structure.

We used 1-decanol as the porogen which allowed us to fabricate Janus solid/macroporous particles. Despite the fact that prepolymer and porogenic phases had a lower value of viscosity the formation of proper biphasic droplet was successful. Being stable as droplets some of Janus beads tended to stick to each other during post polymerisation curing, but subsequent porogen removal with ethanol/cyclohexane mixture loosened most of them. The explanation of particle adhesion lies in the properties of the porous component of the Janus particles. Having a soft structure with a high contact surface the porous part integrated with another one upon contact. Figure III-13 represents the morphology of fabricated solid/macroporous Janus particles.

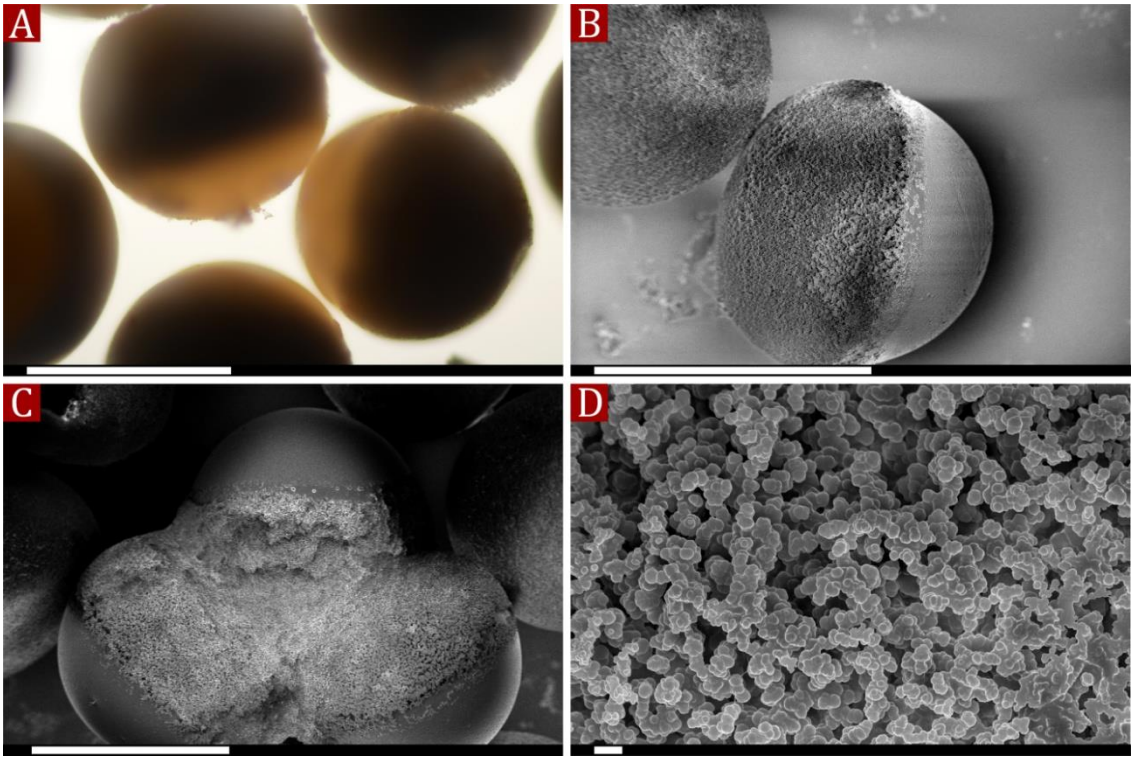

Figure IV-12. Optical and scanning electron microscopy images of solid/macroporous Janus particles. (A) The dark part is porous while light is solid. (B) SEM image clearly defines the biphasic morphology of the particle. (C) Janus triplet as the result of soft-soft interaction between the particles. (D) SEM characterisation of the porosity. (A-C) scale bars are 400 μm, while (D) is 2 μm.

In order to reduce the size of the pores and make them more durable we changed 1-decanol to dibutyl phthalate to reach our goal.[8-10] DBP is well known as an excellent plasticiser introducing elasticity and increasing a value of shock strength of relatively (reduces the brittleness) hard polymers like poly(methyl methacrylate) or polystyrene. We did not detect any differences between the employments of DBP instead of 1-decanol during the Janus droplet generation, but when irradiated with UV light the following the differences were observed. The first one is that Janus droplet solidification did not induce a conglutination. The second one is that both parts of the particles remained transparent until the porogen removal, in contrast to the first case when porous segments instantly whitened. Both differences may indicate completely different morphology of the porous parts of the Janus particles. Our assumptions were

affirmed using optical microscopy and SEM techniques which demonstrated morphological and pore size differences caused by the use of the two types of porogens (see Figure IV-13). We also found that the porous part is covered with a "skin"[9] which formed as a result of complex interfacial interactions during the droplet generation and solidification.[9] In essence it is a less porous layer of the cross-linked polymer, the presence of which did not prevent formation of the normal mesoporous structure underneath.

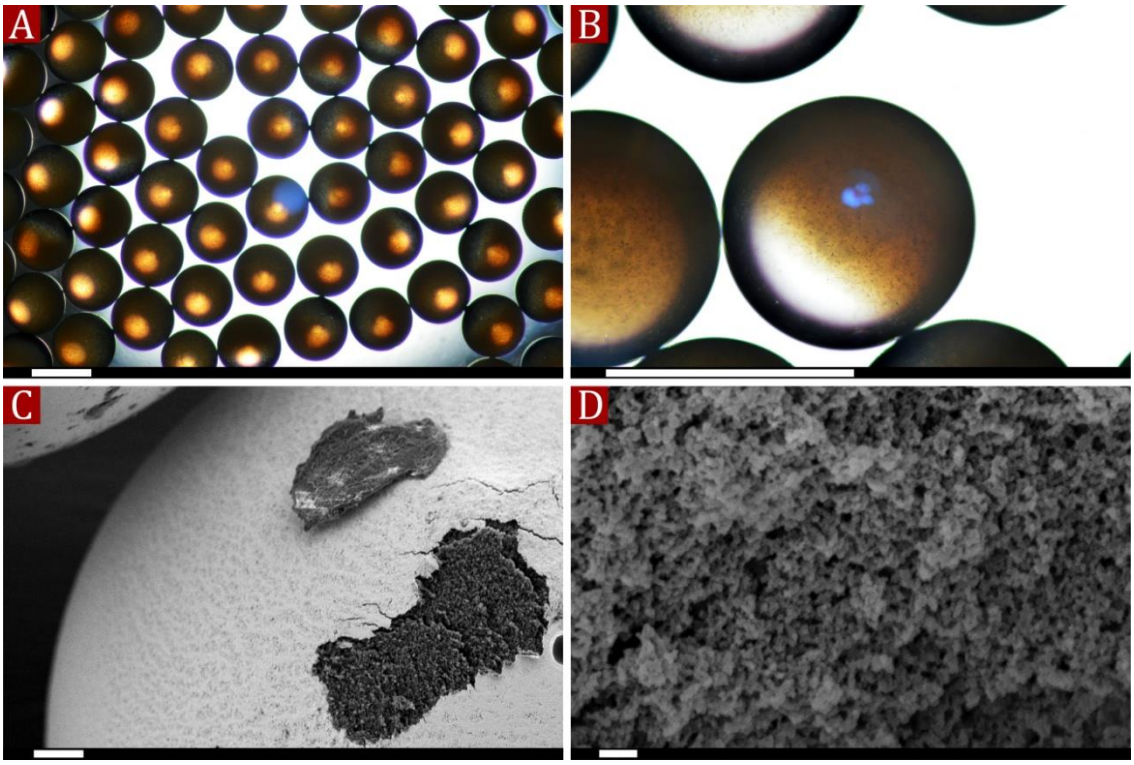

Figure IV-13. Solid/mesoporous Janus particles. (A) Monodisperse solid/mesoporous particles where the darker segment is porous. (B) Closer look at the particles reveals solid segment which is transparent. (C) SEM image of the porous part illustrates a thin layer of "skin"[9] and porous structure under it. (D) SEM characterisation of the porosity. Scale bars (A, B) are 400 µm, (C) is 10 µm and (D) is 400 nm.

We ran a nitrogen sorption porosimetry method to determine pore size distribution also known as Barret-Joyner-Halenda method.[12] According to IUPAC,[13] a mesoporous material has pore sizes in 2-50 nm range, while pores in a macroporous are higher than 75 nm. Figure IV-14A shows that solid/porous particles produced using dibutyl

phthalate have most pores in 200-400 A range (20-40 nm). In the case of 1-decanol we observed that pores are too large to perform nitrogen sorption method. This confirms macroporosity of the Janus particles produced with 1-decanol, which can also be observed on Figure IV-12D, where pores sizes are about 1µm.

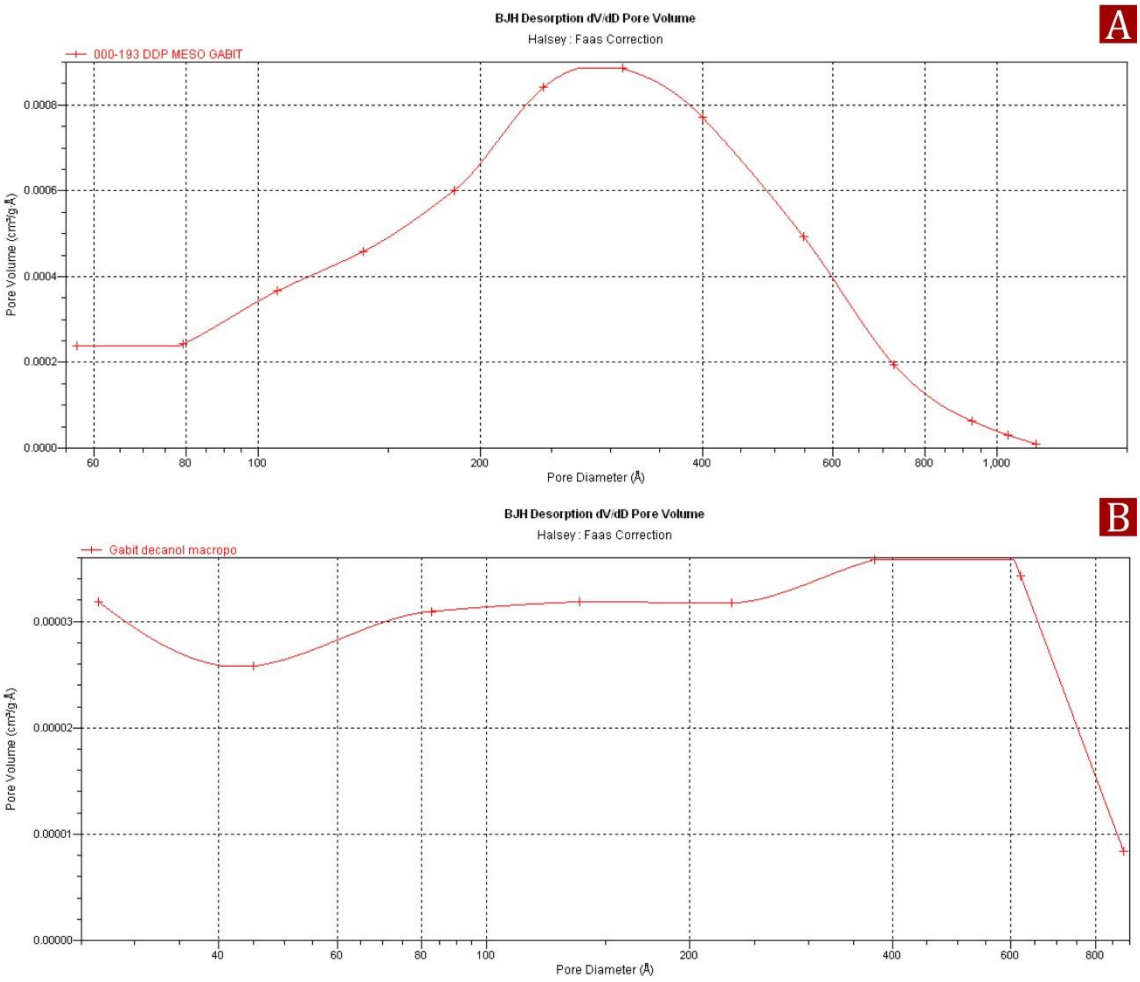

Figure IV-14. Pore size distribution of the Janus solid/porous particles. (A) Pores fabricated using dibutyl phthalate as the porogen. (B) 1-decanol used as porogen.

Apart from the above mentioned potential applications, GMA provides chemical routes to post-utilize a highly reactive epoxy group by running "click" reactions. For instance, this possibility was beautifully realized in fabrication of Janus particles through "sandwich" microcontact printing which was presented by Kaufman and colleagues.[11] In our case, "clicking" of already Janus particles may intricate those more

transforming biphasic particles into triphasic. Aside from above noted phase variations there are possibilities to combine them in a different way. This allows fabricating more intricate particles such as magneto-hydrophobic/hydrophilic, porous/magnetic and porous/hydrophilic Janus beads. In short, despite its simplicity the paired co-flow device robustly generates anisotropic Janus droplets which can be transformed into the particles.

IV.3 Conclusions

More generally it seems hard to deny that our simplified Janus droplet generator provides ample opportunities for fabrication of various anisotropic particles. Computational modelling of the fluid behaviour inside the device allowed us to employ the best layout for effective biphasic droplet generation. The use of viscous dispersed phases significantly extended our choice of compounds appropriate for Janus droplet formation. We also fabricated various types of anisotropic Janus particles including magnetic/non-magnetic or solid/porous particles proving excellent performance of the paired co-flow device layout.

III.4 References

[1] Quevedo, E.; Steinbacher, J.; McQuade, D. T., Interfacial Polymerization within a Simplified Microfluidic Device: Capturing Capsules. *J. Am. Chem. Soc.* **2005**, 127, 10498-10499.

[2] Nisisako, T.; Torii, T., Formation of Biphasic Janus Droplets in a Microfabricated Channel for the Synthesis of Shape-Controlled Polymer Microparticles. *Adv. Mater.* **2007**, 19, 1489-1493.

[3] Nisisako, T.; Hatsuzawa, T., A microfluidic cross-flowing emulsion generator for producing biphasic droplets and anisotropically shaped polymer particles. *Microfluid. Nanofluid.* **2010**, 9, 427-437.

[4] Nisisako, T.; Torii, T.; Takahashi, T.; Takizawa, Y., Synthesis of Monodisperse Bicolored Janus Particles with Electrical Anisotropy Using a Microfluidic Co-Flow System. *Adv. Mater.* **2006**, 18, 1152-1156.

[5] Trappe, V.; Prasad, V.; Cipelletti, L.; Segre, P. N.; Weitz, D. A., Jamming phase diagram for attractive particles. *Nature* **2001**, 411, 772-775.

[6] Ovarlez, G.; Barral, Q.; Coussot, P., Three-dimensional jamming and flows of soft glassy materials. *Nat. Mater.* **2010**, 9, 115-119.

[7] Waitukaitis, S. R.; Jaeger, H. M., Impact-activated solidification of dense suspensions via dynamic jamming fronts. *Nature* **2012**, 487, 205-209.

[8] Dubinsky, S.; Petukhova, A.; Gourevich, I.; Kumacheva, E., Hybrid porous material produced by polymerization-induced phase separation. *Chem. Commun.* **2010**, 46, 2578-2580.

[9] Dubinsky, S.; Park, J. I.; Gourevich, I.; Chan, C.; Deetz, M.; Kumacheva, E., Toward Controlling the Surface Morphology of Macroporous Copolymer Particles. *Macromolecules* **2009**, 42, 1990-1994.

[10] Dubinsky, S.; Zhang, H.; Nie, Z.; Gourevich, I.; Voicu, D.; Deetz, M.; Kumacheva, E., Microfluidic Synthesis of Macroporous Copolymer Particles. *Macromolecules* **2008**, 41, 3555-3561.

[11] Kaufmann, T.; Gokmen, M. T.; Wendeln, C.; Schneiders, M.; Rinnen, S.; Arlinghaus, H. F.; Bon, S. A. F.; Du Prez, F. E.; Ravoo, B. J., "Sandwich" Microcontact Printing as a Mild Route Towards Monodisperse Janus Particles with Tailored Bifunctionality. *Adv. Mater.* **2011**, 23, 79-83.

[12] Barret, E. P.; Joyner, L. G.; Halenda, P. P.; The Determination of Pore Volume and Area Distributions in Porous Substances. I. Computations from Nirtrogen Isotherms. *J. Am. Chem. Soc.***1951**, 73, 373-380.

[13] Rouquerol, J.; Avnir, D.; Faribridge, C. W.; Everett, D. H.; Haynes, J. H.; Pernicone, N.; Ramsay, J. D. F.; Sing, K. S. W.; Unger, K. K.; Reccomendaions

for the Characterization of Porous Solids. *Pure and Appl. Chem.***1994**, 66, 1739-1758.

CHAPTER V

A Simple Microfluidic Device for Microcapsules Fabrication*

In this chapter we show that by using a needle, plastic tubing, two glass capillaries and epoxy glue a microfluidic device can be fabricated. It allows for the production of double emulsions via the generation of droplets-in-droplets. The device is a serial combination of droplet generation by co-flow and a T-junction. To reduce potential issues with channel wetting, we proved that an "obstructed" T-junction outperformed a conventional T-junction. We also illustrate the versatility of our device by producing polymer microcapsules, including ones that contain a waterborne dispersion of a colour changing pigment, and microcapsules with compartmentalized ferrofluidic segments, which are capsules that contain more than one droplet of ferrofluid.

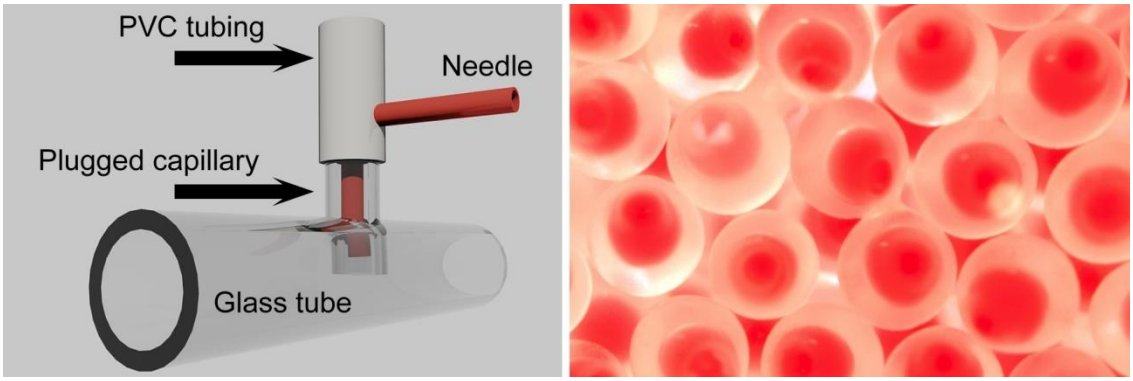

[Graphical abstract]

---

* Part of this chapter has been published:

1. G. Nurumbetov, N. Ballard and S. A. F. Bon, *Polym. Chem.*, 2012, **3**, 1043-1047.

IV.1 Introduction

We were intrigued by the simplicity of the microfluidic set-up reported by McQuade and co-workers[1] in 2005 who in essence used a syringe needle to perforate a plastic tube as a device fabrication strategy towards a T-junction droplet generator. This approach allowed them to produce monodisperse droplets and polymer capsules made through interfacial polymerisation. This simple device fabrication strategy was followed by others, for example Luo and colleagues[2, 3] and us.[4] Inspired by the work of McQuade and co-workers[18] and taking a layout suggested by Choi *et al.*[5] we set ourselves the task to come up with a simplified microfluidic device which was able to generate droplets-in-droplets and that could be assembled and used with ease by the non-specialist polymer community.

Herein we report that by using a syringe needle, plastic tubing, two glass capillaries and epoxy glue, such a microfluidic device can easily be fabricated (see Figure II-7). The device in essence is a serial combination of droplet generation by co-flow and an "obstructed" T-junction. We show versatility of our device through production of polymer microcapsules originating from double emulsions that is droplets-in-droplets.

V.2 Results and discussion

V.2.1 The effect of flow-focussing T-junction

A droplet generation process was described by Clanet *et al.*[6] and further developed by Utada *et al.*,[7] which in general can be characterised as a result of

interaction between dynamic viscous forces, fluid inertia and surface tension. The dimensionless Capillary (Ca) and Weber (We) numbers represent the mentioned forces respectively and are used to describe a droplet generation (see Equitation I-2 and 3). Besides, an important parameter is Reynolds number (Re) characterising local flow behaviour within a droplet generation region (see Equation I-1). Local perturbations can cause instability of the droplet generation process, which in practice affects the monodispersity of the droplets.

One of the variables in both equations is the fluid velocity. The process of droplet generation depends on the fluid velocity in the channels of microfluidic devices. High fluid velocity allows generation of smaller droplets due to the increase of dynamic viscous forces and the reduction of the effects of surface tension, which tend to increase the diameter of the dispersed droplet. In spite of versatility and ease of use of the Ca and We numbers, they generically do not take into account a real fluid velocity profile, which is not homogeneous due to the inner friction of the fluid,[8] resulting in imprecise device assembly and unsteady droplet generation. An influence of fluid flow profiles on the droplet formation and routes to utilization of that effect is debated in the next paragraphs.

Figure V-1 is a schematic representation of the process of double emulsion droplet formation via our simplified microfluidic device. The first step is the formation of droplets of the inner phase into the middle phase via a co-flow set-up, which in essence is a variation of the T-junction device which was reported by McQuade.[1] Making use of a needle bent at 90° facilitates droplet formation and reduces wetting of the walls. In our case (see below) the inner phase is aqueous, and the middle phase is isobornyl acrylate. The second step is generation of the droplet(s)-in-droplet. This is done by making use of an “obstructed” T-junction. With this we mean that by penetrating the capillary into the

glass tube up to a certain distance adds a flow focussing component to the system, which facilitates drop formation and alleviates wetting issues with the walls of the glass tube.

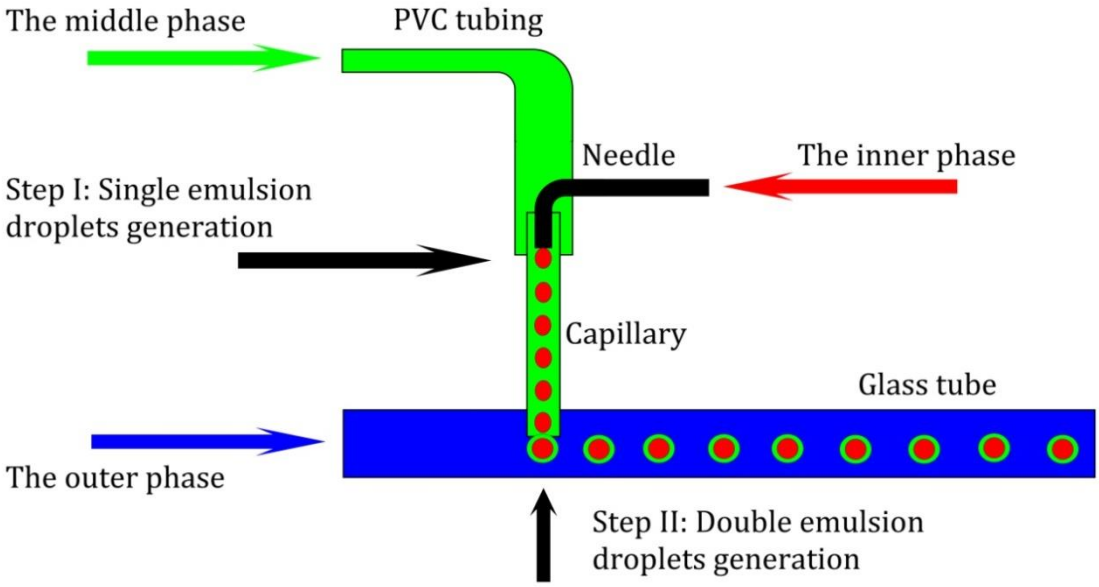

Figure V-1. Schematic representation of double-emulsion droplets generation via our simplified microfluidic device.

The ideal penetration depth was halfway (see below). The outer continuous water phase contains 5 wt% poly(vinyl alcohol), which is added to provide both steric stabilization to the droplets and increases the viscosity of the external water phase.

We carried out fluid flow simulations to understand the influence of the flow rates of the outer phase as a function of the penetration depth of the capillary. Conventionally volumetric flow rates are used whereas it would be more accurate to consider the local flow rate at the tip environment of the capillary. We modelled the capillary as a cylindrical object obstructing the flow of the outer continuous phase in the glass tube. Figure V-2 shows a collection of simulated flow velocity profiles of the liquid in the glass tube. What clearly can be observed is that when the flow in the glass tube is obstructed by the inserted capillary the local velocity increases near its tip.

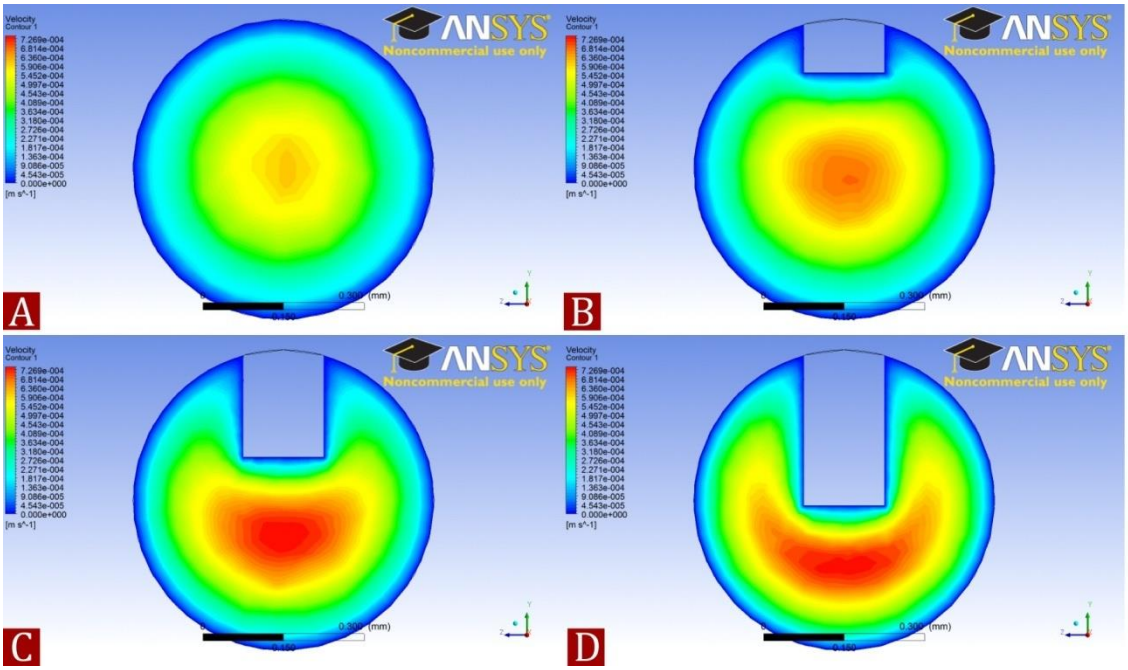

Figure V-2. Fluid flow simulations in a cylindrical tube of inner diameter of 0.58 mm with an orthogonally plugged cylindrical tip of 0.15 mm in diameter. (A) The fluid flow in the tube without obstruction by the capillary and droplets generated by using that layout of the device. (B) The depth of tip penetration is 0.10 mm. (C) The depth is 0.20 mm. (D) The depth is 0.29 mm.

Figure V-3 represents the increase of the flow rate caused by the different penetration depth of the needle.

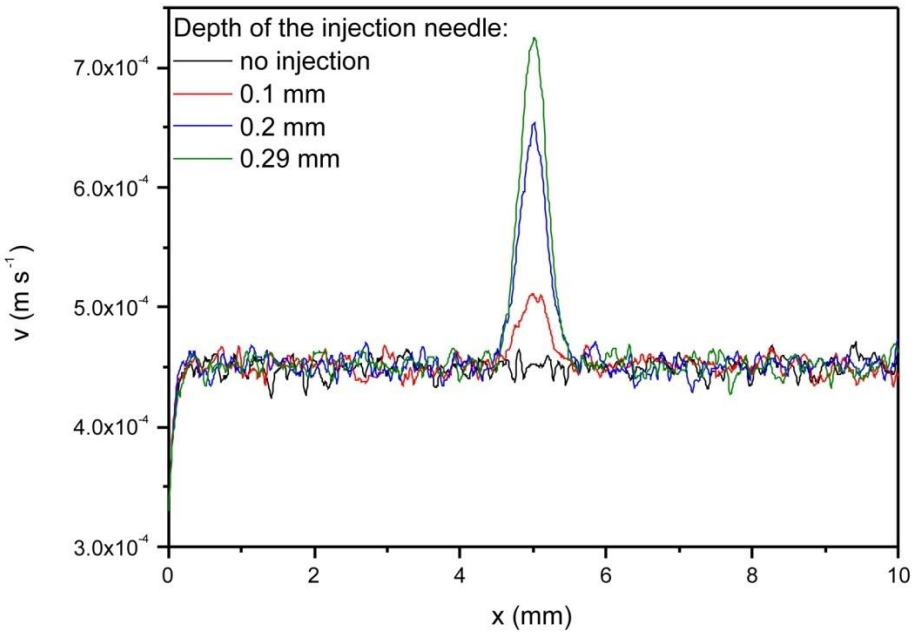

Figure V-3. Velocity distribution at point of the needle tip.

An increase in the local velocity from 4.5×10^{-4} m s^{-1} to 7.5×10^{-4} m s^{-1} raises Capillary number from 9.45×10^{-7} to 1.45×10^{-5} respectively which results in generation of smaller droplets than to be expected on the basis of the average volumetric flow rates.

Table IV-1 represents the experimental parameters of the fluids and channels used in the experiments with various penetration depths.

Table V-1. The parameters for fluids and channels used in optimisation of droplet generation process.

Parameter/Penetration depth	**0 m**	**1.5×10^{-3}m**	**2×10^{-3}m**	**2.9×10^{-3}m**
Main tube diameter, m	0.0058	0.0058	0.0058	0.0058
Cross-tube diameter, m	0.00015	0.00015	0.00015	0.00015
Continuous phase flow rate, mL min^{-1}	0.1	0.1	0.1	0.1
Continuous phase velocity, m s^{-1}*	0.0045	0.0050	0.0065	0.0075
Continuous phase viscosity, kg m^{-1} s^{-1}	0.001	0.001	0.001	0.001
Continuous phase surface tension, N m^{-1}	0.0729	0.0729	0.0729	0.0729
Dispersed phase flow rate, mL min^{-1}	0.01	0.01	0.01	0.01
Dispersed phase velocity, m s^{-1}	0.00944	0.00944	0.00944	0.00944
Dispersed phase flow rate, m^3 s^{-1}	1.66×10^{-10}	1.66×10^{-10}	1.66×10^{-10}	1.66×10^{-10}
Dispersed phase viscosity, kg m^{-1} s^{-1}	0.01	0.01	0.01	0.01
Dispersed phase surface tension, N m^{-1}	0.0317	0.0317	0.0317	0.0317
Dispersed phase density, kg m^{-3}	986	986	986	986

*flow velocity within the tip area according to the simulations.

In order to study the effect experimentally we fabricated a simple T-junction device using a 30 gauge needle, clear C-FLEX® flexible PVC tubing(1/32"ID x 3/32"OD) and

a borosilicate glass capillary (OD 1.0 mm, ID 0.58 mm) in which the needle perforated the capillary and its penetration depth was varied. The continuous aqueous phase (5 wt% PVA solution in water) and dispersed phase (vegetable oil) flow rates were 0.1 mL min^{-1} and 0.01 mL min^{-1} respectively (see Table V-1). The flow rates were kept the same, while penetration the depth was tuned from traditional "on the wall" to the suggested "in the middle of the flow". By placing the needle gradually up to halfway into the capillary indeed the diameters of the droplets generated were reduced from an average value of 418 μm to 282μm (see Figures V-4 and V-5). A general explanation of this effect is that the effective diameter of the main channel is decreasing due to the needle penetration, leading to the increase in the flow velocity and Capillary number. This, in turn, reduces diameter of the produced droplets. The reason why the needle is not placed deeper is that droplets formed will have a larger contact area with the wall upon their formation, which can lead to wetting issues. For this reason we decided that optimized geometry is to place the needle halfway.

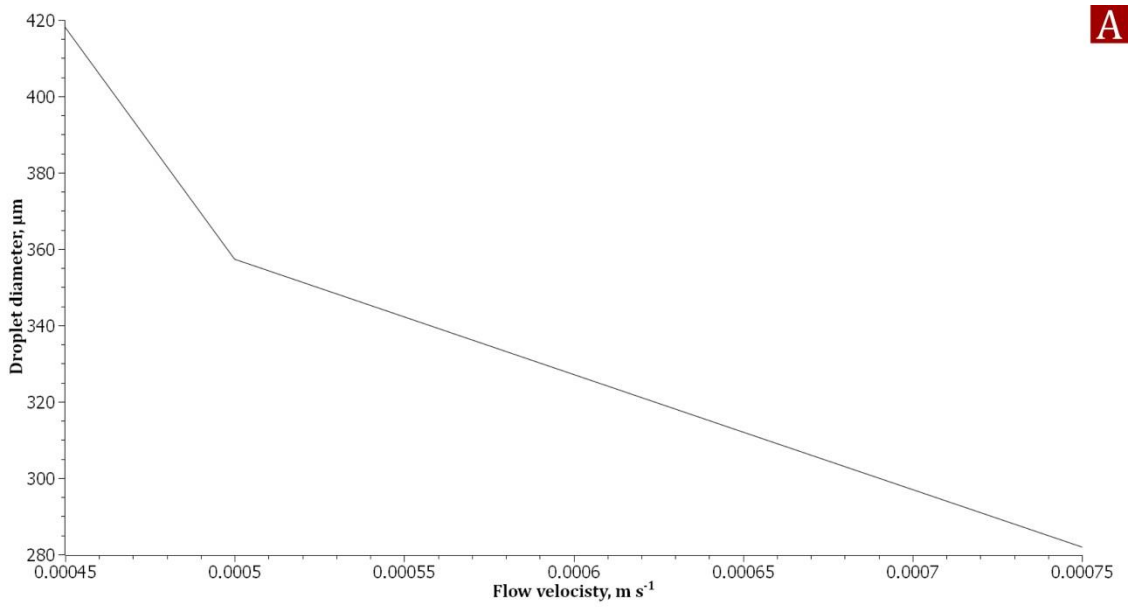

Figure V-4. The fluid flow velocity and droplet size as a function of penetration depth of an orthogonally placed cylindrical tip (OD 0.15 mm) into a cylindrical tube (ID 0.58 mm).

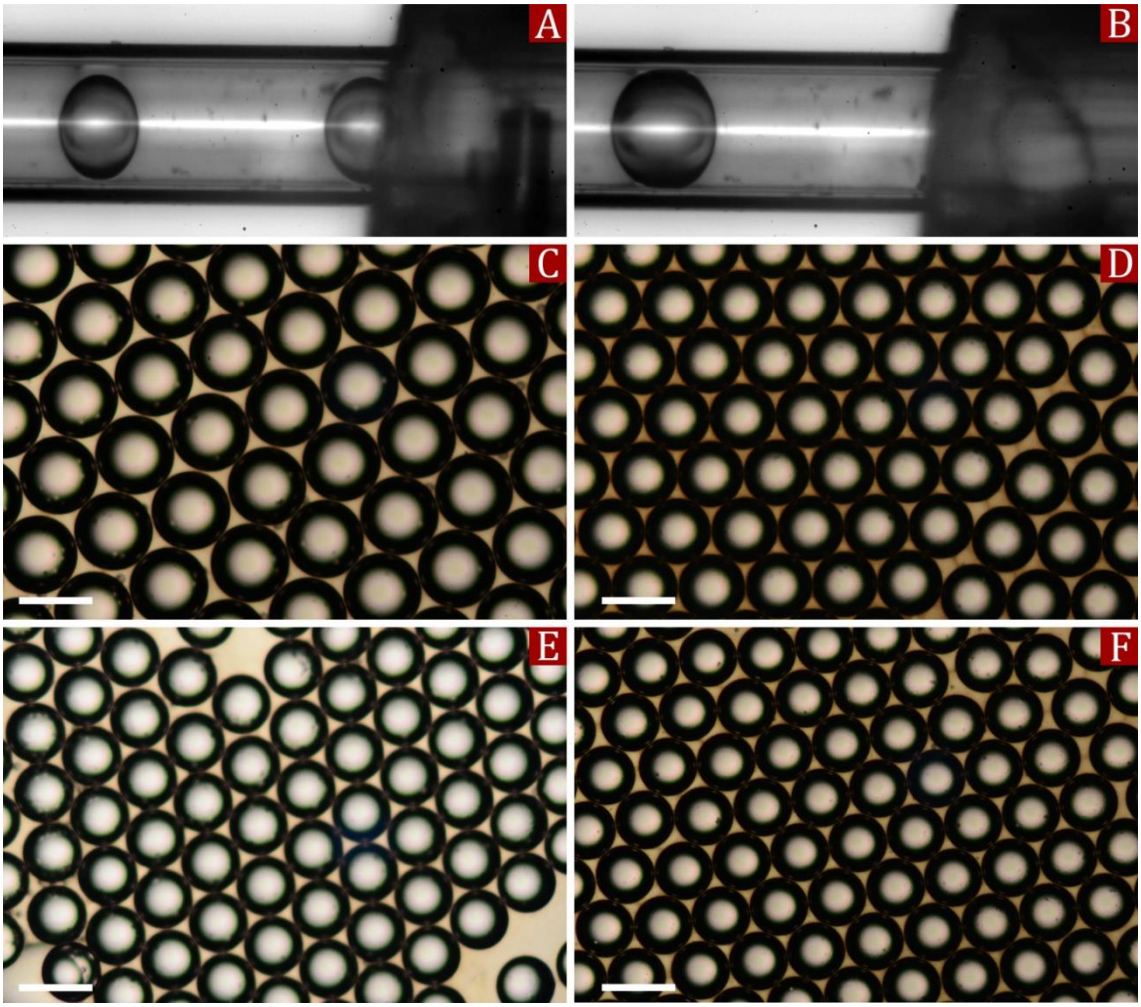

Figure V-5. Visual size reduction of the droplets produced with the different needle penetration depth. (A, B) Droplets in microfluidic channel formed by using obstructed and traditional T-junction. (C) Conventional T-junction, droplet diameter = 418 µm. (D) The penetration depth is 0.10 mm, diameter = 337µm. (E) The depth is 0.20 mm, diameter = 317 µm. (F) The depth is 0.29 mm, diameter = 282 µm. All scale bars are 400µm.

To achieve a high accuracy in the droplet size measurements, we calibrated our Leica DM2500 light microscope by the following procedure. According to Vision Research, the Phantom V7.3 High Speed camera manufacturer, the pixel size on the pictures taken by the camera is 22 microns. So, 1000 µm should be equal to 45.45 pixels. We used 5x magnification lens which increases the amount of pixels to 227.25. In order to check our calculations we took a photograph of 1000 µm calibration standard. Using ImageJ software we found that the standard's length in pixels was

227.15. This value allowed us to perform the precise measurements of droplet sizes analysing images on ImageJ software.

We also performed a statistical analysis of the data obtained from the droplet diameter measurements. We used one hundred values in each case in order to calculate arithmetical mean (X_m), standard deviation (S) and coefficient of variation (C_v) parameters, which are shown in Table V-II. Following equations were used:

$$X_m := \frac{1}{n} \sum_{i=1}^{n} x_i \qquad \textbf{Equation V-1}$$

where n – number of values, x_i – value.

$$S = \sqrt{\frac{1}{n-1} \sum_{i=1}^{n} (x_i - x_m)} \qquad \textbf{Equation V-2}$$

where n – number of values, x_i – value, x_m – arithmetic mean.

$$C_v = \frac{S}{X_m} \qquad \textbf{Equation V-3}$$

where S – standard deviation, x_m – arithmetic mean.

Table V-2. Statistical analysis of droplet diameters.

Statistical parameter	**Penetration depth/ Droplet diameter, µm**			
–	0 mm	0.10 mm	0.20 mm	0.29 mm
Arithmetical mean, µm	418	337	317	282
Standard deviation, µm	1.89	3.11	2.09	2.15
Normal distribution*, µm	418±3.78	337±6.22	317±4.18	282±4.30
Coefficient of variation	0.004%	0.009%	0.006%	0.007%

*according to the Central Limit Theorem 95% of the microcapsules lies in this distribution

V.2.2 Production potential of the device

Our microfluidic set-up (see Figures II-7 and V-1) was used to fabricate polymer capsules with a wall made from poly(isobornyl acrylate) and one or more liquid water-based compartments. Tuning the flow rates of the inner phase and the middle phase allowed for easy control of how many droplets are encapsulated inside a single isobornyl acrylate droplet. Figure V-6 illustrates a monomer molecule employed to fabricate the shell.

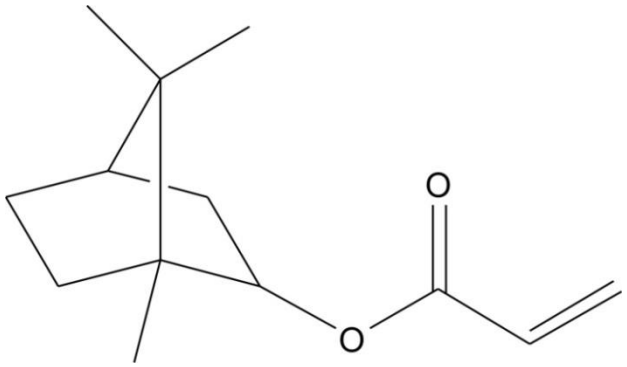

Figure V-6. Isobornyl acrylate

Figure V-7 shows optical micrographs of the capsules produced with different flow rates, while Table V-2 shows the values used to tune the shell thickness and the number of cores. If the flow rate of the inner phase is high enough to form several droplets while the middle phase transforms into a single droplet, multicompartment droplets can be formed.

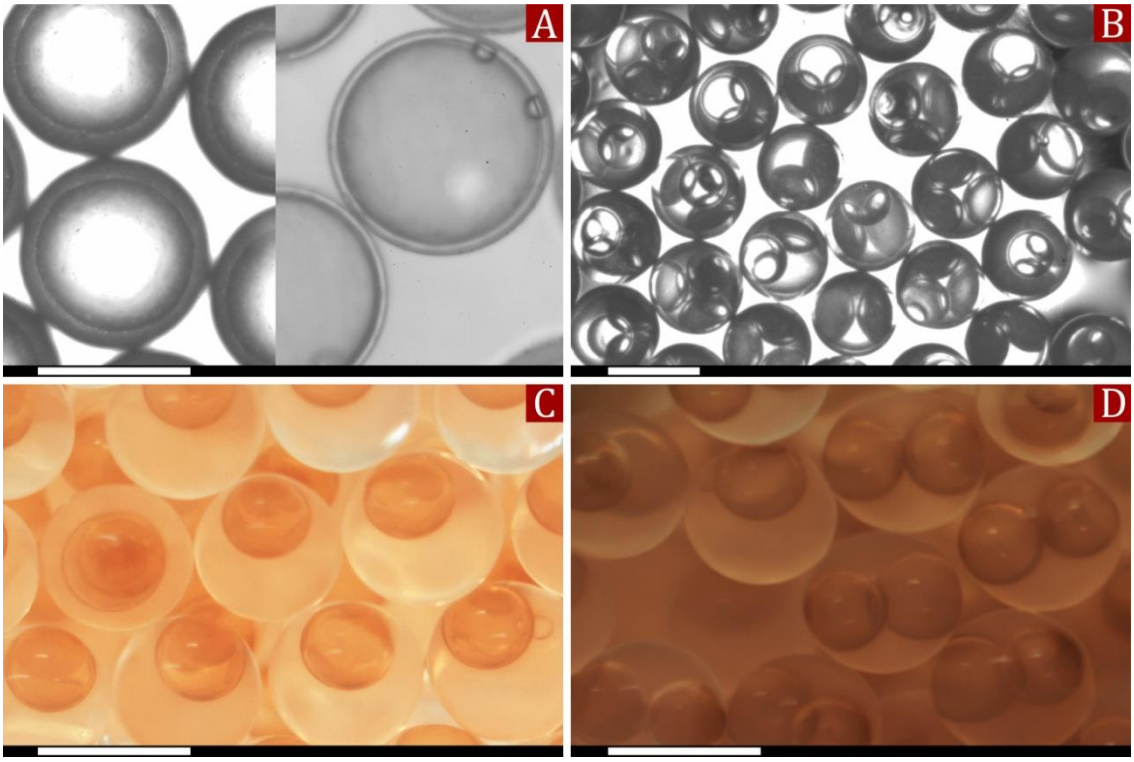

Figure V-7. The capsules with water as encapsulated material. (A, B) Control over the shell thickness and compartmentalisation by tuning flow rates. (C, D) Capsules where the core containing a water-based ferrofluid is surrounded with a poly(IBA) shell. All scale bars are 500 μm.

Table V-3. Flow ratios of the inner and middle phases led to formation of the various types of capsules.

Inner phase flow rate, mL min^{-1}	Middle phase flow rate, mL min^{-1}	Type of capsule
0.004	0.021	Single core, thick shell
0.006	0.019	Single core, thinner shell
0.009	0.016	Single core, thinnest shell
0.011	0.014	Double core
0.012	0.013	Double/triple core

The outer phase flow rate was 0.25 mL min^{-1}in all cases, so that only the inner structure tuned while the size of the droplets unchanged. It is important to realise, that values

given in Table V-2 are exactly applicable only for the device employed in our experiments, because any change of the device geometry will affect the droplet generation parameters. We recommend using given flow rate ratios between the inner and the middle phases as initial values and experimentally clarify the appropriate values for another device, utilizing the obstructed T-junction layout.

Complimentary to the ability to tune the morphology of the capsules, functionality can be achieved by encapsulating various materials into the polymer capsules. For example, by modifying the colour of the cores functional particles that can be valuable as macromarkers or for encapsulating pigments can be fabricated. Figure V-8 shows optical micrographs of coloured water encapsulated in a poly(isobornyl acrylate) shell by curing the middle phase in water-in-IBA-in-water droplets generated *via* the simplified microfluidic device.

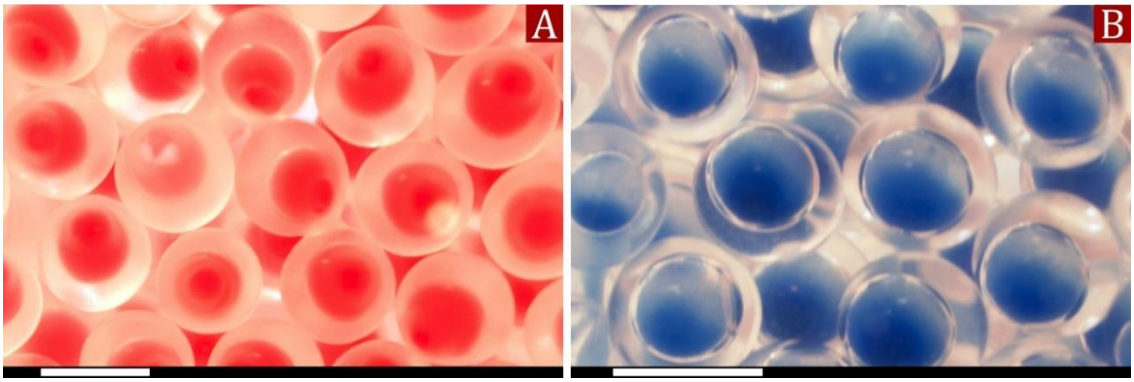

Figure V-8. The capsules with water-based colouring as encapsulated material. (A) Single-core capsules populated with a red pigment surrounded with a poly(IBA) shell. (B) Monodisperse capsules space-filled with a blue pigment. All scale bars are 500μm.

Taking a step forward, the capsules can contain a pigment demonstrating an ability to change from one colour to another under an external stimulus. Figure V-9 shows optical micrographs of the capsules with ChromaZone® heat sensitive pigment, in the core at room temperature and at 40 °C. Due to the ability to reversibly change colour from blue

to white when the temperature rises above 31 °C, these capsules can potentially be used as heat sensors.

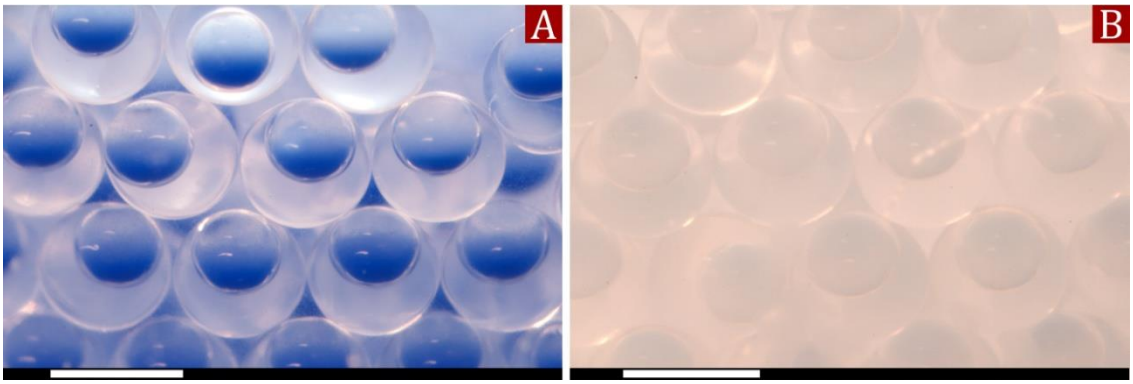

Figure V-9. Colour changing suspension encapsulated in the polymeric shell. (A) The "chameleonic" capsules at room temperature. (B) Monodisperse capsules after temperature increase to 40 °C. Subsequent cooling reverses the effect by making the capsules blue. All scale bars are 500μm.

As well as fabricating particles with interesting optical properties we produced polymer microcapsules with a magnetic core (or multiple cores if so desired). Figure V-8 shows optical micrographs of the magnetically sensitive capsules. Fe_3O_4 particles stabilized by two layers of surfactant in water solution were used as inner phase during the double emulsion droplet generation. During the droplet generation process flow rate of the inner phase was tuned in order to fabricate the multicored droplets. This process does not demand any other modifications to the device so that it is easy to tune the number of core droplets online during the droplet generation process. Subsequent solidification of the middle phase in ferrofluid-in-IBA-in-water led to the formation of magnetically responsive capsules (see Figure V-10).

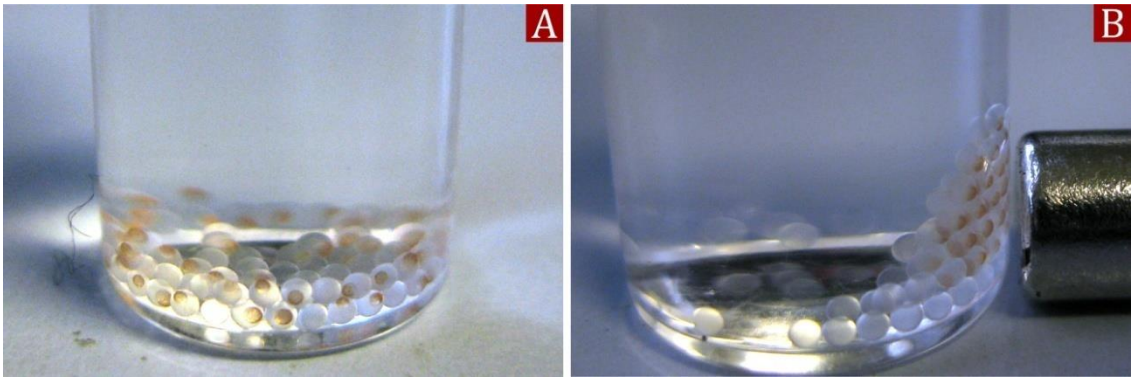

Figure V-10. (A) Magnetic capsules in the vial without applied magnetic field. (B) External field created by neodymium magnet attracted encapsulated ferrofluid and forced capsules to move.

V.3 Conclusions

In this chapter, fabrication of a simplified microfluidic device that can easily be used by polymer chemists for preparation of microcapsules was demonstrated. Fluid flow simulations allowed for the design of an inexpensive, simple and effective microfluidic device for double emulsion droplet generation. This device was successfully used in fabrication of various types of functional materials including heat sensitive capsules which can be used as sensors, and magnetically attractive capsules that offer mobility under application of external forces.

V.4 References

[1] Quevedo, E.; Steinbacher, J.; McQuade, D. T., Interfacial Polymerization within a Simplified Microfluidic Device: Capturing Capsules. *J. Am. Chem. Soc.* **2005**, 127, 10498-10499.

[2] Chen, Y.; Wang, Y. J.; Yang, L. M.; Luo, G. S., Micrometer-sized monodispersed silica spheres with advanced adsorption properties. *AIChE Journal* **2008**, 54, 298-309.

[3] Xu, J.; Li, S.; Tostado, C.; Lan, W.; Luo, G., Preparation of monodispersed chitosan microspheres and *in situ* encapsulation of BSA in a co-axial microfluidic device. *Biomed. Microdevices* **2009**, 11, 243-249.

[4] Gokmen, M. T.; Van Camp, W.; Colver, P. J.; Bon, S. A. F.; Du Prez, F. E., Fabrication of Porous "Clickable" Polymer Beads and Rods through Generation of High Internal Phase Emulsion (HIPE) Droplets in a Simple Microfluidic Device. *Macromolecules* **2009**, 42, 9289-9294.

[5] Choi, S.-W.; Zhang, Y.; Xia, Y., Fabrication of Microbeads with a Controllable Hollow Interior and Porous Wall Using a Capillary Fluidic Device. *Adv. Funct. Mater.* **2009**, 19, 2943-2949.

[6] Clanet, C.; Lasheras, J. C., Transition from dripping to jetting. *J. Fluid Mech.* **1999**, 383, 307-326.

[7] Utada, A. S.; Fernandez-Nieves, A.; Stone, H. A.; Weitz, D. A., Dripping to Jetting Transitions in Coflowing Liquid Streams. *Phys. Rev. Lett.* **2007**, 99, 094502.

[8] Persson, B. N. J., *Sliding Friction. Physical Principles and Applications*. 2nd ed.; Springer: **2000**; p 516.

CHAPTER VI

Microfluidic Fabrication of Armoured Polymer Vesicles

In this chapter we report fabrication of stimuli responsive polymer vesicles using a simplified co-flow double emulsion droplet generator. We show that by using needles and capillaries a high performance microfluidic device can be manufactured. This device was employed to generate double emulsion droplets, which were further transformed into the polymer vesicles. We used PBMA-co-PDMAEMA amphiphilic diblock copolymer to form a bilayer upon solvent evaporation from the middle phase of double emulsion droplets. Chemically active colloids were used to "armour" the bilayer, which further were employed to release the contents of the polymer vesicle or to move them in a controlled manner. Catalytic decomposition of hydrogen peroxide by platinum nanoparticles or MnO_2 was used as the main reaction.

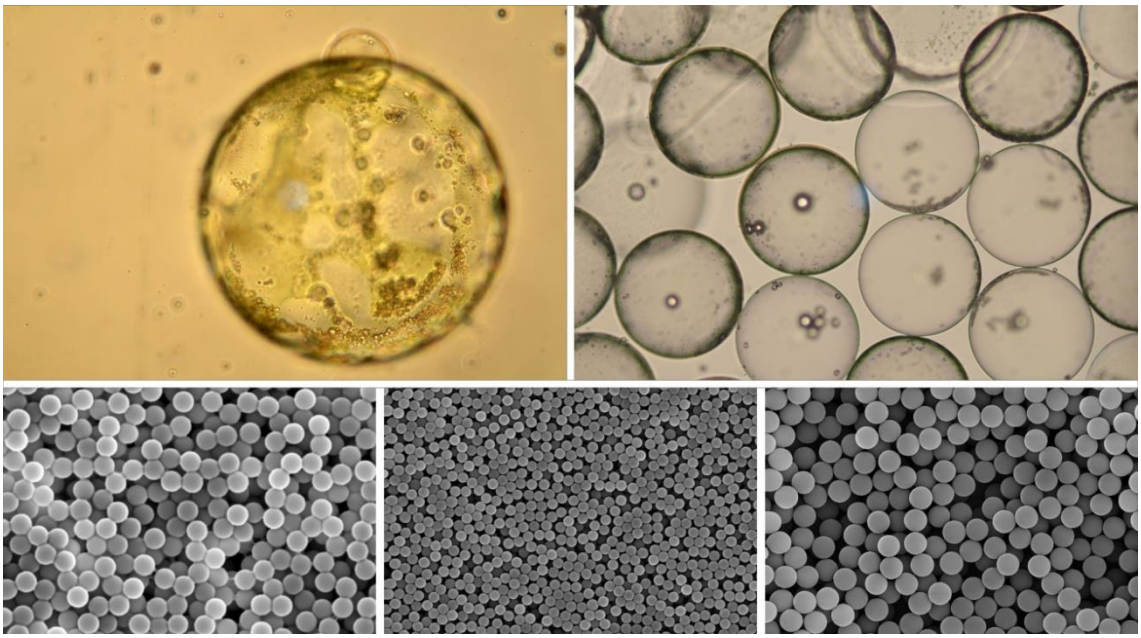

[Graphical abstract]

VI.1 Introduction

We were inspired to develop a plain double emulsion droplet generator by a work presented by McQuade and colleagues,[1] which employs a needle and plastic tube to fabricate microcapsules. In contrast to the device presented in Chapter V we decided to implement a co-flow layout instead of obstructed T-junction, in order to expand the range of simple devices appropriate for the polymersomes fabrication. Moreover, we set ourselves a goal to impregnate stimuli-responsive colloidal particles into the bilayer in order to add functionality such as controlled motility or contents release.

In this chapter we report a fabrication of a simple double emulsion droplet generator based on the co-flow layout, which was employed to produce polymer vesicles. We show synthesis of highly monodisperse polymer colloids which are responsive to external chemical or physical signals. We intricate polymer vesicles by plating a "colloidal armour" on their surface *via* droplet microfluidics.

VI.2 Results and discussion

VI.2.1 Generation of double emulsion droplets

The device employed in our experiments built under the co-flow/flow focussing scheme which implies a step by step dispersion of the inner phase in the middle phase which then should be redispersed in the continuous outer phase. This approach separates the process of double emulsion generation for two areas allowing simplification and increasing the performance of the device. As well as the obstructed T-junction layout presented in Chapter V, this device allows controlling the various parameters of the

droplet formation. First of all, the diameter of the double emulsion droplets and the volumetric ratio between the inner and middle phases, which in turn has an impact on the bilayer thickness of the polymer vesicles. In addition, it allows controlling compartmentalisation producing multiples-core droplets, which later form as non-spherical polymersomes. Figure VI-1 illustrates a versatility of the sectionalised co-flow droplet generation employing the simplified microfluidic device.

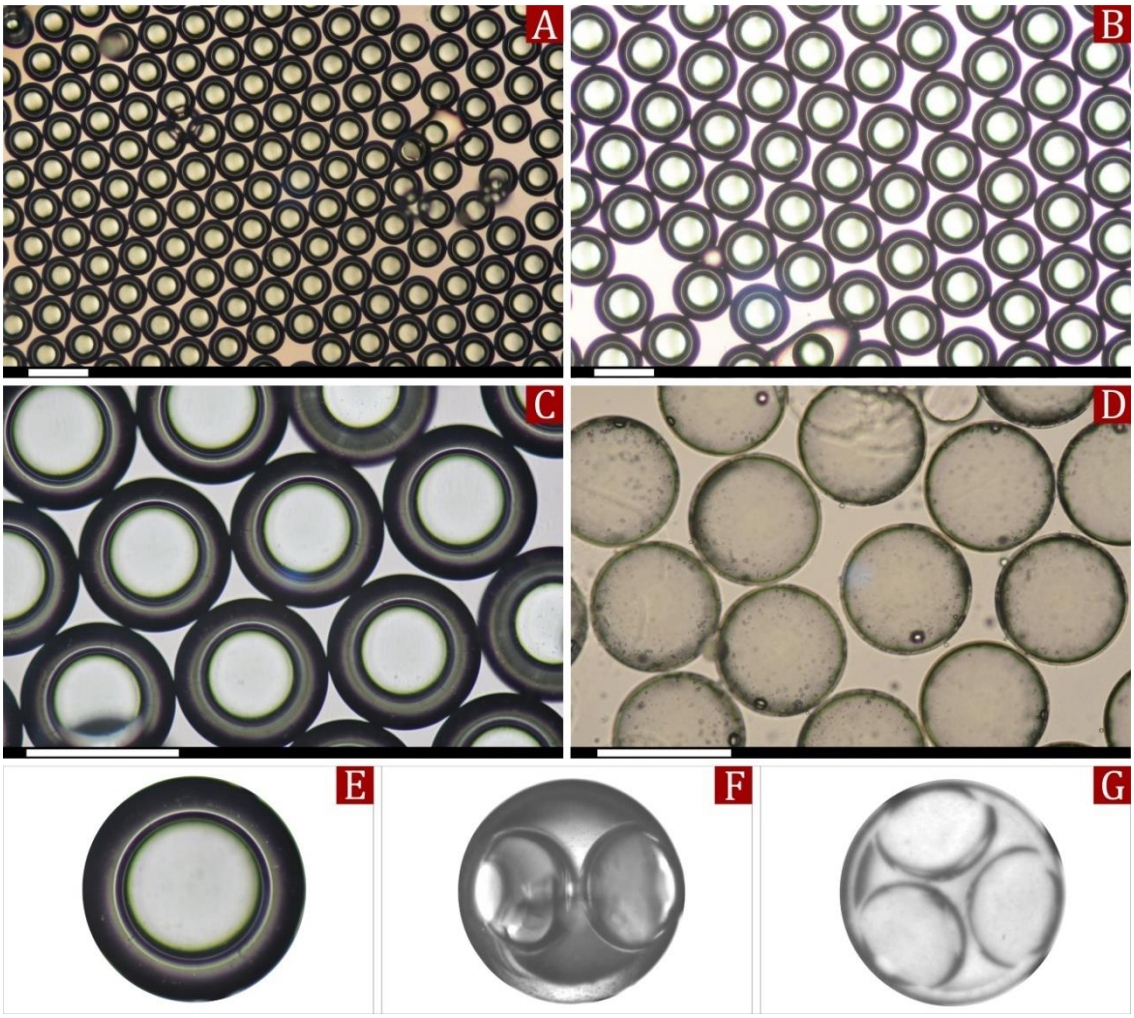

Figure VI-1. A control over the size and shell thickness of double emulsion droplets. (A) Monodisperse water-in-oil-in-water droplets. (B) A reduction of the flow rates led to the fabrication of bigger droplets. (C) The volume of the middle phase is two times higher. (D) A tuning the volumetric flow ratio in favour of the inner phase allowed production of thinned walls droplets. (E) Single-core droplet. (F) Double-core. (G) Triple-core. All scale bars are 150 μm.

All these modifications were carried out by tuning the flow rates during the double emulsion droplets generation. According to our experimental data the size of the droplets primarily depends on the flow rate ratio between the outer phase and cumulative value of the middle and inner phases, while a desired shell thickness and compartmentalisation achievable by changing the flow ratios between the inner and middle phases. Mainly this can be explained by the geometry of the microfluidic device, where processes of the core and shell formation are separated, i.e. each parameter defined by interaction of only two phases. Table VI-1 represents the values of the flow rates for each phase employed to control above noted characteristics of the double emulsion droplets.

Table VI-1. Typical flow rates of the inner (F_I), middle (F_M) and outer (F_O) phases used to control the parameters of the droplets.

F_I, mL min^{-1}	F_M, mL min^{-1}	F_O, mL min^{-1}	Type of double emulsion droplet
0.005	0.015	0.15	Single core, thick shell, size ≈ 150 μm
0.005	0.015	0.23	Single core, thick shell, size ≈ 100 μm
0.007	0.013	0.15	Single core, thin shell, size ≈ 150 μm
0.010	0.013	0.15	Single core, thin shell, size ≈ 150 μm
0.005	0.010	0.15	Double core, size ≈ 150 μm
0.006	0.009	0.15	Triple core, size ≈ 150 μm

An important point which sometimes overlooked is that double emulsion droplet generation is an experimental process, where any theoretical predictions are not reliable. The main reasons are particular geometry of the channels along with physical and chemical properties of the solutions used, which directly affects critical droplet

formation parameters such as Reynolds (Re), Capillary (Ca) and Weber (We) numbers as it comes from the equations describing them (see Equations I-1, 2 and 3).

For all these reasons, any direct use of the flow rate values on another double emulsion droplet generator build under the proposed scheme needs to be treated with caution, because the final results may be different. Nevertheless, the ratios between the flow rates are good starting point which can be experimentally adjusted for a particular device.

VI.2.2 Synthesis of the functional colloidal armour

Due to the usage of the toluene and chloroform as the middle phase, colloidal particles should be highly cross-linked to be employed as "armour". Synthesizing these particles we faced following problems. A fabrication of the poly(divinylbenzene) homopolymer particles using dispersion polymerisation is not reliable due to a high dependence on the stirring rate. The reaction very often ends with coagulation. An employment of the styrene/divinylbenzene mixtures also led to coagulation after the two hours from the reaction initiation. We found that the most effective method is two-stage dispersion polymerisation reported by Winnik and co-workers.[2] The essential difference from the conventional one-stage reaction is that cross-linker does not take part in the nuclei formation since its addition on the second stage. This makes the whole reaction much more stable allowing fabrication of the monodisperse highly cross-linked polymer particles. Despite the fact that original recipe suggests an addition of the pure cross-linker, we found that mixture of the styrene (50 vol%) and EGDMA (50%) performs better. The synthesized polymer particles were easily dispersed in the

toluene/chloroform mixture using the sonication. Figure VI-2 shows the particles synthesized using two-stage dispersion polymerisation.

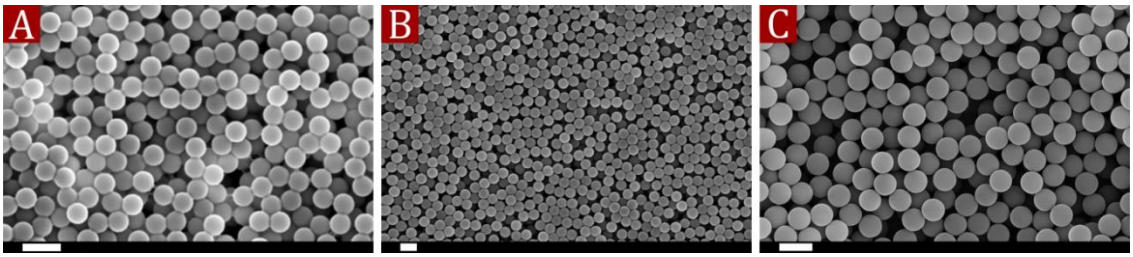

Figure VI-2. Growth of the highly cross-linked polymer particles. (A) SEM image of the particles after the first stage, D_{avg} = 1.20µm. (B) After the second stage, D_{avg} = 1.70µm. (C) After the cross-linker addition, D_{avg} = 1.85 µm. All scale bars are 3 µm.

Obtained particles were functionalised by coating with the platinum nanoparticles. This allowed us to use them as catalytic centres after the impregnation into the bilayer of the polymer vesicles.

VI.2.3 Formation of the bilayer from the liquid middle phase

Solvent evaporation from the middle phase has a high impact of this process on the formation of the bilayer. The PBMA-block-PDMAEMA copolymer dissolved in the middle phase has an amphiphilic structure since the PBMA is hydrophobic, while PDMAEMA is hydrophilic. This dual nature forces the molecule of copolymer act as a surfactant in the middle phase of the double emulsion droplet. Theoretically, hydrophilic blocks seeking to minimize the surface free energy should be in the aqueous medium, whereas hydrophobic should remain in the non-polar middle phase just like molecular surfactants. In the case of double emulsion droplets the inner aqueous phase should be stabilised within the middle phase as the result of such behaviour of the block copolymer. We found that in practice the performance of the PBMA-block-PDMAEMA was fully consistent with theoretical assumptions, since the inner phase was robustly

stabilised solely by the copolymer. In addition to the inner/middle interface, double emulsion droplets have the middle/outer at which the copolymer presumably acts likewise. Subsequent solvent evaporation from the middle phase from such droplets led to the formation of the bilayer (see Figure I-11).

What sort of picture do these considerations allow us to construct? The molecules of the amphiphilic block copolymer are thermodynamically oriented at the two water/oil interfaces available in the structure of the double emulsion droplets. The solvent removal from the middle phase causing compression of the two interfaces which results in the bilayer formation. If the amphiphilic behaviour is proven experimentally, the formation of the proper bilayer remains unverified. The crucial question therefore is whether the shell forming after the solvent evaporation is the bilayer? Armes and colleagues reported an employment of transmission electron microscopy, confocal laser scanning microscopy, atomic force microscopy, and fluorescent microscopy to study the morphology of the micro- and nanometer-sized polymersomes.[3-5] In this chapter we used transmission electron microscopy to observe the structure of the polymer vesicles as the main analysis technique. We also used cryogenic scanning electron microscopy as the auxiliary method. Figure VI-3 shows the micrographs of the microfluidically synthesized polymer vesicles obtained *via* above mentioned techniques. The thickness of the bilayer allows us to say, that by using microfluidics it is possible to fabricate polymer vesicles rather than capsules.

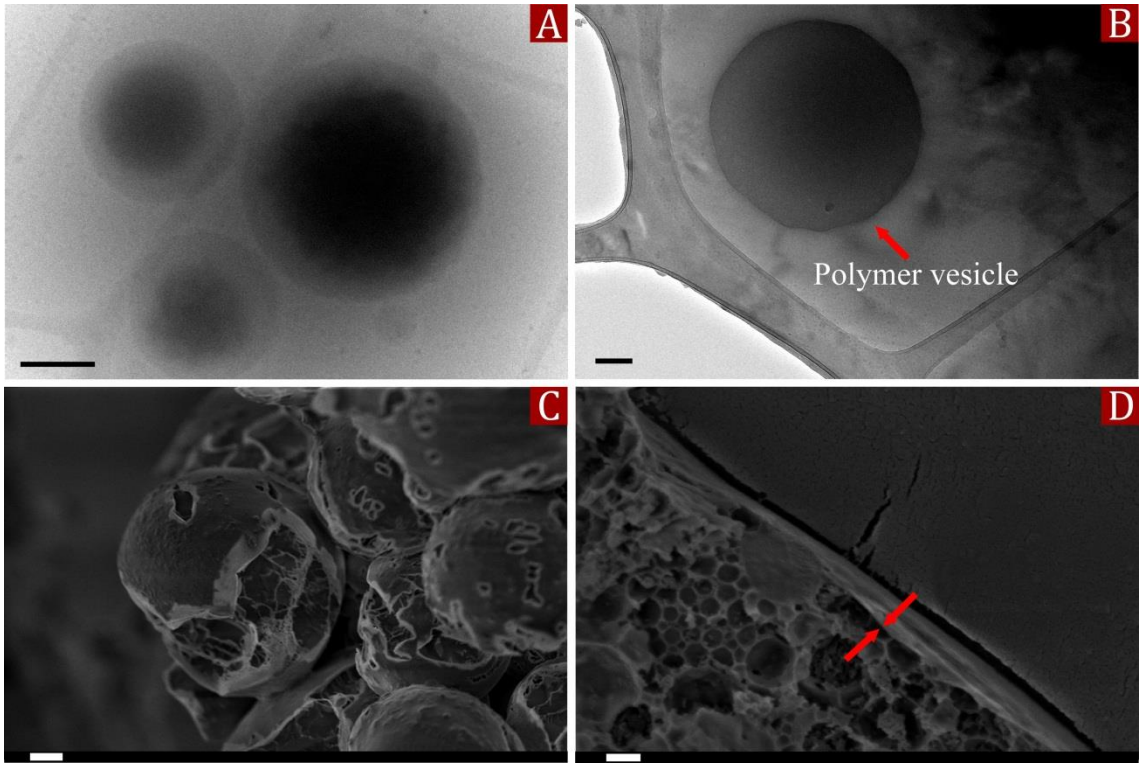

Figure VI-3. TEM and Cryo-SEM images of polymer vesicles. (A, B) TEM images of polymer vesicles. (C, D) Cryo-SEM images. The bilayer between the ice (smooth area) and vesicles contents (bubbly area). Scale bars are 500 nm (A) and 200 nm (B), 2 μm (C), 400 nm (D)

Another important question is the concentration of the block copolymer in the middle phase. It should be low to provide the bilayer formation rather than a polymer shell, but enough to stabilise the inner phase droplet to employ the microfluidic approach. We ran three experiments when the concentration of the polymer in the middles phase was 1 g L^{-1}, 5 g L^{-1}, and 10 g L^{-1}. We found that double emulsion droplets are not stable in the first case, whilst the non-stabilised inner phase rapidly diffused through the middle. In the second and third cases the middle phase robustly compartmentalised the inner preventing a diffusion and droplet breakage. We decided to use 5 g L^{-1} and, because it provided the robust droplet stabilisation.

VI.2.4 Stimuli responsive polymer vesicles

The microfluidic method for fabrication of polymer vesicles allowed impregnation of synthesized colloids which are responsive to an external physical or chemical stimulus into the bilayer. This in turn made brought more intricacy, which allowed us to control the motility of the polymersomes or break the bilayer when desired. Such behaviour of the armoured polymer vesicles is important, because it is providing an opportunity to deliver and release the contents at the exactly right location.

First of all, we experimentally verified our approach by fabricating polymer vesicles which contain highly cross-linked polystyrene particles in the bilayer. The concentration of the particles in the middle phase was 0.001 g mL^{-1}, because the higher amount led to the formation of clusters of the particles in the bilayer, while initial goal was to spread them evenly. Apart from the higher solid content clustering could be caused by a fast evaporation process, when the gas bubbles in the middle phase creating an interface where the particles prefer to be acting as Pickering stabilizers.[6, 7] Figure VI-4 illustrates an impact of the middle phase evaporation on the particles distribution in the bilayer.

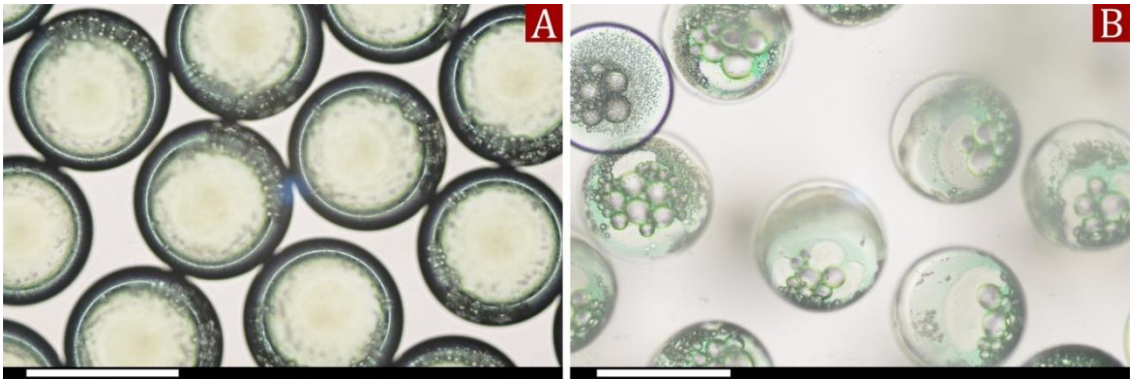

Figure VI-4. Solvent evaporation leading to the particle aggregation. (A) Double emulsion droplets heated to 35 °C which caused bubbling in the middle phase. (B) Polystyrene particles aggregated around the bubbles. All scale bars are 150 μm.

To avoid this phenomenon we maintained the temperature constant at 25 °C and rotated a vial with double emulsion droplets throughout the evaporation process, which allowed removing the solvent more evenly.

Finding a strategy to distribute the particles throughout the bilayer we replaced the highly cross-linked polystyrene beads with particles having platinum nanoparticles on deposited on their surface. In theory, these particles impregnated into the polymer vesicles should provide an opportunity to move them or break the structure of the bilayer due to reactivity with hydrogen peroxide. Platinum catalysed decomposition of the hydrogen peroxide:

$$2H_2O_2 \rightarrow 2H_2O + O_2\uparrow \qquad \textbf{Reaction A}$$

However, in practice polystyrene beads covered with platinum nanoparticles did not show a desired behaviour. This problem has two aspects: a partial coverage of the polymer particles by metal nanoparticles and the size of the colloidal platinum. The sputter coating technique covered only the half of the spherical particles while other remained inactive. This in turn means that all impregnated polystyrene particles can settle in the bilayer so that active part will be a part of interior, because it is difficult to orientate polystyrene particles in the bilayer, so that all deposited platinum will be in contact with hydrogen peroxide. The size of the particles does not preclude their full coverage with the bilayer, which also reduces catalytic activity of the colloidal platinum even if all particles have their active halves turned to the outer surface. Figure VI-5 represents the experiments carried out with the highly cross-linked particles partially covered with colloidal platinum. The polymer vesicles having those particles in the bilayer did not moved or break like we expected upon blending with 30 wt% H_2O_2 solution, we observed only a small deformation and micro-bubbles on the surface.

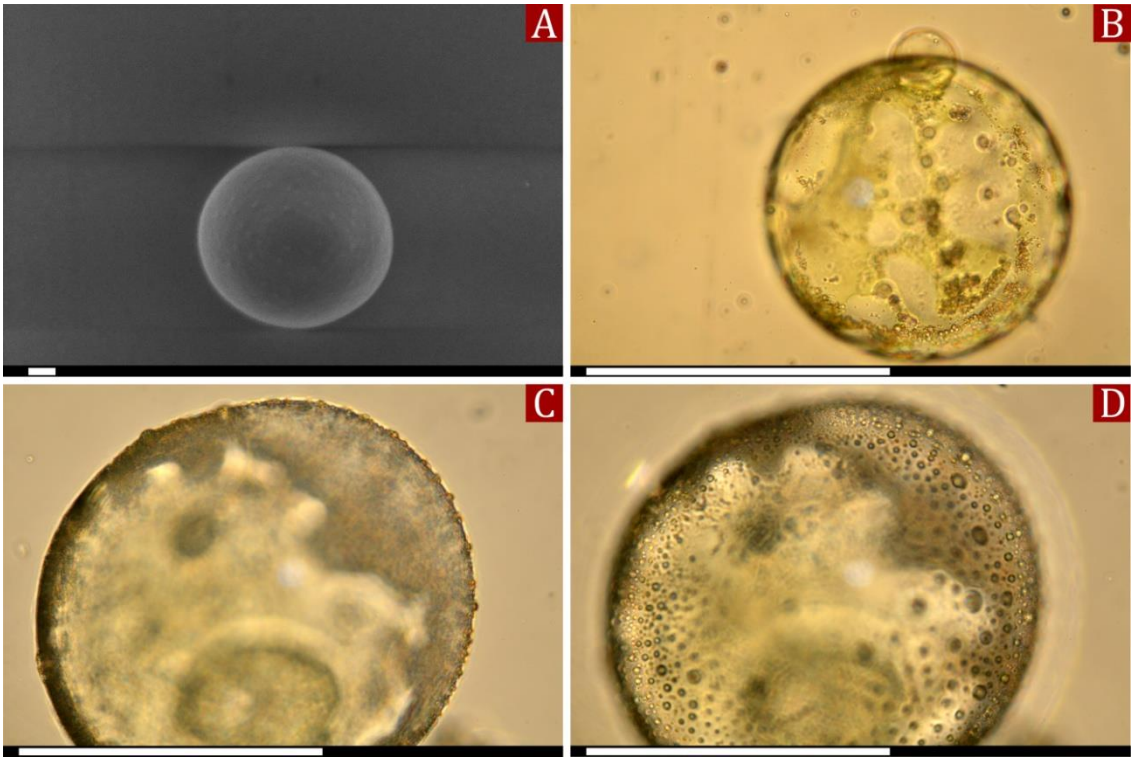

Figure VI-5. SEM image of the platinum covered polystyrene particle and optical micrographs of the polymer vesicles reaction with H_2O_2.(A) Platinum particles can be seen as the tiny light spots on the surface. (B) Polymer vesicle before H_2O_2 addition.(C) An addition of the hydrogen peroxide caused deformation, but vesicle remained unbroken. (D) Closer look at the surface. Scale bars are 200 nm (A) and 150μm (C-E).

In order to prove our assumptions concerning the orientation of the polystyrene particles in the bilayer as well as the activity of the platinum colloids on their surface, we checked the reactivity of the free particles. Figure VI-6 clearly illustrates catalytic activity of the polystyrene particles which decompose the hydrogen peroxide upon the contact. We also captured a short video, which can be found on the attached CD-drive.

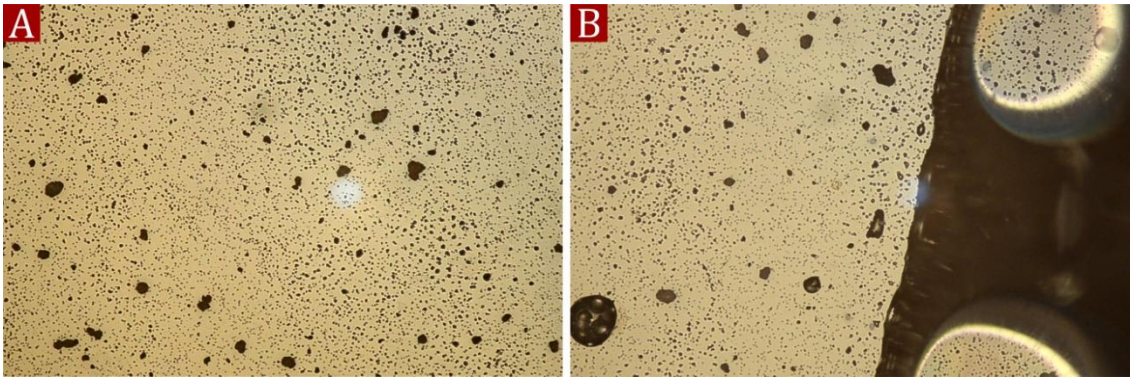

Figure VI-6. Decomposition of the H_2O_2 catalysed by the platinum covered polystyrene particles. (A) Particles on the glass slide. (B) A drop of the hydrogen peroxide solution (dark area) on the surface immediately starts the reaction which can be observed as oxygen bubbles (light area) inside the solution.

Obtaining the evidence of the limited functionality of the noble metal covered polystyrene particles, we tried to found an alternative option to achieve our goals. Nothing can detract from the central fact that particles which supposed to be "micro-engines" for the polymer vesicles should not have the disadvantages noted above. Namely, orientation of the particles in the bilayer should not affect a catalytic activity while the size should be significantly bigger than the thickness of the bilayer. Our choice fell on the manganese oxide particles. First of all, MnO_2 like platinum catalytically decomposes the H_2O_2using the same scheme as Reaction A. Secondly, the orientation in the bilayer is no longer critical due to the reactivity of whole particle. Thirdly, the size (>5μm) of the MnO_2 particles allowed us to assume that surface will not be covered a thin layer of the bilayer preventing the decomposition of H_2O_2.Considering significant differences between the polystyrene (>2μm, spherical shape, ρ = 1060 kg m^{-3}) and MnO_2 (>5 μm, tetragonal shape, ρ = 5026 kg m^{-3}) particles, we first validated the replacement in terms of double emulsion droplets generation and their transformation into the polymer vesicles. We employed the same droplet generation parameters as in the case with the polystyrene particles and generated two types of double emulsion droplets: single core, thick shell and double core, both ≈ 150

µm in diameter (see Table VI-1). We did not notice any differences during the double emulsion droplet generation, but further analysis using the optical microscopy revealed following peculiarity. According to the micrographs MnO_2 particles were distributed more evenly over the middle phase, which is certainly a positive effect. We assume that higher surface area and density of the MnO_2 particles in comparison to the polystyrene ones reduced the Brownian motion preventing aggregation. Figure VI-7 shows the double emulsion droplets with MnO_2 particles dispersed in the middle phase.

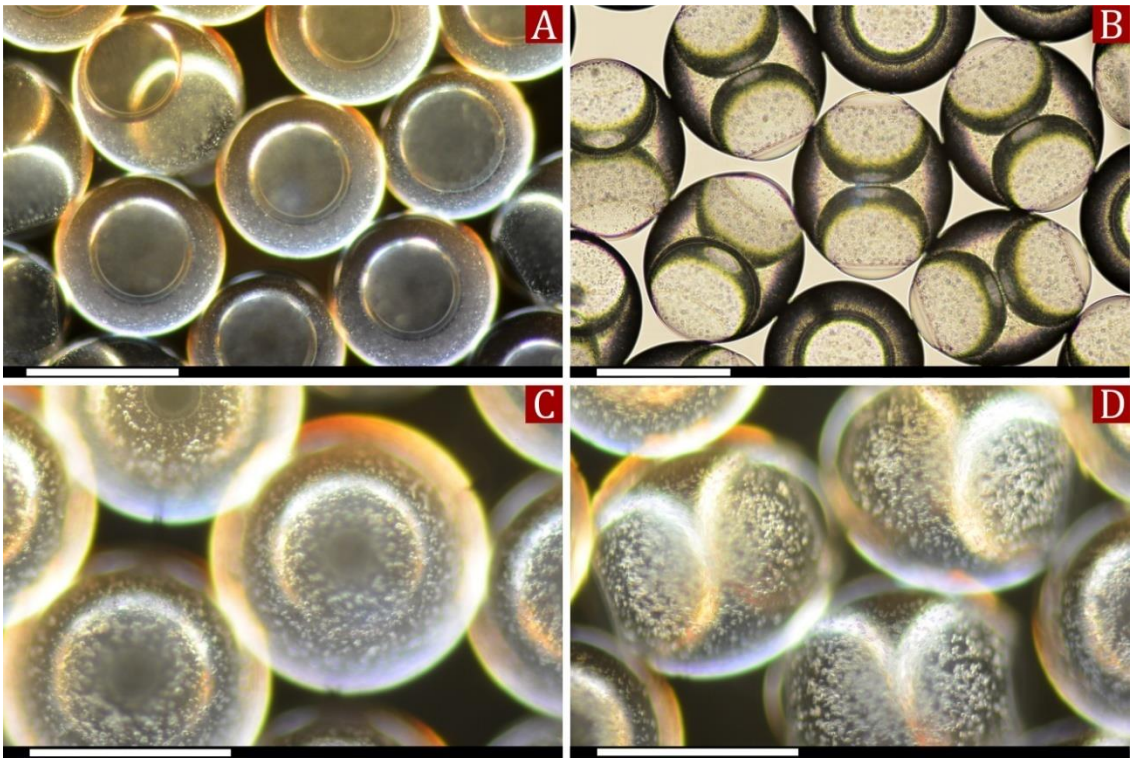

Figure VI-7. Optical micrographs of the double emulsion droplets containing MnO_2 particles in the middle phase. (A) Single core droplets. (B) Double core droplets. (C) Focussing on the surface reveals the MnO_2 particles which can be seen as tiny spots on the images A and B. (D) Surface of the double emulsion droplet. All scale bars are 100 µm.

Verifying the possibility to employ pure MnO_2 particles instead of platinum covered polystyrene, we steadily evaporated the solvent in order to transform the double emulsion droplets into the polymer vesicles. We gently evaporated the solvent from the middle phase to prevent dewetting instabilities[8] resulting in a premature breakage of the

polymer vesicle within a period of 24 h. After that we mixed vesicles with hydrogen peroxide solution. As we expected the catalytic decomposition of the H_2O_2 ran more vigorously breaking polymer vesicles. Figure VI-8 illustrates an interaction of the H_2O_2 solution with MnO_2 "armoured" polymer vesicles.

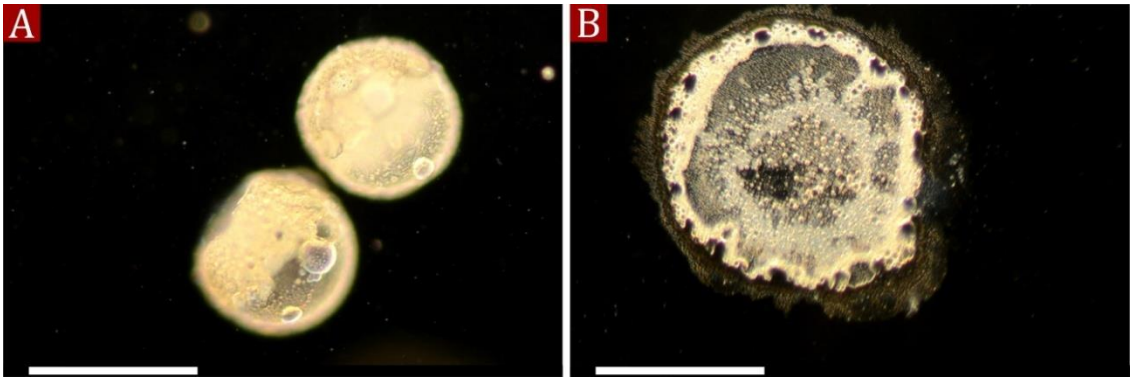

Figure VI-8. A destruction of the polymer vesicles. (A) Upon contact with H_2O_2 solution the surface of the polymer vesicles starts to bubble. (B) This phenomenon ends with a complete destruction of the polymer vesicles. All scale bars are 150 µm.

The proposed method of influence on the bilayer integrity allows releasing contents, but motility of the polymer vesicles still remains uncontrolled. Even if we assume that oxygen release resulting from the reaction between H_2O_2 and MnO_2 would be enough to jet pulse the polymer vesicle, the motion will be erratic. To move it in a controlled manner we replaced the MnO_2 particles with Fe_3O_4 magnetic nanoparticles. Again, in terms of double emulsion droplet formation it had no effect allowing employment of the same parameters (see Table V-1). Despite a low concentration (0.001 g mL^{-1}) of the Fe_3O_4 nanoparticles in the middle phase, their high magnetic strength made polymer vesicles responsive to an external magnetic field. Figure VI-9 represents the magnetic properties of the Fe_3O_4 "armoured" polymer vesicles.

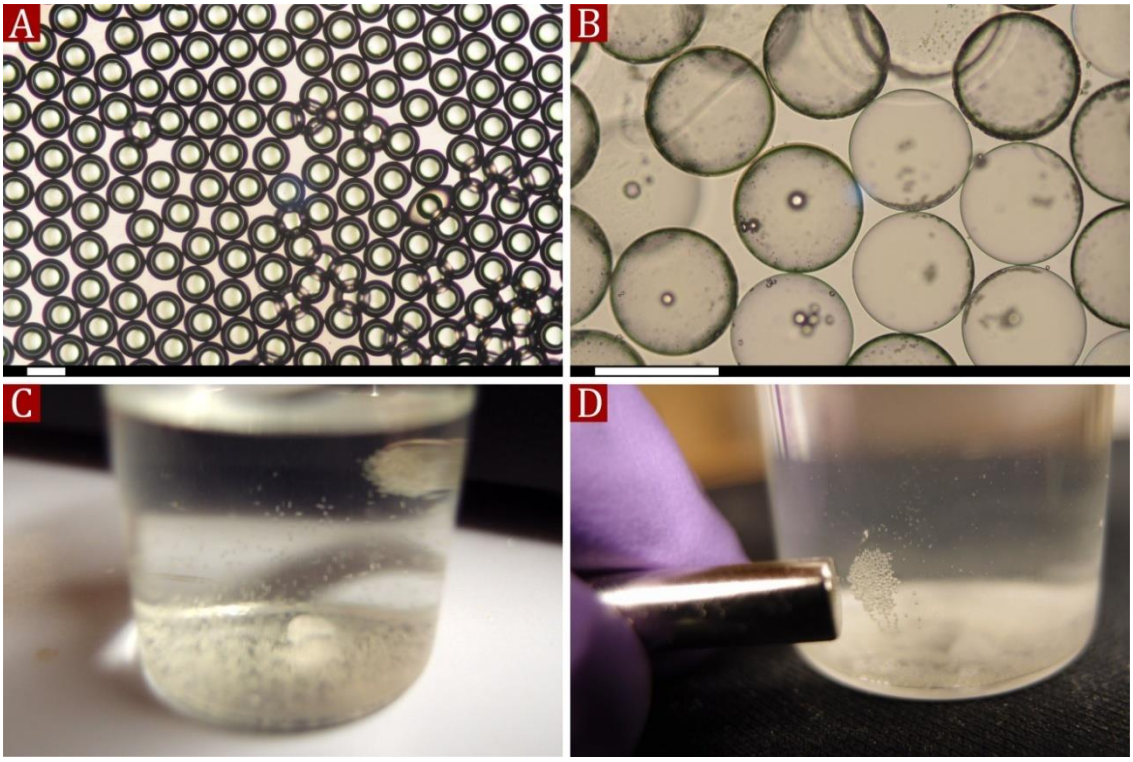

Figure VI-9. Polymer vesicles containing Fe_3O_4 nanoparticles in the bilayer. (A) Double emulsion droplets after the generation where the middle phase contains Fe_3O_4 magnetic nanoparticles. (B) Polymer vesicles after the solvent removal. (C-D) 0.5 kg magnet attracts polymer vesicles from the vials bottom.

In short, colloidal particles impregnated into the bilayer provide ample opportunities to modify polymer vesicles allowing control over the contents release and motility.

VI.3 Conclusions

It is difficult to escape the conclusion that microfluidic fabrication of the polymer vesicles is an excellent tool not only to produce, but also intricate them. The simplified double emulsion droplet generator allowed robust and reproducible synthesis of the various types of the polymer vesicles. The use of the amphiphilic diblock copolymer led to the formation of the bilayer as the result of interfacial phenomena. An employment of

the chemically or physically responsive colloids dispersed in the middle phase of double emulsion droplets allowed to synthesize stimuli responsive polymer vesicles.

VI.4 References

[1] Quevedo, E.; Steinbacher, J.; McQuade, D. T., Interfacial Polymerization within a Simplified Microfluidic Device: Capturing Capsules. *J. Am. Chem. Soc.* **2005**, 127, 10498-10499.

[2] Song, J.-S.; Winnik, M. A., Cross-Linked, Monodisperse, Micron-Sized Polystyrene Particles by Two-Stage Dispersion Polymerization. *Macromolecules* **2005**, 38, 8300-8307.

[3] Sugihara, S.; Blanazs, A.; Armes, S. P.; Ryan, A. J.; Lewis, A. L., Aqueous Dispersion Polymerization: A New Paradigm for in Situ Block Copolymer Self-Assembly in Concentrated Solution. *J. Am. Chem. Soc.* **2011**, 133, 15707-15713.

[4] LoPresti, C.; Massignani, M.; Fernyhough, C.; Blanazs, A.; Ryan, A. J.; Madsen, J.; Warren, N. J.; Armes, S. P.; Lewis, A. L.; Chirasatitsin, S.; Engler, A. J.; Battaglia, G., Controlling Polymersome Surface Topology at the Nanoscale by Membrane Confined Polymer/Polymer Phase Separation. *ACS Nano* **2011**, 5, 1775-1784.

[5] Blanazs, A.; Madsen, J.; Battaglia, G.; Ryan, A. J.; Armes, S. P., Mechanistic Insights for Block Copolymer Morphologies: How Do Worms Form Vesicles? *J. Am. Chem. Soc.* **2011**, 133, 16581-16587.

[6] Pickering, S. U., XXXIII.-Note on the arsenates of lead and calcium. *J. Chem. Soc., Trans.* **1907**, 91, 307-314.

[7] Bon, S. A. F.; Chen, T., Pickering Stabilization as a Tool in the Fabrication of Complex Nanopatterned Silica Microcapsules. *Langmuir* 2007, 23, 9527-9530.

[8] Hayward, R. C.; Utada, A. S.; Dan, N.; Weitz, D. A., Dewetting Instability during the Formation of Polymersomes from Block-Copolymer-Stabilized Double Emulsions. *Langmuir* **2006**, 22, 4457-4461.

CHAPTER VII

Conclusions and Future Work

VII.1 Conclusions

Droplet microfluidics is a versatile tool to fabricate various types of polymer particles and capsules. Employing physical and chemical phenomena like fluid dynamics or polymerisation process, it allows controlling the size of the produced objects in a range of 25–1000 μm and tuning their properties. Microfluidically synthesized microparticles and capsules are widely used in many areas of science and industry.

At the same time a practical implementation of the droplet microfluidic methods often requires specialist technologies, especially in for the device manufacturing. The purpose of this work was to design simple microfluidic devices and employ them to fabricate anisotropic polymer particles and capsules. We used readily available materials and equipment to reach the goal and suggested different device geometries depending on the required properties of the produced objects. Each device was used to fabricate polymer-based particles and microcapsules which have different characteristics.

In Chapter III we showed the fabrication of the single emulsion droplet generator which was employed to synthesize anisotropically-shaped amphiphilic “microbuckets”. An internal phase separation phenomenon allowed us to transform monomer droplets containing non-polymerisable oil into the “microbuckets” upon solidification in a UV-reactor. Having a water soluble 2-hydroethyl methacrylate as the component of the monomer phase allowed us to modify the surface of the “microbuckets” making the exterior hydrophilic whilst the cavity retained hydrophobic.

We than changed the geometry of the microfluidic device which allowed us to produce biphasic polymer particles described in Chapter IV. We combined two needles

making a paired co-flow single emulsion droplet generator. Biphasic polymer particles also known as Janus were obtained by the dispersion of the different prepolymer solutions through that paired channel. We tuned the properties of the prepolymer solutions by adding magnetic nanoparticles, porogen or hydrophilic monomer. This allowed us to fabricate 400 μm Janus droplets which were post cured to transform into particles.

In Chapter V we developed the simplified device for fabrication of polymer microcapsules. The design of the device was based on the tradition T-junction layout, but we placed the tip of dispersion channel into the middle of the main channel. The productivity of this obstructed T-junction geometry was computationally and experimentally studied showing better results. We prepared the water-based ferrofluid, thermoresponsive suspension and coloured solutions and used them as the inner phase. Using our device we generated double emulsion droplets where the middle phase was curable isobornyl methacrylate, whilst the inner varied between the above noted solutions. Photopolymerisation of the middle phase led to formation of the polymer microcapsules with various properties.

Further in Chapter VI we manufactured the double emulsion droplet generator which is based on the co-flow geometry of the channel. We used this device to synthesize the capsule-like objects known as polymer vesicles from the double emulsion droplets. In parallel, we impregnated reactive colloidal particles into the bilayer which allowed us to control the integrity and motility of the polymer vesicles. We employed platinum covered polystyrene and MnO_2 particles as the colloidal "armour" in order to create catalytic centres on the surface of the polymer vesicles. This allowed us to decompose hydrogen peroxide solution upon mixing with polymer vesicles. However, we found that platinum covered polystyrene particles did not perform as we expected.

Besides, we used magnetic Fe_3O_4 nanoparticles as the colloidal "armour" which added the responsiveness to the external magnetic fields to the polymer vesicles.

To conclude, we developed high performance microfluidic devices using relatively cheap materials and tools, which allowed us to fabricate anisotropic polymer microparticles and capsules.

VII.2 Future work

In spite of the wide use of droplet microfluidics in the academic field it lacks industrial large scale applications. The main reason is that droplet microfluidics does not provide a high product yield by mass which makes it non-profitable. If dispersion of monodisperse single emulsion droplets can be solved with existing technologies like Shirasu Porous Glass, industrial generation of double emulsion droplets remains unattainable. The double emulsion devices introduced in this work can be taken as the basis for: (*i*) design of devices providing the same productivity as batch reactors and (*ii*) investigation of optimal operation parameters.

We believe that the fabricated particles can be further studied for potential applications. Thus, amphiphilic "microbuckets" can be employed to carry a hydrophobic phase in its cavity and release it when desired. The behaviour of solid/porous Janus particles at the water-oil interface could also be interesting, since capillary pressure can firmly stick the particles at the interface. Potentially, they should outperform traditional solid particles used to stabilise liquid interfaces known as Pickering stabilisation.[1, 2]

VI.3 References

[1] Pickering, S. U., XXXIII.-Note on the arsenates of lead and calcium. *J. Chem. Soc., Trans.***1907**, 91, 307-314.

[2] Bon, S. A. F.; Chen, T., Pickering Stabilization as a Tool in the Fabrication of Complex Nanopatterned Silica Microcapsules. *Langmuir* **2007**, 23, 9527-9530.